Radiation damage of polymers in ultrasonic fields

Dissertation

zur

Erlangung des Doktorgrades (Dr. rer. nat.)

der

Mathematisch-Naturwissenschaftlichen Fakultät

der

Rheinischen Friedrich-Wilhelms-Universität Bonn

vorgelegt von

Poornnima Anbalagan

aus

Chennai, Indien

Bonn 2008

Angefertigt mit Genehmigung der Mathematisch-Naturwissenschaftlichen Fakultät der Rheinischen Friedrich-Wilhelms-Universität Bonn.

Declaration

I hereby declare that the work in this thesis is original and has been carried out by me at the Helmholtz Institut für Strahlen- und Kernphysik, Universität Bonn, under the supervision of Prof. Dr. Karl Maier and in partial fulfillment of the requirements of the Doctor rerum naturalium (Dr. rer. Nat) degree of the University of Bonn. I further declare that this work has not been the basis for the awarding of any degree, diploma, fellowship, associateship of similar title of any university or institution.

Poornnima Anbalagan

February 2008

Helmholtz Institut für Strahlen- und Kernphysik,

Universität Bonn,

Nußallee 14-16, 53115 – Bonn,

Germany

Abstract

Radiation damage has always been a topic of great interest in various fields of sciences. In this work, an attempt is made to probe into the effect of sub-threshold ultrasonic waves on the radiation damage created by irradiation of deuterons in polymer samples wherein the polymer samples act as model systems. Two equal volumes of radiation damage were produced in a single polymer sample wherein a standing wave of ultrasound was introduced into one. Three polymers namely, Polycarbonate, Polymethylmethacrylate and Polyvinyl chloride were used in this work. Four independent techniques were used to analyze the irradiated samples and visualize the radiation damage. Interferometric measurements give a measure of the refractive index modulation in the irradiated sample. Polymers, being transparent, do not absorb in the visible region of the electromagnetic spectrum. UV-Vis absorption spectroscopy shows absorption peaks in the visible region in irradiated polymer samples. Ion irradiation causes coloration of polymers. The light microscope is used to measure the absorption of white light by the irradiated polymers. Positron annihilation spectroscopy is used to obtain a measure of the open volume created by irradiation in polymers. A comparison between the irradiated region and the region exposed to ultrasonic waves simultaneously with irradiation in a polymer sample shows the polymer specific influence of the ultrasonic standing wave.

Contents

1 Introduction

Radiation damage is a sophisticated tool to modify properties of materials making them available for various applications in everyday life. It has numerous applications in the medical field, material testing, food technology, etc. It is extensively used in radiation therapy for cancer.

Radiation damage in polymers is used as a means of modifying and studying polymer properties in a simple and controllable way. It brings about modification of chemical bonding in polymers and finds a broad application in production of optical components.

The polymers chosen for study are namely **Polycarbonate (PC)**, **Polymethylmethacrylate (PMMA)** and **Polyvinyl chloride (PVC)**. These polymers are widely in use in the modern chemical industry.

Polycarbonate fills an important niche as one of the most popular engineering resins in the medical device market. Possessing a broad range of physical properties that enable it to replace glass or metal in many products, PC offers an unusual combination of strength, rigidity, and toughness that helps prevent potentially life-threatening material failures. The major properties of PC—clarity, high strength and impact resistance, good heat resistance, low water absorption, and biocompatibility—have led to its use in a wide range of critical medical devices. PC is also used in the manufacture of compact discs, lab equipment, safety glasses etc.

 Polymethylmethacrylate has a good degree of compatibility with human tissue and can be used for replacement intraocular lenses in the eye when the original lens has been removed in the treatment of cataracts. Hard contact lenses are frequently made of this material. In orthopaedics, PMMA bone cement is used to affix implants and to remodel lost bone. In cosmetic surgery, tiny PMMA microspheres suspended in some biological fluid are injected under the skin to reduce wrinkles or scars permanently. PMMA is a versatile material and is used as an alternative to glass because of its low density, high impact strength and high transmittance of light in comparison to glass. It does not shatter but instead breaks into large dull pieces. PMMA has excellent environmental stability and is therefore often the material of choice for outdoors applications. It finds use in the manufacture of aircraft windows, laserdiscs, furniture etc.

Polyvinyl chloride it is one of the most valuable products of the chemical industry. It is a widely used building material and extensively used in pipe systems because of its flexibility. It is used in magnetic stripe cards, plumbing fixtures, insulation on electric wires, etc.

All three polymers are transparent, making them suitable for optical methods of analysis. In this work, these polymers are used as a model system to study the influence of ultrasound on radiation damage. High energy ions are implanted in polymer samples and the effect of introduction of ultrasound simultaneously in this sample system that is being rapidly modified is studied. The results are presented and discussed.

2 Theory

2.1 Polymers

The word polymer literally means "many parts". Solid polymers can be distinguished into the amorphous and the semicrystalline categories. Amorphous solid polymers are either in the glassy state, or – with chain cross-linking – in the rubbery state. Those amorphous polymers for which the glass transition temperature is higher than $25^{\circ}C$ are in the glassy state at room temperature. The usual model of the macromolecule in the amorphous state is the "random coil" as shown in Figure 2.1 [3].

Figure 2.1: Schematic diagram of random coil macroconformation in amorphous glassy polymers [3].

2.2 Structure and bonding

2.2.1 Polymer structure

The polymer molecule consists of a "skeleton" (which may be a linear or branched chain or a network structure) and peripheral atoms or atom groups.

Amorphous polymers are plastics where the polymer chains have no well defined order in the solid state. Every polymer structure can be considered as a summation of structural units. In solid amorphous polymers, each structural unit or repeat unit is part of a chain and concomitantly finds itself inserted in a matrix formed by other structural units [6]. Examples of such materials are Polycarbonate (PC), Polymethylmethacrylate (PMMA) and Polyvinylchloride (PVC).

As a general rule, any polymer which can be produced in a clear glass form is an amorphous type. In the glassy state, thermal energy is not sufficient to permit even segments of the polymer chains to move relative to one another. Thus it is an essentially frozen structure in which thermal motion is limited to vibrational energy in place. Self-diffusion and other mobility-related phenomena are not supported in the glassy state [7].

6

2.2.2 Bonding within the polymer

The most common interaction between the atoms within a polymer molecule is the covalent bond. This type of chemical bonding not only produces a stable bond of high strength, but also allows the entire polymer molecule to remain uniformly strong with each additional bond added to it.

2.2.3 Bonding between polymeric molecules

The van der Waals force acts as the cohesive mechanism to hold polymeric molecules together. This force is usually about 1% of the covalent bond strength within the polymeric molecule. With increased proximity of the molecules, increased size of the molecules, high ionic character to the backbone bonds and ionic pendants, the value of the van der Waals force will increase and may reach about 10% of the covalent bond strength.

2.2.4 Configuration of the polymer molecule

The majority of polymeric molecules are based on organic carbon derived from naturally occurring hydrocarbons, which already have some form and structure. Most of them are short chains with repeating units or monomers, with carbon comprising the backbone of the chain and other atoms or groups of atoms satisfying the remaining bonding possibilities.

2.3 Defects in polymers

As any other solid, polymers also contain defects. For example, side chains might be missing (giving rise to radicals) or an incorrect unit might show up in a polymer chain. All these defects act to increase the specific volume and to lower the melting point. Furthermore, microvoids are always present in polymers, their volumes ranging from 1 to 10^{-9} vol.%, their densities ranging from 10^6 to 10^9 cm^{-3}, and their diameters ranging up to 4 μm. Typical microvoids are, however, as small as 10 to 30 nm [5].

2.4 Radiation damage in polymers

Ion irradiation in solid polymers is a controlled means to introduce damage. The interaction of ions with polymers leads to bond breaking, formation of free radicals (paramagnetic defects) and various phenomena that are induced by the complex secondary chemical processes along the trajectory of the ion [8]. The fundamental events involved in ion irradiation of polymers are electronic excitation, ionization, chain scission and cross-linking as well as expulsion of material from the original solid thereby producing an irreversible change. Not only the physical processes but

also the chemical processes of energy deposition determine the modification of a polymer.

2.4.1 Mechanisms of Particle-Polymer Interaction

2.4.1.1 Particle-Particle interaction

2.4.1.1.1 Basis Expressions

The interaction of two particles, projectile a and target A, resulting in the creation of two (identical or different) particles b and B:

$$a + A \rightarrow b + B + Q \tag{2.1}$$

is usually written in the form: $A(a,b)B$. In the case of a nuclear reaction, the change in the total mass of both reaction partners leads to an additionally occurring quantity, the nuclear reaction energy Q:

$$Q = -[M_b + M_B - (M_a + M_A)]c^2, \tag{2.2}$$

with $c =$ velocity of light, and M_i being the atomic masses of the particles i ($i = a, A, b, B$). If $Q < 0$, one talks about "endothermal", and for $Q > 0$ about "exothermal" reactions. The case of $Q = 0$ is defined as "elastic scattering". Q is transferred to both reaction partners as kinetic energy [5].

For a reaction $A(a,b)B$, one can define a "differential cross-section" $d\sigma(\Theta)/d\Omega$ as the probability of finding the reaction product b escaping in the direction Θ within the solid angle $d\Omega$. Integration over the whole solid angle yields the total cross-section:

$$\sigma_{tot} = \int_0^{4\pi} \sigma(\Theta)/d\Omega. \tag{2.3}$$

The unit of the cross-section is usually given in barn (10^{-24} cm^2).

2.4.1.1.2 Nuclear Potentials

The potential of a nucleus consists of two different regions: In the central area, one has a deep negative (attractive) potential region, which is necessary to keep the nucleons together in the nucleus. Beyond the "nuclear radius" R, one encounters a high (repulsive) potential well with its maximum being the so-called Coulomb barrier $E_c = Z_1 Z_2 e^2/R$. For the impact of light projectiles (H, He, Li, B, …) onto light target atoms (H, C, O, ...) characteristic for polymers, $E_c \approx 1\ to\ 25\ MeV/amu$. Irradiation of polymers with highly energetic

particles with $E > E_c$ leads to nuclear reactions (essentially with embedded heavy impurities), which renders them radioactive.

2.4.1.1.3 Elastic Collisions

In the case of elastic scattering ($a = b$, $A = B$, and no target excitation, i.e., $Q = 0$), one distinguishes between potential scattering and resonance scattering. The case of potential scattering, also referred to as "shape elastic scattering", means that the projectile is scattered elastically (i.e., without energy loss of the total system) at the surface of the target nucleus, i.e., the projectile does not penetrate onto the target, hence does not produce any compound nucleus.

2.4.1.1.4 Resonances

In the case of resonance scattering, or "compound elastic scattering" the projectile penetrates into the target nucleus and forms a compound nucleus, which subsequently decays. Most nuclear reactions are a coherent mixture of both elastic and resonance scattering. Resonances exist in the case of charged projectiles and neutral emitted particles.

2.4.1.1.5 Inelastic Collisions

In the case of inelastic collisions, part of the nuclear reaction energy Q is used to excite the target nucleus (positive excitation energy E^*), and $a = b$ and $A = B$ hold.

2.4.1.2 Energy-Loss Processes of Ions in Matter

The energy-loss processes of an ion penetrating into solids has been studied by many investigators such as N. Bohr, H. Bethe, F. Bloch, J. Lindhard among others and as a consequence, many studies dealing with the slowing down of energetic ions into the matter have come up.

In general, two principal features characterize the passage of charged particles through matter: (a) a loss of energy by the particle and (b) a deflection of the particle from its incident direction. These effects are primarily the result of inelastic collisions of the charged particles with the atomic electrons of the material and elastic scattering of the charged particles from the nuclei. At very high energies (larger than several hundred MeV), bremsstrahlung is produced by electrons and Cherenkov radiation is produced by muons. At lower energies (which is the region of interest), the slowing down of ions is traditionally separated into two distinct processes: electronic and nuclear slowing down or

stopping power. The sum of these two processes is called the total stopping power:

$$S(E) = \frac{dE}{dx} \qquad (2.4)$$

which gives a measure of the projectile's energy loss dE per pathlength dx. This quantitiy is also denoted as "linear energy transfer (LET)".

2.4.1.2.1 Nuclear stopping power

The nuclear stopping power is related to the kinetic-energy transfer from the incoming ion to the target atoms. For energies higher than some eV the slowing down of a heavy ion in the matter can be described by a sequence of binary collisions with the target atoms. Then, the projectile trajectory can be specified by the projectile and target masses, ion energy, impact parameter and particularly by the force law describing the interaction.

The calculation of the nuclear stopping power has been performed by considering elastic collisions. At low energies, the cross-section for inelastic collisions vanishes with decreasing ion energy.

Thus, within the elastic-collision approximation, the energy transfer from the projectile atom to the target atom reads

$$T = \frac{\gamma E \sin^2 \theta}{2}, \qquad (2.5)$$

with

$$\gamma = \frac{4M_1 M_2}{(M_1 + M_2)^2}, \qquad (2.6)$$

where M_1, M_2 are the ion and the target masses, E is the incident energy and θ is the scattering angle in the center-of-mass (CM) frame. Assuming the projectile-target-atom interaction represented by a central potential $V(r)$, the scattering angle θ can be written as a function of the impact parameter p and energy E as:

$$\theta(p, E) = \pi - 2 \int_{r_0}^{\infty} \frac{p\,dr}{r^2 \sqrt{(1 - V(r)/E_{CM} - p^2/r^2}}, \qquad (2.7)$$

where $E_{CM} = \frac{M_1}{M_1 + M_2} E$ is the energy in the centre-of-mass frame and r_0 is the distance of closest approach determined by the zero of the square root in the above equation. With the help of the above expression, the differential scattering cross-section can be calculated.

In the case of **amorphous materials** we have a random distribution of the target atoms. Let us consider N target atoms per volume unit ($atoms/cm^3$), then the number of collisions specified by impact parameters between p and $p + dp$ in a target thickness Δx is $dn = N\Delta x 2\pi p dp$. Then the mean energy-loss per unit path due to elastic collisions is

$$\left(\frac{dE}{dx}\right)_n = N \int_0^\infty dp 2\pi p T(p) = NS_n(E),$$

(2.8)

where $T(p)$ is given by eq.2.5. S_n is the nuclear stopping cross-section, which depends only on the parameters of a binary collision. Similarly, the energy-loss straggling due to the fluctuation in the number of collisions can be also obtained:

$$W_n = N \int_0^\infty dp 2\pi p T^2(p).$$

(2.9)

Interatomic Potential: The collision between two atoms is a complex many-body problem. Indeed, in a single collision, there exist $N_1 + N_2 + 2$ bodies, where N_1 and N_2 are the number of electrons of the projectile and target atom, respectively, interacting essentially via Coulomb forces.

The concept of an interatomic potential governing the motion of two atoms arises from the possibility of separating the nuclear and electronic motions. This separation will be valid in the case of a very small approximation rate between the two nuclei allowing a relaxation of the electronic system at each time. This is the well-known adiabatic or Born-Oppenheimer approximation. It leads to an effective potential given by the sum of the Coulomb interaction between the two nuclei $Z_1 Z_2 e^2 / R$ and the ground-state energy $E_{el}(R)$ of the electronic system in the field of the two nuclei separated by a distance R

$$V(R) = \left(\frac{Z_1 Z_2 e^2}{R}\right) + E_{el}(R) - E_{el}(\infty).$$

(2.10)

$Z_1 e$ and $Z_2 e$ are the projectile and target atom charges.

2.4.1.2.2 Electronic stopping power

Inelastic collisions are almost solely responsible for the energy loss of heavy particles in matter. At high energies, the energy loss of ions penetrating matter is dominated by electronic collisions, mainly target excitation and ionization, and is well described by the Bethe Bloch formula [9]. The Bethe formula

provides reliable values for the electronic stopping power for high energies but at energies lower than about 100 keV it becomes very difficult to determine the electronic stopping theoretically.

The Bethe-Bloch Formula

In the quantum-mechanical calculation performed by Bethe, Bloch and others, the energy transfer is parameterised in terms of momentum transfer rather than impact parameter which serves well as the momentum transfer is a measurable quantity whereas the impact parameter is not. The formula obtained is then

$$-\frac{dE}{dx} = 2\pi N_a r_e^2 m_e c^2 \rho \frac{Z}{A} \frac{z^2}{\beta^2} \left[ln\left(\frac{2m_e\gamma^2 v^2 W_{max}}{I^2}\right) - 2\beta^2 \right]. \quad (2.11)$$

Equation 2.11 is commonly known as the Bethe-Bloch formula and is the basic expression used for energy loss calculations. In practice, however, two corrections are added: the density effect correction δ, and the shell correction C which are important at high and low energies respectively, so that

$$-\frac{dE}{dx} = 2\pi N_a r_e^2 m_e c^2 \rho \frac{Z}{A} \frac{z^2}{\beta^2} \left[ln\left(\frac{2m_e\gamma^2 v^2 W_{max}}{I^2}\right) - 2\beta^2 - \delta - 2\frac{C}{Z} \right], \quad (2.12)$$

with

$2\pi N_a r_e^2 m_e c^2 = 0.1535$ MeVcm^2/g

r_e: classical electron radius $= 2.817 \times 10^{-13}$ cm

m_e: electron mass

N_a: Avogadro's number $= 6.022 \times 10^{23}$ mol^{-1}

I: mean excitation potential

Z: atomic number of absorbing material

A: atomic weight of absorbing material

ρ: density of absorbing material

z: charge of incident particle in units of e

$\beta = v/c$ of the incident particle

$\gamma = 1/\sqrt{1-\beta^2}$

δ: density correction

C: shell correction

W_{max}: maximum energy transfer in a single collision.

12

The maximum energy transfer is that produced by a head-on or knock-on collision. For an incident particle of mass M, kinematics gives

$$W_{max} = \frac{2m_e c^2 \eta^2}{1 + 2s\sqrt{1 + \eta^2} + s^2},$$ (2.13)

where $s = m_e/M$ and $\eta = \beta\gamma$. Moreover, if $M \gg m_e$, then

$$W_{max} \cong 2m_e c^2 \eta^2.$$ (2.14)
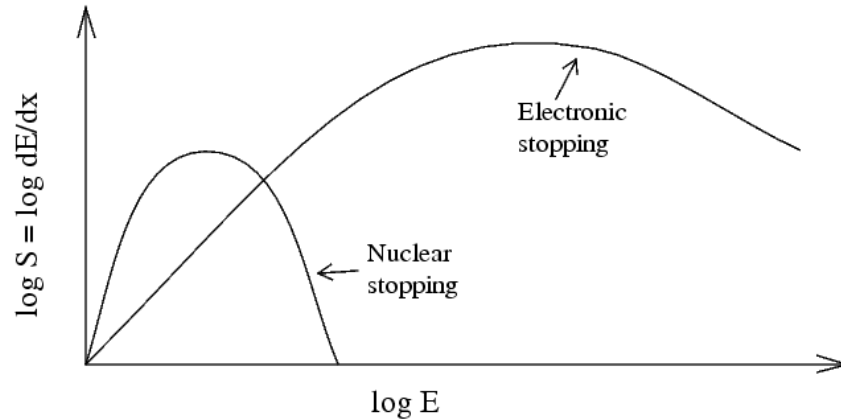
Figure 2.2: A graphical representation of the ratio between nuclear and electronic stopping power. The maximum of the nuclear stopping curve typically occurs at energies between 10-100 keV, of the electronic stopping power at MeV energies [10].

2.4.1.3 Range Distribution

For a given material, the penetration depth of an implanted ion depends largely on the energy of the ion. Ionizing radiation has a large penetrating ability in polymers in comparison to other forms of radiation (ultraviolet radiation).

When energized, charged particles such as deuterons, pass near orbiting electrons, the positive charge of the deuteron attracts the negatively charged electrons, pulling them out of their orbits. This is called ionization, which changes the characteristics of the atom and, consequentially, the character of the molecule within which the atom resides. The sample is ionized at the expense of the energy of the particle until the particle is stopped. It is well known that the damage depends not only on the number of ions produced in the material, but also upon the density of ionization. The dosage is proportional to the ionization per centimetre of path, or specific ionization, and this varies almost inversely with the energy of the particle. Thus the specific ionization or dose is many

13

times less where the particle enters the sample at high energy than it is in the last section of the path where the ion is brought to rest and hence the effects near the end of the range will be considerably enhanced due to greater specific ionization, the degree of enhancement depending critically upon the type of material irradiated. This point, where the high-dose region of energy release occurs, is called the Bragg peak.

Practically, the ion range is calculated using SRIM 2006, a program which simulates the ion trajectories in the sample of interest[1]. There are distinct differences between low- and high-energy ion trajectories. This difference results from different interatomic potentials. At very low energies, particle scattering behaves like hard-sphere collisions, with isotropic directional changes. At high energies, the particle interaction is governed by Coulomb scattering with a 1/r potential, which implies strong forward scattering. The resulting differences in the depth profile shapes are demonstrated in Figure 2.3. We observe that the curve slopes down over a certain spread of thickness and does not drop immediately to the background level. This is due to the fact that the energy loss is not in fact continuous, but statistical in nature [5].

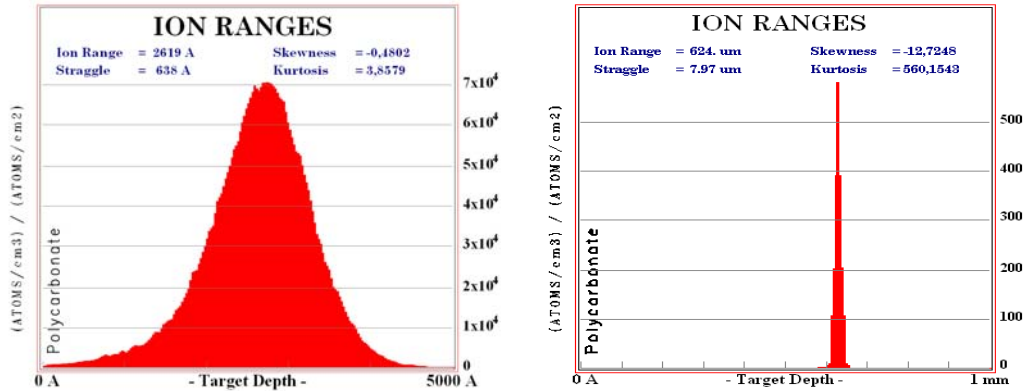Figure 2.3: The concentration distributions of the deposited particles. Pronounced differences show up for low and high energies [5].

From a theoretical point of view, the mean range of a particle of a given energy, T_0, can be calculated by:

$$S(T_0) = \int\limits_0^{T_0} \left(\frac{dE}{dx}\right)^{-1} dE.$$

(2.15)

---

[1] More information on SRIM available in http://www.srim.org/SRIM/SRIM2006.htm

Polymers properties

Radiation damage by energetic ions is usually far more complex in polymers than in, e.g., metals or semiconductors. Ion polymer interaction involves a lot of primary and secondary effects. The energy lost by the incident ions results in primary ionization and formation of excited states in the target. This process is fast ($< 10^{-13}$ sec) and it takes place before the nuclei can move significantly. If the energy of the electrons produced by ionization is less than 100 eV, their range in the target will be small and any secondary process takes place close to the ion path (within a few Angstroms). If the electron energy is above 100 eV they will produce secondary tracks branching off from the ion path (δ-rays) and the lost energy may not be absorbed locally.

In general the energy deposited by the incoming ion in a polymer sample, in steady state condition, results in crosslinks or scission of the original chain. The prevalence of one effect on the other depends on the polymer structure: for example PMMA undergoes scissions because the tetra-substituted carbon atoms tend to degrade the main chains, while the presence of benzene rings in the Polycarbonate structure increases its stability by trapping the excitation energy. Together with crosslinks and scission production, gas depletion from polymer is always observed. During irradiation, electronic excitation and ionization produce excited and ionized species, and radicals (which may recombine due to diffusion effects), and Coulomb interactions among these ions can cause excessive bond stretching or breakage, and nuclear reactions can cause atomic displacement. These processes are responsible for chemical changes, alterations in the internal structure and changes in mechanical, optical, electrical properties of polymers.

Polymers as a class of material can display very similar optical properties. They can be clear, glossy and colourless in appearance, under some conditions. The clarity comes about due to the completely bound nature of the electrons. With the electrons all associated with specific atoms and tightly bound in defined orbitals, the polymer has a great deal of "open space" through which a photon of light may pass without "striking" a particle.

Coloration occurs in a material if the elements that comprise that material are able to absorb photons of light and re-emit them in the visible range while absorbing some of the energy associated with the wavelength of the colour it will display. Polymers are comprised of lightweight elements which do not absorb or re-emit energy in the visible range even when they may be struck with visible light. Ion irradiation produces absorption centers in the UV and visible regions of the spectra. With increasing doses, the samples appear light yellow, yellow, brown and even black for doses above 10^{15} ions/cm^2.

Polymers are capable of having very smooth surfaces, and little light will be lost to reflection on this type of surface. As light is transmitted through the surface of the polymer, all except that which is reflected becomes refracted by the polymer. The amount of refraction is dependent on the density of the material through which the light passes and can be calculated using the index of refraction and Snell's law. Upon emergence from the polymer, the light refracts again in accordance with the index of refraction of the new medium through which it is passing. Ion irradiation leads to buildup of density fluctuations in the polymer resulting in a change in the refractive index of the polymer which reflects the changes in the polymer structure. The refractive index changes are very high for aliphatic polymers (PMMA) and relatively low for the aromatic polymers (PC).

2.5   Ultrasound in polymers

Sounds with a frequency above 20 kHz are called ultrasonic (beyond the range of human hearing). Speed of sound itself varies from one material to another. The speed also depends on temperature, pressure and other factors.

Ultrasonic waves are propagated in gaseous, liquid and solid media. In solids, transverse as well as longitudinal waves occur. This work deals with longitudinal ultrasonic waves in solids. Figure 2.4 shows the sound propagation in a solid. The particles oscillate in the direction of propagation of the wave.

Figure 2.4: Longitudinal wave

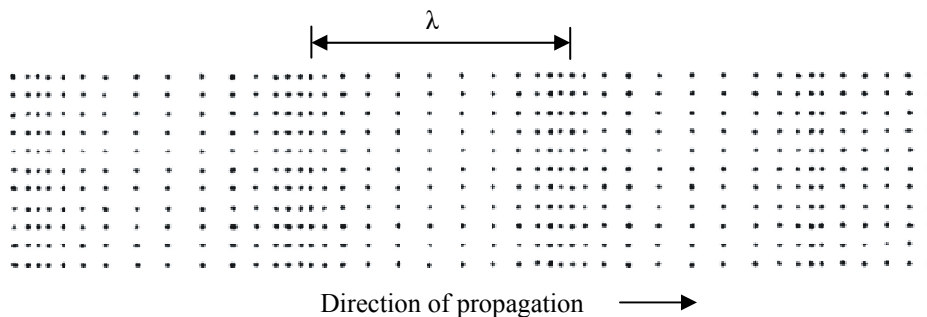The velocity of ultrasound is a characteristic value for a particular medium. The velocity of longitudinal waves in a solid is given by

$$c_{long} = \sqrt{\frac{E}{\rho}\frac{1-\mu}{(1+\mu)(1-2\mu)}} \qquad 2.16$$

where E is the modulus of elasticity, ρ is the density and μ is the Poisson's ratio. The frequency of the ultrasonic waves is determined by the source of the acoustic

16

vibrations. Particles of a medium are displaced relative to their position of rest by the passage of ultrasonic waves. The displacement x of a particle in relation to the time t obeys a sine law:

$$x = A sin2\pi vt,$$ 2.17

where A is the displacement amplitude, or the maximum displacement.

Acoustic vibrations propagating in a medium create a pressure in addition to the mean pressure in the medium. This additional pressure is called the sound pressure [11]. It is the pressure of a sound wave at any point in the medium in relation to time and can be written as:

$$P = P_0 sin2\pi vt,$$ 2.18

where P is the pressure at any instant, and P_0 is the pressure amplitude at the given point.

The sound pressure of a plane progressive wave is related to the vibrational velocity by:

$$\frac{P}{v} = \rho c.$$ 2.19

The product (ρc) of the density of the medium and the sound velocity in this medium is known as the specific acoustic impedance (Z) of the medium. The greater the acoustic impedance for a given particle velocity amplitude, the greater the sound pressure amplitude: $P_0 = v_0 \rho c$.

Ultrasonic frequencies can be obtained by using piezoelectric materials. A piezoelectric is a non-centrosymmetric, non-polar material which becomes polarised when a stress is applied or which changes shape when an electric field is applied. An applied stress separates centres of positive and negative charge, leading to polarisation

$$P = d\sigma$$ 2.20

where d is the piezoelectric coefficient and σ is stress (tension/compression or shear). σ can be multi-axial; this means that d is actually an array of coefficients (a third rank tensor). Hence a rapidly alternating electric field causes the material to vibrate. The frequency at which the crystal vibrates most readily in response to the electrical input, and most efficiently converts the electrical energy input to mechanical energy is the resonance frequency at which the electrical impedance is minimum. The vibrations are then passed through any adjacent material as a

17

longitudinal wave i.e., a sound wave is produced. The exact fraction of the incident sound which is transmitted or reflected depends on the acoustic impedance of the two materials on each side of the boundary. The greater the difference in impedance, the more sound will be reflected rather than transmitted.

By using piezoelectric ceramics, ultrasonic waves are inducted into polymer samples. The frequency (5MHz) and amplitude of the ultrasound pulses (not more than 30 $V_{peak-peak}$) inducted into the samples are chosen such that the change in temperature in the samples is very small. Hence the intensity of ultrasound used is sub-threshold, causing no measurable damage to the polymer samples unlike in another method of ultrasound treatment in polymers, **Ultrasonic Welding.**

Ultrasonic welding is a plastics welding process, in which two work pieces are bonded as a result of a pressure exerted to the welded parts combined with application of high frequency acoustic vibration (ultrasonic). The plastic melts in the contact area (due to local heating), the polymer molecules are cross-linked, forming a strong joint. The frequency of acoustic vibrations is in the range 20 to 70 kHz. The amplitude of the acoustic vibrations is about 0.05 mm.

3 Experiment

3.1 Sample preparation

3.1.1 Material description

3.1.1.1 Polycarbonate (PC)

Polycarbonates are polymers having functional groups linked together by carbonate groups (-O-(C=O)-O-) in a long molecular chain. Polycarbonate is an aromatic material. The chemical structure is depicted in Figure 3.1.
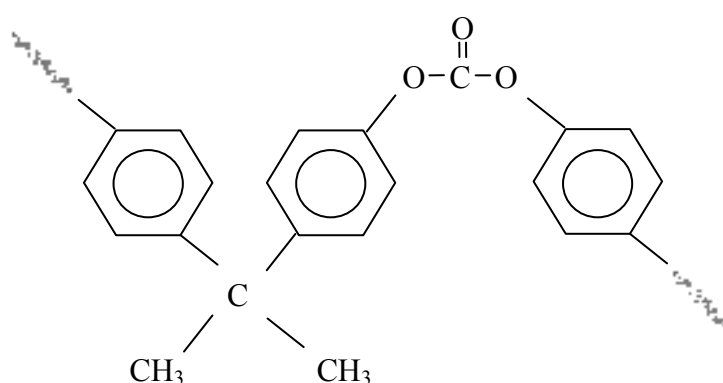
Figure 3.1: Chemical representation of Polycarbonate chain

Polycarbonate (in the form of sheet) was manufactured by Bayersheet GmbH. Polycarbonate sheets were prepared by polycondensation of the two monomers. Samples of dimension $30\times5\times5$ mm^3 were cut out from the Polycarbonate sheet. The density of Polycarbonate is 1.2 g/cm^3. The velocity of ultrasound in Polycarbonate is ~2200 ms^{-1}.

3.1.1.2 Polymethylmethacrylate (PMMA)

Polymethylmethacrylate is the synthetic polymer of methylmethacrylate. PMMA is an aliphatic material and a polar polymer. This thermoplastic and transparent plastic is commercially known as Plexiglas. Its chemical structure is depicted in Figure 3.2.

$$
\begin{array}{cc}
\mathrm{CH_3} & \mathrm{CH_3} \\
| & | \\
\mathrm{\sim\!\!\sim\!\!\sim\!-\!\!\!\lceil CH_2 - C - CH_2 - C \rceil\!\!\!-\!\!\sim\!\!\sim} \\
| & | \\
\mathrm{C = O} & \mathrm{C = O} \\
| & | \\
\mathrm{OCH_3} & \mathrm{OCH_3}
\end{array}
$$

Figure 3.2: Chemical representation of a PMMA chain

PMMA (in the form of sheet) was obtained from Quinn Plastics. The production of PMMA sheets involved mass polymerisation of the monomer, methylmethacrylate. Samples of dimension $30 \times 5 \times 5$ mm^3 were cut out of the PMMA sheet. The density of PMMA is 1.19 g/cm^3. The velocity of ultrasound in PMMA is ~2700 ms^{-1}.

3.1.1.3 Polyvinyl chloride (PVC)

Polyvinyl chloride is produced by polymerization of the monomer vinyl chloride. PVC is a thermoplastic. It is a polar polymer and an aliphatic material. Its chemical structure is shown in Figure 3.3.

$$
n \left[\begin{array}{ccc}
\mathrm{H} & & \mathrm{Cl} \\
\diagdown & & \diagup \\
 & \mathrm{C = C} & \\
\diagup & & \diagdown \\
\mathrm{H} & & \mathrm{H}
\end{array} \right]
$$
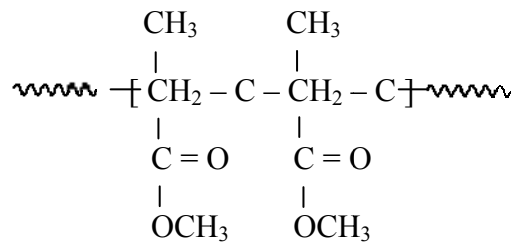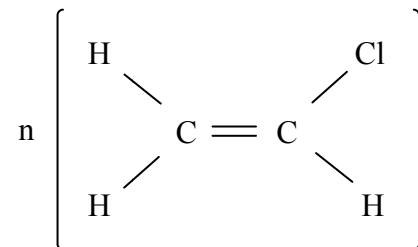
Figure 3.3: Chemical representation of a PVC chain

PVC (in the form of sheet) was manufactured by Röchling Engineering Plastics KG. The PVC sheets were prepared from the monomer by Tension polymerisation. A blue dye is added during the preparation and hence the sample although transparent has a blue tinge. Samples of dimension $30 \times 5 \times 5$ mm^3 were cut out the Polyvinyl chloride sheet. The density of the Polyvinyl chloride samples used is 1.68 g/cm^3. The velocity of ultrasound in Polyvinyl chloride is ~2400 ms^{-1}.

3.1.1.4 Additives

The process of production of all polymers involves the incorporation of additives. Additives include all substances that are intentionally added to a polymer mixture, but which do not form primary chemical bonds. Plasticizers are additives used to increase the flexibility or plasticity of the polymer. Filler defines virtually anything added to a polymer for purposes other than plasticization. It also means a non-reacting additive used primarily to add bulk. Reinforcement additives are powders and fibres added to a polymer to serve to reinforce or increase the tensile strength of the polymer.

3.1.2 Ultrasonic transducers

The piezoelectric effect occurs in a number of natural crystals including quartz, but the most widely used substance is a synthetic ceramic, Lead zirconate titanate.

Lead zirconate titanante $(Pb[Zr_xTi_{1-x}]O_3 \ 0<x<1)$, also known as PZT is a ceramic perovskite material that shows a marked piezoelectric effect. Being ferroelectric, it develops spontaneous polarization which can be reversed in the presence of an electric field. This compound is a solid solution of ferroelectric $PbTiO_3$ and anti-ferroelectric $PbZrO_3$. The ferroelectric Curie temperature of PZT (about $320^\circ C$) is dependent on the composition. PZT ceramics do not have a phase transition point in the temperature range from room temperature to Curie temperature. Thus it is widely used for piezoelectric application. Its composition shows large electromechanical coupling factor. One of the most commonly used chemical composition is $PbZr_{0.52}Ti_{0.48}O_3$.

Lead atoms, several oxygen atoms (cubic-face-centered) and a titanium and/or a zirconium atom (pseudocubic-body-centered) are arranged in a cubic regional structure. The titanium atom takes the cubic-body-centered position above the curie temperature. At temperatures below the curie temperature, the titanium atom moves somewhat from its central situation out and the before electrically neutral lattice becomes a dipole. This dipole lattice exhibits now piezoelectric characteristics.

Lead meta niobate (LMN), also a piezoelectric material, is a ferroelectric without perovskite structure. This compound has a curie temperature near $570^\circ C$ and is orthorhombic system in room temperature and this compound shows very low mechanical quality factor (Q_m), which gives a measure of the ability of the transducer to work over a range of frequencies. It shows large orientation for direction of polarization [12].

PZT was largely used in our experiments although LMN was also used in some of our experiments. In principle, there were no observable effects in the samples due to the change in the ultrasound transducer used.

Effect of an alternating field:

For linear dielectrics, the polarisation is aligned with and proportional to the electric field E and the P-E curve is linear. For ferroelectrics, the P-E curve exhibits hysteresis. The unit cell is spontaneously polarised below the Curie temperature, T_c. At $T<T_c$, the polarisation can always be switched by applying a large enough electric field.

Figure 3.4 shows a typical hysteresis curve created by applying an electric field to a piezoelectric ceramic element until maximum polarisation, P_s, is attained, reducing the field to zero to determine the remanent polarisation, P_r, reversing the field to attain a negative maximum polarisation and negative remanent polarisation, and re-reversing the field to restore the positive remanent polarization. The tracing below the hysteresis curve plots the relative change in the dimension of the ceramic element along the direction of polarisation, corresponding to the change in the electric field. The electric field applied is of the order of a few thousand volts/mm.

In this work, polarised piezoceramics with a thickness of half the wavelength are used. They are manufactured by applying high electric field at elevated temperature. The electric field is then removed and the ceramic is in the state of remanent polarisation. A maximum voltage of 30 $V_{peak-peak}$ is applied to the piezoceramic during the experiment and hence the change in polarisation due to the applied electric field oscillates about the remanent polarisation of the polarised piezoceramic and the corresponding elongation and contraction of the piezoceramic is very small in dimension in comparison with the shown dimension changes in Figure 3.4.

(a) hysteresis curve for polarization

(b) relative increase/decrease in dimension (strain, S) in direction of polarization
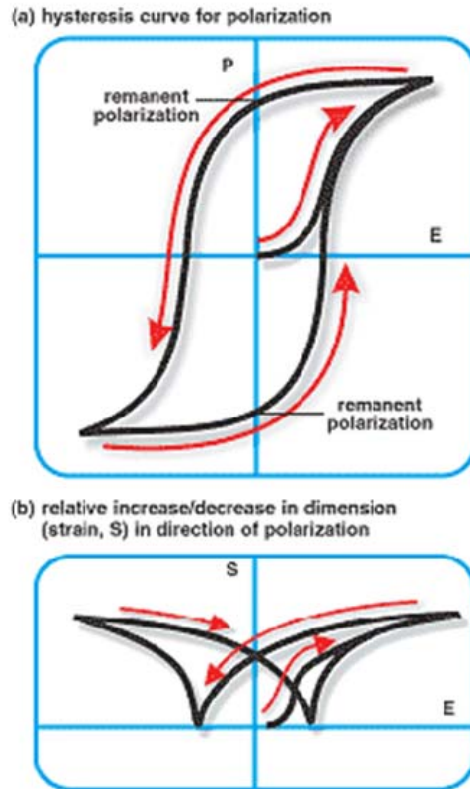
Figure 3.4: Effects of electric field (E) on polarisation (P) and corresponding elongation/contraction of ceramic element [4]

3.1.3 Sample fabrication

The polymer samples are fixed with ultrasound transducers and the final sample looks as shown in Figure 3.5.
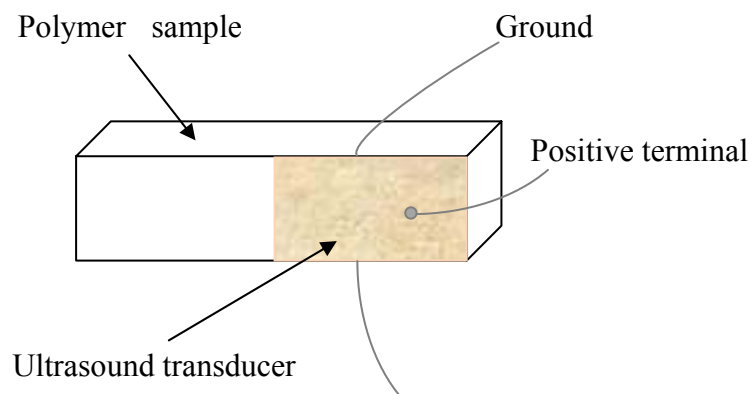
Figure 3.5: Sample fixed with an ultrasound transducer

3.2 Bonn Cyclotron

Ion irradiation of the polymer samples was carried out at the experimental site 8 in the Bonn Cyclotron. A complete view of the Bonn Cyclotron is shown in Figure 3.6. Deuterons were obtained from an Electron Cyclotron Resonance ion source. The ions extracted were then accelerated to an energy of 26 MeV/nucleon and brought to experimental site 8.
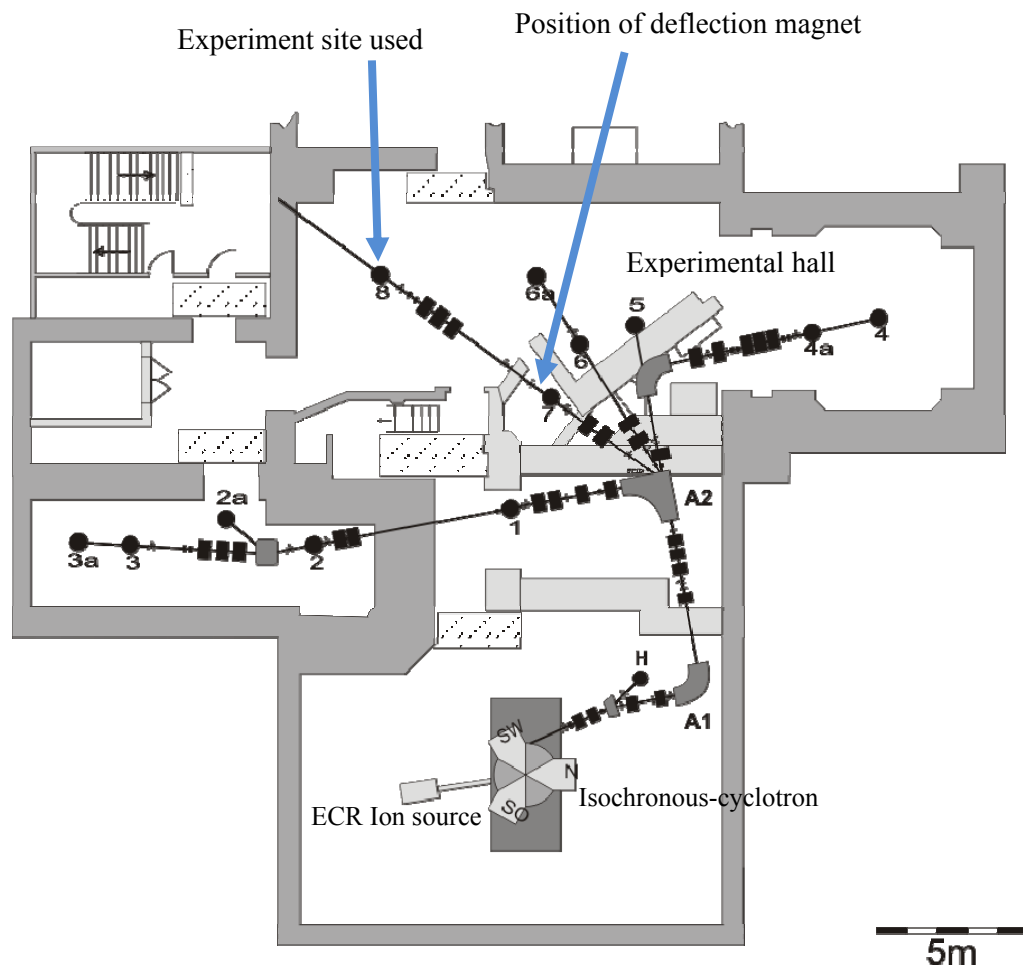
Figure 3.6: The Bonn Cyclotron. The passage of the deuteron beam to experimental site 8, after being deflected by magnet A2 is almost a straight line. This stretch of the beam line consists of a series of stoppers, steerers, slits, valves and quadrupoles.

24

3.3 Experimental details

The beam line from experimental site 7 to experimental site 8 (in Figure 3.6) had to be modified in order to produce a pulsed deuteron beam and to obtain two equal volumes of radiation damage in the polymer samples. The modifications involved are explained in detail in this section.

3.3.1 Deflection of the Deuteron beam

At experimental spot 7 (Figure 3.6), a narrow flexible tube with a diameter of 20mm is plugged into the beam line. This tube is enclosed within a 27mm wide slit in a standard 50Hz iron core magnet. This magnet consists of six coils (6V and 100A across each). The best configuration to achieve maximum output current was to connect each set of three coils in series and then connect the two sets of coils in parallel (Figure 3.7). The magnet is driven by a set up consisting of two high current transformers (2kVA) and a variable transformer. The output terminals of the two high current transformers were connected in series. The output from the variable transformer is fed into one of the two high current transformers connected in series. A 1Ω resistor is connected to the input of the other. The variable transformer operates at a chosen output voltage.

The magnetic field measured at the magnet varies linearly with the output voltage of the variable transformer. Also the magnetic field varies as a sine wave as the current that drives the magnet is sinusoidal. When the deuteron beam passes through the tube enclosed by the magnet, it is deflected. This deflection of the deuteron beam at the magnet corresponds to a spread of the beam over a length of 20 cm at the experimental site 8.

Eddy currents are created when a stationary conductor encounters a varying magnetic field. Eddy currents create losses through joule heating and hence reduce the efficiency of many devices that use changing magnetic fields. They are minimized in this case by using thin sheets of magnetic material called laminations. Electrons cannot cross the insulating gap between the laminations.
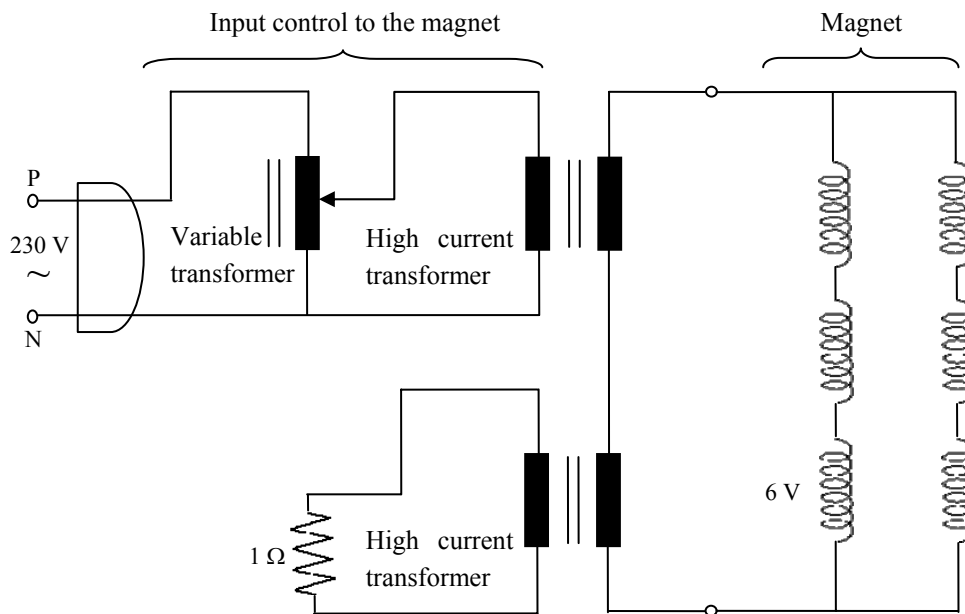
Figure 3.7: Transformer set up to deflect the deuteron beam

3.3.2 Reduction of activation

Graphite rings are fitted in the beam line at various positions to reduce the activation of the beam line due to the narrow passage and deflection of the beam. These rings have an inner diameter of 20mm and are 10mm thick. One of these is positioned just before the stainless steel elastic tube so that the beam is stopped in the graphite if the beam diverges from the narrow passage. Another is positioned to absorb the beam diverging outside a diameter of 20mm. A graphite block with a 14mm aperture is placed in the chamber at experimental site 8 (Figure 3.6) and a 10mm thick graphite ring with an inner diameter of 12mm is fitted into the aluminium flansch which forms the end of the beam line, for the same purpose. This helps reduce the activation of the parts of the beam line to a great extent.

3.3.3 Beam profile view

A screen is placed in the chamber at the end of the beam line in experimental site 8 (Figure 3.6). It consists of a quartz glass slide of dimensions $75 \times 25 \times 1$ mm^3 fitted into one of the surfaces of a graphite block of dimensions $80 \times 30 \times 10$ mm^3. The thickness of the quartz glass slide is such that the beam passes through it and stops in the graphite block. A white illumination against the black background is seen where the beam falls on the quartz glass. The spread of the deflected beam is also visible on this screen.

26
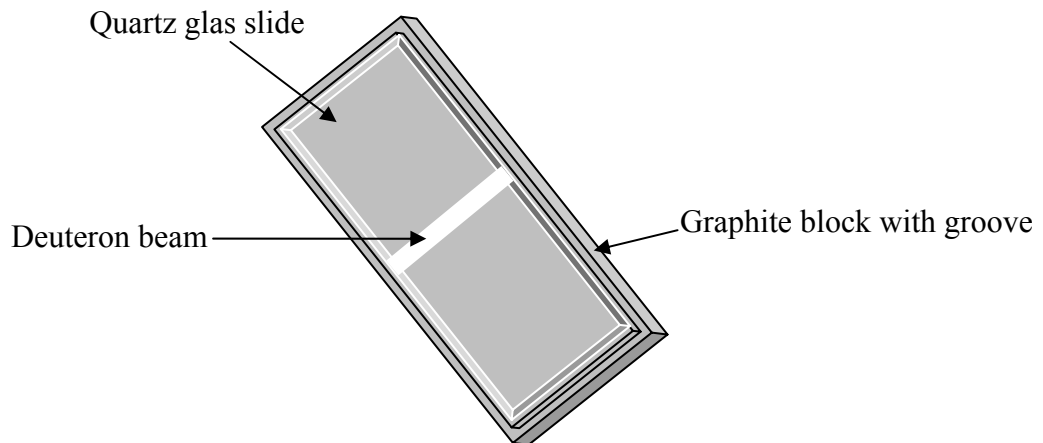
Figure 3.8: Deuteron beam profile as seen on the graphite screen

This screen proves to be a better replacement for a fluorescent screen in which a mixture of zinc sulphide and sodium silicate is coated on a piece of pure aluminium, as the coated mixture becomes highly activated in comparison to the quartz glass slide for a very small beam current. Also continuous usage of the fluorescent screen leads to constant degradation of the coated layer and in the course of time, a clear picture of the beam is not visible.

3.3.4 Beam outlet

An aluminium flansch with an aperture of diameter of 12 mm forms the end of the beam line at experimental site 8. A 30 μm thick aluminium foil covering the aperture, seals the evacuated beam line.

A 2.5 mm thick piece of (99.9%) pure aluminium is cold rolled and two holes with a diameter of 4 mm were drilled 1 mm apart in it. This is fixed on to the aluminium flansch such that the two apertures are aligned with the outlet of the flansch and are also horizontally aligned. These two outlets are positioned exactly in the central part of the deflected deuteron beam ensuring equal beam current passage through both the outlets. Thus we obtain two equally implanted volumes in our samples.
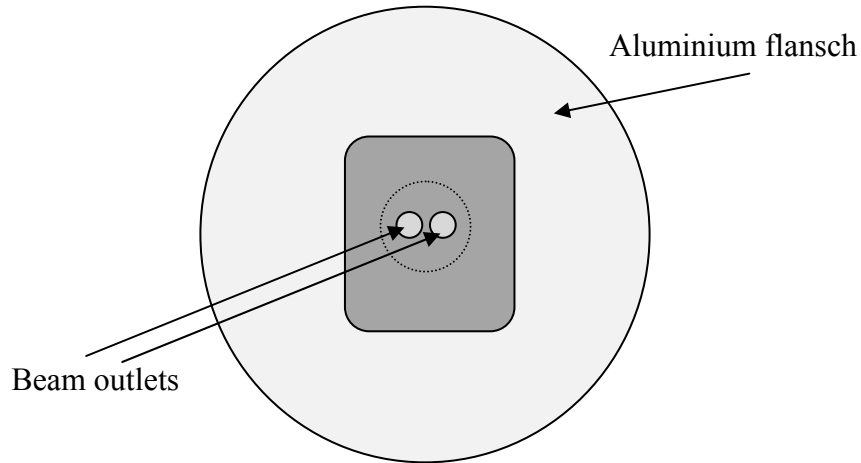
Figure 3.9: Deuteron beam outlet as seen from the front

3.3.5 Faraday cup

A faraday cup is a conductive (graphite) cup designed to catch charged particles. The resulting current can be measured. The faraday cup is positioned corresponding to an ion beam shooting position. When a beam of ions hits the graphite, it gains a small net charge while the ions are neutralized. The graphite can then be discharged to measure a small current equivalent to the number of single charged impinging ions.

$$\frac{N}{t} = \frac{I}{e}$$

where N is the number of ions observed in time t (in seconds), I is the measured current (in amperes) and e is the elementary charge ($\sim 1.6 \times 10^{-19}$ C). Thus a measured current of 0.2 nA corresponds to about 1 billion ions striking the faraday cup each second.

3.3.6 Ionization chamber

An ionization chamber is a device for detection and measurement of ionizing radiation. The electrodes of the ionization chamber used here are made up of 5 μm thick aluminium foils. Three foils are arranged vertically where the first and the third foil are connected and form the cathode. The foil in the middle forms the anode. A negative high voltage of -100 V is applied across the cathode. The beam passing through the ionization chamber produces secondary electrons which travel

28

towards the central aluminium foil and an integral electron current is measured at the anode. This measured ionization current is calibrated with the Faraday cup. Thus the measured ionization current helps to detect the passage of the ion beam through the chamber and gives a measure of the ion current in terms of the ionization current. The ionization current varies as a function of the input high voltage. So a fixed voltage lying in the linear region is used. The ionization chamber is mounted on a stand and placed right in front of the outlet of the deuteron beam.
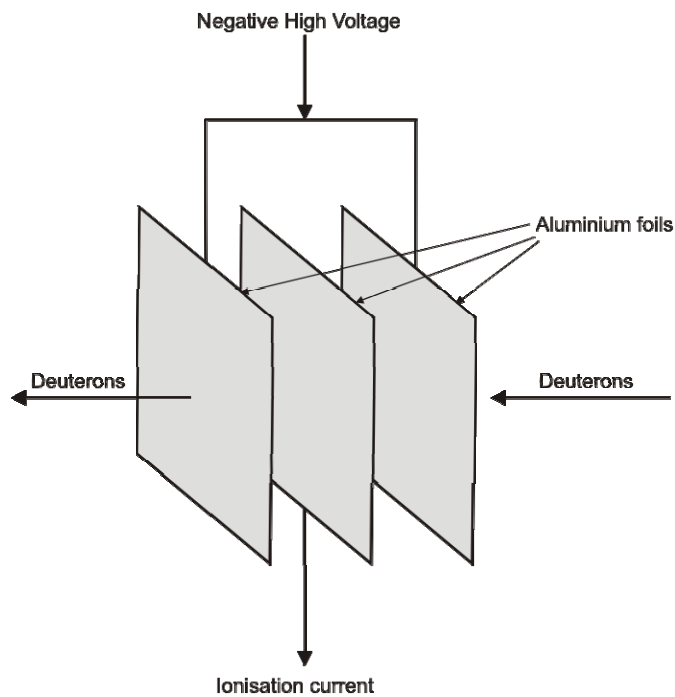
Figure 3.10: The set up consisted in the ionisation chamber

3.3.7 Scintillation detectors

The scintillation detector is one of the most useful particle detection devices in nuclear physics today. It is comprised of two main components: first, a scintillator which absorbs incident radiation and converts the energy deposited by ionization into a fast pulse of light and second, a photomultiplier. This second component converts the light pulse into a pulse of electrons and also amplifies the electron pulse to be recorded or processed. Many different types of scintillators exist for example, an organic liquid solution, a plastic, or a crystal (organic or inorganic).

The light output of a scintillator is proportional to the deposited energy so the amplitude of the electrical signal will be proportional to this energy.

The main requirements for scintillators are high effieciency for detection of the desired radiation, high light output and a short decay time for the emission of light so that fast counting is possible. This means that the time difference between two events can be obtained accurately with scintillator detectors. In scintillators, the decay time of emitted light is affected by the type of incident radiation, since different types of incident particles have different ionization powers. Higher ionization density will lead to higher concentrations of excited molecular states for intermolecular interactions, and therefore a higher probability for an excited molecule to meet and interact with another excited molecule. This results in a higher fraction of slow-component light. The photomultiplier tube converts the weak light of the scintillation pulse into a corresponding electrical signal. Light signals are converted into a current pulse without adding a large amount of noise to the signal. A photomultiplier tube consists of

- A photocathode that deposits the light energy from the scintillator to electrons by absorbing incident photons and transferring the energy of each photon to an electron within the photoemissive material. The electron then escapes from the surface of the photocathode.

- A series of electrodes which are called dynodes operated at positive potentials greater than the cathode potential. When electrons hit these dynodes, several electrons are released. This multiplication is necessary for a detectable pulse.

- An anode that collects these "multiplied" electrons resulting in electric pulses.

3.3.7.1 Liquid scintillator neutron detector

The neutron detector employed in the experiment consists of a liquid scintillator followed by a photomultiplier tube. The radiation impinging on the liquid scintillator consists of neutrons and gammas that are produced by highly excited nuclei. Elastic scattering of neutrons by hydrogen nuclei generates recoil protons while gamma rays interact via Compton scattering yielding recoil electrons. The recoil protons have a short mean free path and produce a large number of ionization events. The recoil electrons have a long mean free path producing very few ionization events. The rise time (light decay constants) of the recoil protons is shorter than that of the recoil electrons. But in the case of a deuteron beam, the observed signal constitutes of an almost equal contribution from neutrons and gammas. Thus an integral signal obtained from the neutron detector

is used to mark the position of the pulsed deuteron beam impinging the sample. To obtain a precise signal, a plastic scintillator is brought in to use.

3.3.7.2 Plastic scintillators

Plastic scintillators consist of a solid solution of organic scintillating molecules in a polymerized solvent. Because of the ease with which they can be shaped and fabricated, plastic scintillators have become an extremely useful form of organic scintillator.

The scintillation emission of a typical plastic scintillator has a maximum around 400nm. Plastic scintillators are characterized by a relatively large light output and a short decay time, on the order of a nanosecond. This makes the material well suited for fast timing measurements. Because the density and atomic number are rather low, the material is not very well suited for efficient detection of gamma rays. Since they exhibit very short response times, they are extensively used in experiments where accurate measurements of very short time intervals (ns) must be obtained in spite of prodigiously high count rates.

Organic scintillators contain aromatic hydrocarbon molecules that have suitable vibrational excited states which can be excited by ionizing radiation. They are de-excited via the emission of electromagnetic radiation. Scintillation light results from transitions made by free valence electrons of the molecules. This production of photons in organic scintillators is a molecular process most easily described by using the potential-energy diagram (Figure 3.11). The lower curve represents the potential energy when all of the electrons are in the ground state and the upper curve shows the potential energy of an excited state.
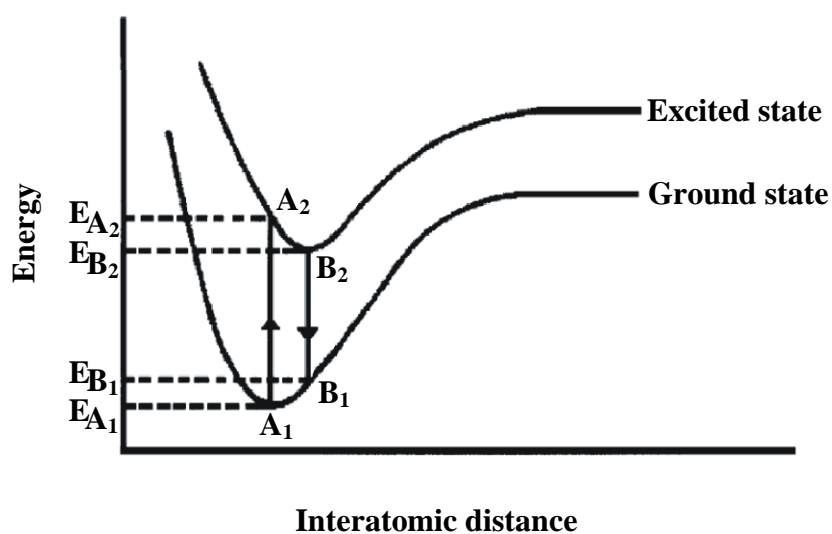

Figure 3.11: Energy diagram (simplified) of an organic scintillator [1]

31

The Franck-Condon principle states that the energy deposited by a charged particle, not dissipated as heat, causes a transition from A_1 to A_2 ($E_e = E_{A2} - E_{A1}$) in a time (~0.1 ps) that is short compared to the vibration time of the molecule. Some energy is lost through lattice vibrations moving the molecule to B_2. After a time (~10 ns) that is long compared to the vibration time, the excited state may decay to the ground state (B_2 to B_1), the excess energy ($E_p = E_{B2} - E_{B1}$) being carried away by an emitted photon. This fluorescent emission produces approximately 1 photon for every 100 eV of energy deposited. Since the energy required to produce an excited state (E_e) exceeds that carried away by photons (E_p), the probability for re-absorption of the emitted photon is small i.e., the scintillator is transparent to the light that it generates. Secondary scintillators are frequently used to 'shift' this emitted light to longer wavelength, near the peak of a photomultiplier spectral-response curve. These secondary fluors have a high absorption cross section at the wavelengths generated by the primary scintillator and respond to the energy deposited in exactly the same manner as described earlier, except that all energy level are somewhat lower (wavelengths are longer) – the scintillator is transparent to the light it generates. The scintillator and the photomultiplier are housed in a dark box so that the only light detected is caused by cosmic rays.

The plastic materials that have found the widest application consist of those manufactured from thermosetting plastics which include polystyrene, polyvinyl toluene and various acrylic polymers. The generation of light from these plastics is accomplished through the addition of small amounts of many different combinations of organic molecules known to have fluorescent properties of high efficiency.

To obtain a precise signal so as to differentiate (resolve) the deuteron pulses from the two equivalent apertures, a plastic scintillator is used. It is placed such that a clear, sharp signal of one of the deuteron beams is obtained. From the signal obtained, we can roughly calculate the number of particles impinging. The position of this signal obtained from the plastic scintillator is marked with respect to the signal obtained from the neutron detector. This helps to synchronise the pulsing of the ultrasound input to the sample with the deuteron beam.

3.3.8 Sample placement

A motorized X-Y table with an attached platform that can be moved horizontally as well as vertically is used to hold and position the sample at a desired location.

The X-Y table is controlled with a Turbo Pascal program. The sample is placed in front of the ionization chamber.

3.3.9 Standing wave of ultrasound

Polymers samples fixed with piezoelectric transducers act as resonators as the ultrasonic wave transmitted by the transducer into the polymer is reflected by the open surface of the polymer due to the large difference in acoustic impedance between the polymer and air. A standing wave is created in the sample at the resonance frequencies of the resonator. When a laser beam is passed perpendicularly through the sample, a diffraction pattern is observed at the resonance frequencies of the sample system. The resonance frequency at which the diffraction pattern is most intense is chosen. As the density of the polymers used is large, we can view only the first maxima in the diffraction pattern, clearly. Two right-angled prisms are used to direct the laser beam into the sample and direct the out-coming pattern onto a screen placed at a distance so that a clear pattern is seen. The diffraction pattern is monitored using a camera to ensure a standing wave of ultrasound in the sample throughout the irradiation.

3.3.10 Temperature measurement

To measure the temperature change in the sample during irradiation, Fe/CuNi thermocouple and Ni/NiCr thermocouple were used together with a Zero degree reference cell. The thermocouples were glued to the edges of the samples. The maximum difference in measured voltage during irradiation corresponded to 0.15°C.

3.4 The Experiment

3.4.1 Ion irradiation

The ionized particle used for irradiation in polymer samples is the deuteron ($^2H^{1+}$). The energy of the deuterons used for irradiation is 26 MeV. The most obvious advantage in using deuterons with energy in the order of MeV is their greater range in materials among all of the particles produced in the Bonn cyclotron. Enhancing the ion range provides us with a larger overall modified polymer volume to study. Also interaction between high energy ions and polymer chains involves high values of energy loss and spatial distribution of the deposited energy ensuring enough damage in the polymer for analysis with various techniques. The thickness of the sample is chosen such that the range of ions is smaller than the thickness of the sample and hence the incident ions are stopped and trapped within the sample producing cylindrical zones of damage. The deflected deuteron beam

passes through the two identical beam outlets and impinges on a single sample in two regions thus creating two equal volumes of radiation damage in the polymer sample. A standing wave of ultrasound is simultaneously introduced in one half of the sample containing one of the two equal regions undergoing radiation damage as depicted in Figure 3.13.

As a crude but useful rule-of-thumb, the maximum deposited power should not exceed some 25 mW when irradiating polymers. Keeping this in mind, the beam current used was kept as low as 0.25 nA to avoid excessive heating of the target. A 100 Hz beam current signal was on each of the implanted volumes. A ventilator is employed to cool the sample uniformly throughout the irradiation. Temperature measurements of the sample during ion irradiation show nearly no change.

The polymers used in this work are Polycarbonate, Polymethylmethacrylate and Polyvinyl chloride, properties of which can be found in Section 3.1.1. The total ion charges deposited in the samples range between 200 nC to 6700 nC. The range of the ions in the polymers was obtained using SRIM 2006. Figure 3.12 shows the simulation of ion trajectories in a Polycarbonate sample.
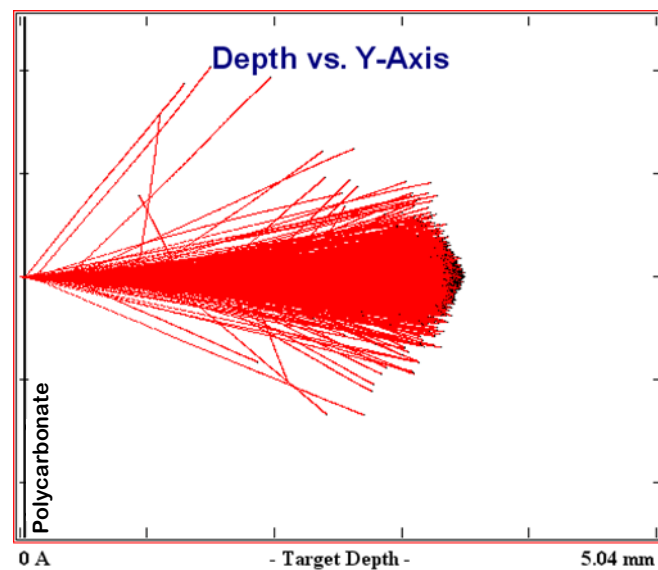
Figure 3.12: SRIM-simulation of the trajectories of deuterons with energy of 26 MeV/nucleon in a Polycarbonate sample
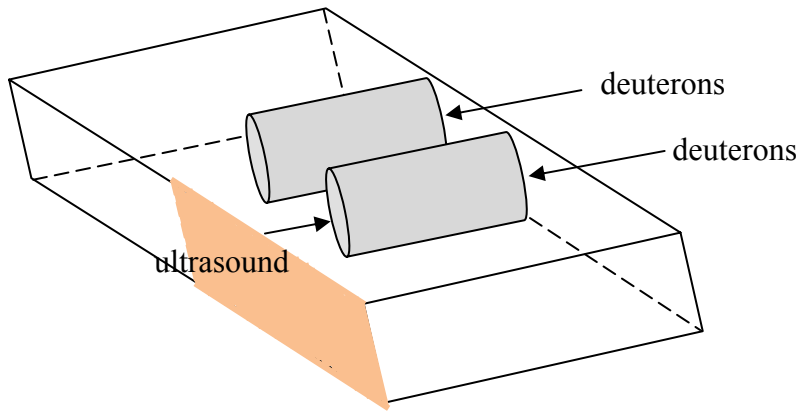
Figure 3.13: A schematic representation of the sample during ion implantation (not to scale).

3.4.2 Introduction of Ultrasound

The piezoelectric transducers used have a frequency in the range between 4 and 5 MHz and have a thickness equal to half the wavelength of the ultrasound frequency, ensuring that most of the energy is emitted at the fundamental frequency. The ultrasound was introduced into the samples simultaneously during ion irradiation (as shown in Figure 3.13).

The electronics set up for introduction of pulsed ultrasound in the sample is shown in Figure 3.12.
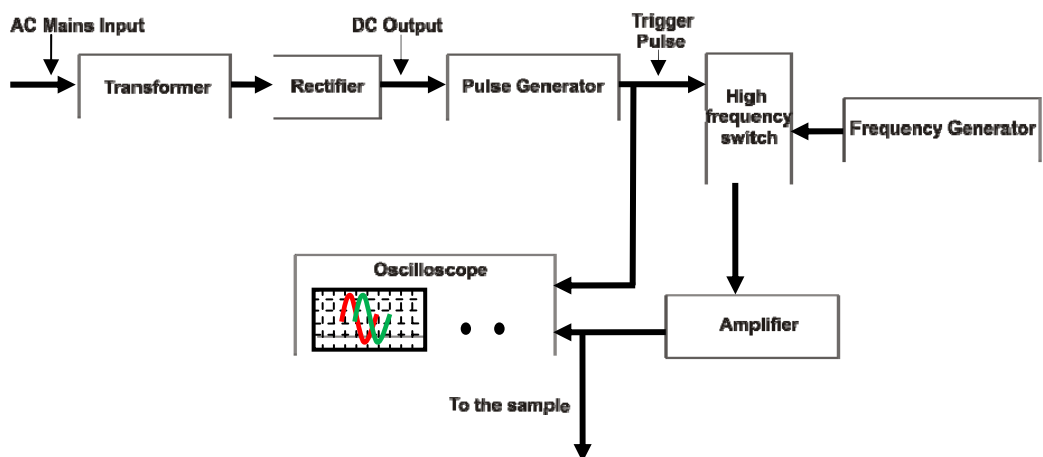
Figure 3.1 The electronics set up for the introduction of pulsed ultrasound in the sample

The resonance frequencies of the sample fixed with ultrasound transducer (resonator) are obtained using an impedance analyser. A standing wave is created at frequencies in which an integer multiple of half the wavelength is contained inside the sample. At the chosen resonance frequency of the sample system, a periodic variation of sound pressure builds up in the sample (Figure 3.13).
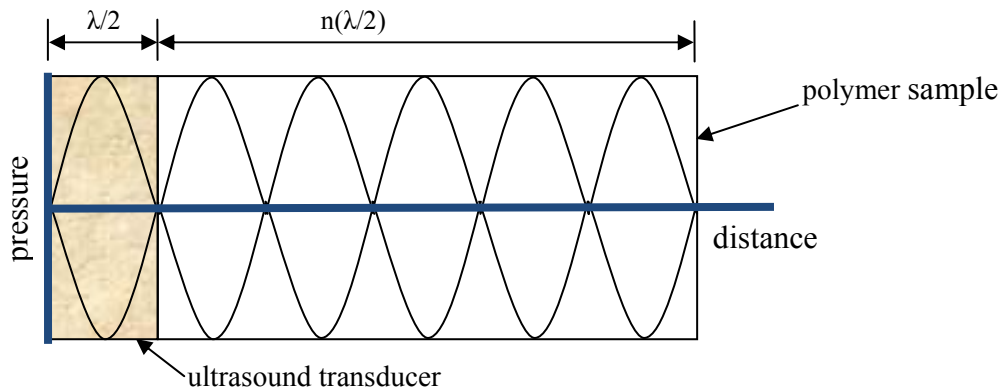
Figure 3.2 Simplified representation of the variation of sound pressure inside a polymer sample fixed with an ultrasound transducer.

Pressure variations cause particles of the medium to vibrate due to increase and decrease of density. Thus the introduction of a standing wave of ultrasound creates a stationary vibration pattern consisting of nodes – points where the medium doesn't move, and antinodes – points where the motion is maximum, in the polymer sample. The ultrasound was pulsed with a duty cycle of 0.03 or 3%. The power of ultrasound was maintained at a sub-threshold value with respect to each of the polymers used.

3.4.3 Synchronsation of ultrasound with the deuteron beam

The signal from the neutron detector and the signal from the plastic scintillator, due to the deuteron beam, are viewed in an oscilloscope simultaneously. The signal from the plastic scintillator signifies the deuteron beam from a single beam outlet and is precise compared to the signal from the neutron detector which signifies the deuteron beam from both the beam outlets. But the plastic scintillator cannot be continuously used for more than two hours as it would get damaged. Also it needs to be placed very close to the ion beam outlet which will hinder the placement of the sample. So we mark the position of the signal from the plastic scintillator in comparison to the position of the signal from the neutron detector in

the oscilloscope monitor. Now the sample is brought to position in front of the beam outlet.

A standing wave is created in the sample which is verified as described in Section 3.3.9. The trigger used to pulse the ultrasound is viewed in the oscilloscope and synchronised with the position of the signal from the plastic scintillator in the signal from the neutron detector. This synchronisation leads to the introduction of the standing wave of ultrasound into the sample exactly when the deuteron beam impinges on that part of the sample.

3.5 Experimental methods

3.5.1 Interferometry

Interferometry is an elegant branch of optics which provides versatile and sensitive tools for a wide range of physical measurements. Optical interferometry is a technique of interferometry combining light from multiple sources in an optical instrument in order to make various precise measurements[13].

3.5.1.1 Theory

Ion irradiation in polymer samples causes refractive index modulation and deformation of the sample surfaces. Measuring these changes is the goal of interferometry applied here.

The phase φ of a monochromatic light wave of wavelength λ passing through a sample of thickness d and refractive index n is given by

$$\varphi = \left(\frac{2\pi}{\lambda}\right) nd$$

3.3

The phase of an incident plane wave propagating through an ion implanted sample changes spatially inhomogeneously. The contribution to the change in phase is accounted for not only by refractive index modulation in the sample but also due to surface deformation of the sample. Surface deformation majorly includes a wedge-shaped sample with non-parallel surfaces and fluctuations in sample thickness due to ion irradiation. This can be expressed as:

$$\Delta T(x, y) = \Delta W(x, y) + \Delta d(x, y)$$

where $\Delta T(x, y)$ is the total surface deformation, $\Delta W(x, y)$ is the local thickness (3.4) variation due to the sample wedge and $\Delta d(x, y)$ is the local thickness modulation by ion irradiation.

37

The phase change can now be expressed in simple terms as a total differential of two contributions:

$$\Delta\varphi(x,y) = \left(\frac{\partial\varphi}{\partial n}\right)\Delta n(x,y) + \left(\frac{\partial\varphi}{\partial T}\right)\Delta T(x,y) = \Delta\varphi_n(x,y) + \Delta\varphi_T(x,y). \quad (3.5)$$

To determine the change in phase after transmission through the sample, the two contributions mentioned are considered. Let us consider two light waves of identical wavelength λ passing through a sample at two points as shown in Figure 3.15. The two waves with phases φ_1 and φ_2 are in phase with each other before impinging on the sample.
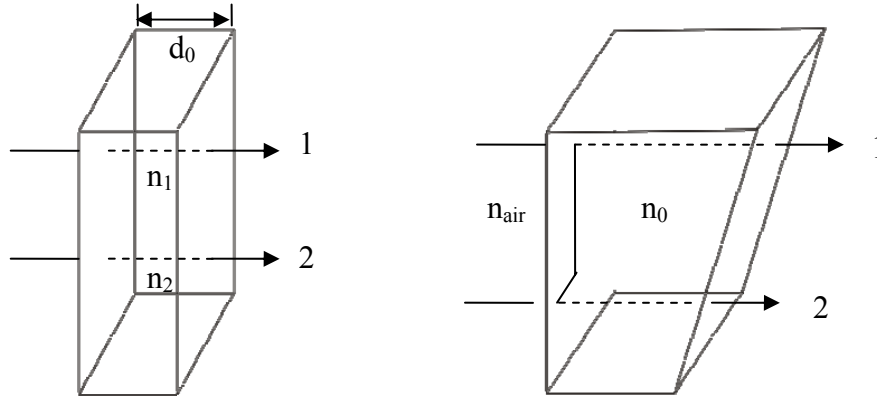
Figure 3.3 Light waves passing through a sample. Left: Thickness of sample is constant. Right: Refractive index of the sample is constant.

If only the refractive index in the sample varies and the thickness d remains constant, the change in phase is given by

$$\Delta\varphi_n(x,y) = \left(\frac{2\pi}{\lambda}\right)d_0\Delta n(x,y), \quad (3.6)$$

where Δn is the variation in the refractive index.

In the second case, the thickness of the sample varies but the refractive index n remains constant. Then the phase difference is given by

$$\Delta\varphi_T(x,y) = \left(\frac{2\pi}{\lambda}\right)(n_0 - n_{air})\Delta T(x,y). \quad (3.7)$$

In general, both cases occur and Δn and ΔT are small compared to n_0 and d_0 respectively. Hence the total phase change can be expressed as:

$$\Delta\varphi(x,y) = \left(\frac{2\pi}{\lambda}\right)[d_0\Delta n(x,y) + (n_0 - n_{air})\Delta T(x,y)]. \quad (3.8)$$

38

By rearranging, we obtain:

$$\Delta n(x,y) = \left(\frac{\lambda}{2\pi}\right)\Delta\varphi(x,y) - \frac{(n_0 - n_{air})}{d_0}\Delta T(x,y). \qquad (3.9)$$

Thus the total phase change $\Delta\varphi(x,y)$ and the total change in thickness $\Delta T(x,y)$ are measured and the change in refractive index $\Delta n(x,y)$ is calculated.

To determine the refractive index modulation $\Delta n(x,y)$ of the samples with good spatial resolution, a unique apparatus consisting of both Mach-Zehnder interferometer and Michelson interferometer in a single setup was brought into use.

3.5.1.2 Measurement setup and measurement method

Mach-Zehnder interferometer (named after physicists Ernst Mach and Ludwig Zehnder) is used to measure the total phase shift $\Delta\varphi(x,y)$ of an initially plane wave travelling through the sample. Michelson interferometer (invented by Albert Abraham Michelson), the most common configuration for optical interferometry, was used to determine the thickness modulation $\Delta T(x,y)$ in the sample. Both interferometers employ division of amplitude.

To have a single well-defined coordinate system and to avoid spatial displacement between measurements, both the interferometers were combined in one setup. The sample was placed on a rotating and tilting stage (Figure 3.4). The sample is placed such that the laser beam passes through the sample perpendicular to the direction of ion irradiation. This way, the entire diameter of the implanted volume is analysed. There are three modes of operation of the interferometer setup namely transmission mode, wedge determination mode and reflection mode.

3.5.1.2.1 Transmission Mode

The transmission mode involves the Mach-Zehnder interferometer setup (Figure 3.4) to measure the total phase shift $\Delta\varphi(x,y)$. A He-Ne laser ($\lambda_1 \approx 632.8\ nm$) is used as the source of light for the measurement. The light beam from the He-Ne laser is expanded. This expanded light beam falls on the beam splitter BS1 in the interferometer. The signal arm consists of the mirrors M3 and M4 and the sample stage S (and hence the sample) ending at BS2. The reference arm consists of the mirrors M1 and M2, the beam splitter BS2, a mirror mounted on a combined translator stage PM, which consists of a piezo translator on a motor-driven translator stage, and ends at BS2. The signal beam and the reference beam interfere and the resultant interference pattern is

focused by the lens L, reflected by the mirror M5 and captured by a CCD camera on to the chip.
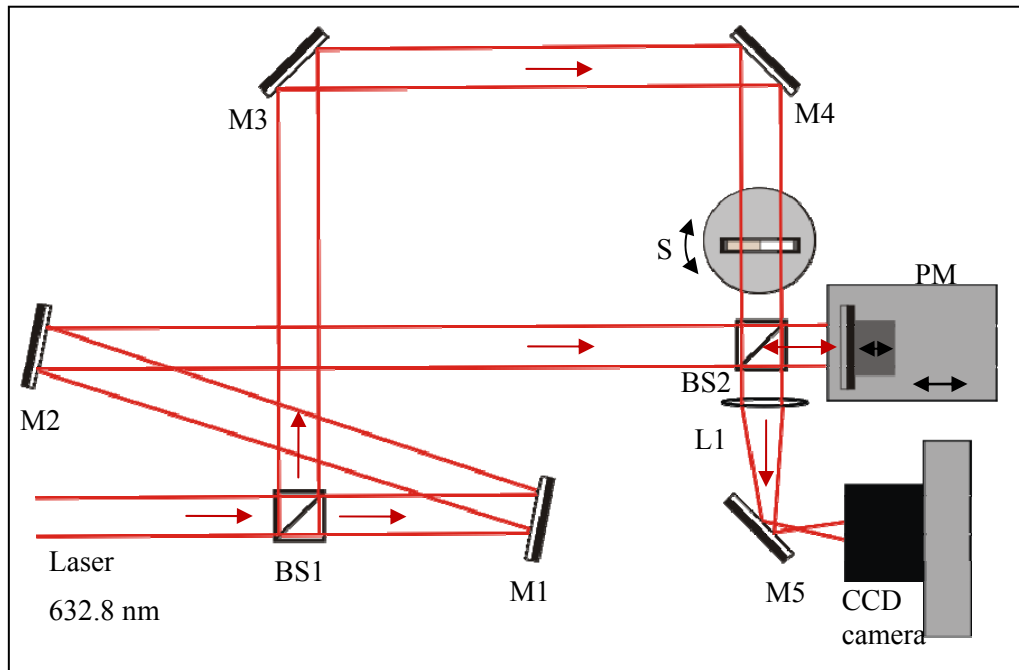
Figure 3.4: Mach-Zehnder Interferometer set up for measuring the total phase shift

3.5.1.2.2 Wedge determination mode

In the "wedge determination mode", a reference plate is placed next to the sample on the rotating stage S. The interferometric setup involving Michelson-Interferometer is represented schematically in Figure 3.5. The signal arm of the interferometer in the transmission mode is blocked here by B1. The reference arm consists of the mirror mounted on the piezo translator stage and the beam splitter BS2. The signal arm consists of the sample surface and the beam splitter BS2. The signal beam is reflected by both the sample and the reference plate surfaces.

40
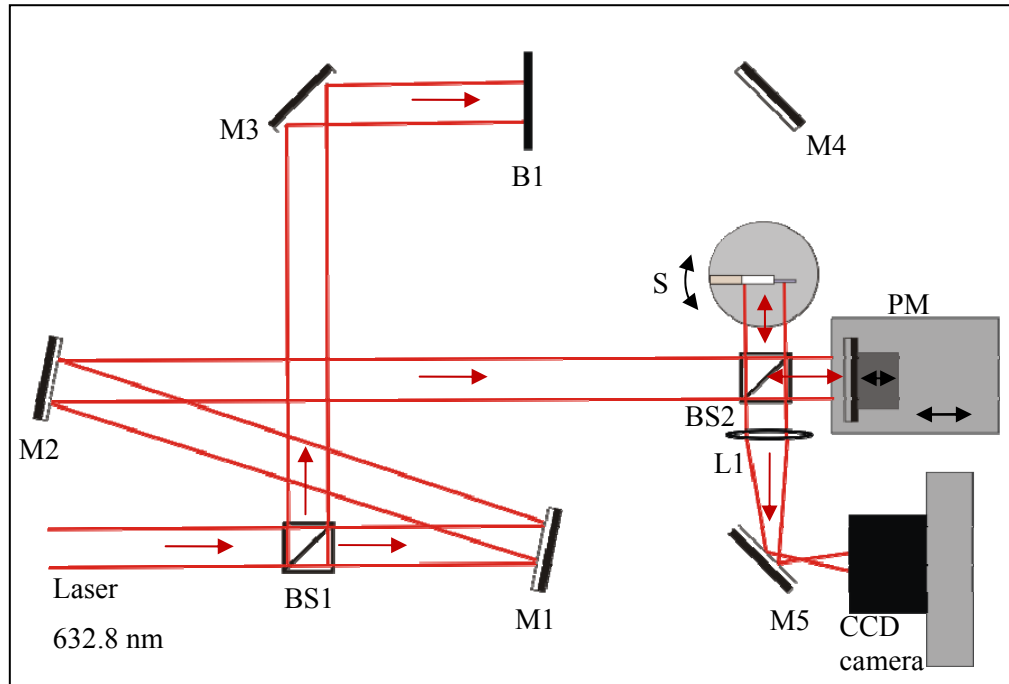
Figure 3.5: Michelson Interferometer set up for measurement of wedges in the sample

The signal arm and the reference arm together represent Michelson's interferometer. Care is taken to align the surface of the sample such that the reflected wave is parallel to the incident wave. This is achieved by making sure that the number of fringes in the interferogram observed is minimum. To determine the wedge associated with the aligned sample surface, the number of steps required to align the front surface of the reference plate is counted. The reference plate is tilted horizontally as well as vertically to achieve this. The same procedure is carried out on the rear side after a 180° turn of the sample stage S. The angular resolution is 28µrad. By this manner, complete information regarding the wedge associated with a sample can be obtained and thus $W(x, y)$ can be determined. The samples used for our experiment were found to have no wedges associated with them.

3.5.1.2.3 Reflection Mode

The reflection mode involves the setup (Figure 3.6) required to measure the surface deformation of the sample, $\Delta d(x, y)$. The apparatus setup is similar to that in the wedge determination mode except that instead of the laser light, the red light ($\lambda_2 \approx 650nm$) of a light emitting diode with a coherence length of about 15 µm is collimated by the lens L2 and used as the light beam for measurement. The sample surface and the beam splitter BS2 form the signal arm and the piezo mirror and the beam splitter BS2 form the reference arm, thereby using a Michelson interferometer setup. The short coherence length of

the LED (≈25 μm) avoids the superimposition of reflections from the rear surface of the sample. The phase difference $\Delta\varphi_1$ due to the surface deformation of the sample Δd_1 is given by

$$\Delta\varphi_1(x,y) = \frac{2\pi}{\lambda} 2\Delta d_1(x,y). \tag{3.10}$$

The factor 2 before $\Delta d_1(x,y)$ in equation 3.10 is accounted for by the light travelling from the beam splitter BS2 to the sample surface being reflected by the sample surface back to the beam splitter BS2. Since the phase change can be obtained from the interference pattern captured by the CCD camera on to the chip, the surface deformation can be obtained from the equation above. By rotating the sample stage by 180° horizontally, the surface deformation for the other surface of the sample Δd_2 can be obtained. The entire thickness modulation by surface deformation is given by:

$$\Delta d = \Delta d_1 + \Delta d_2. \tag{3.11}$$

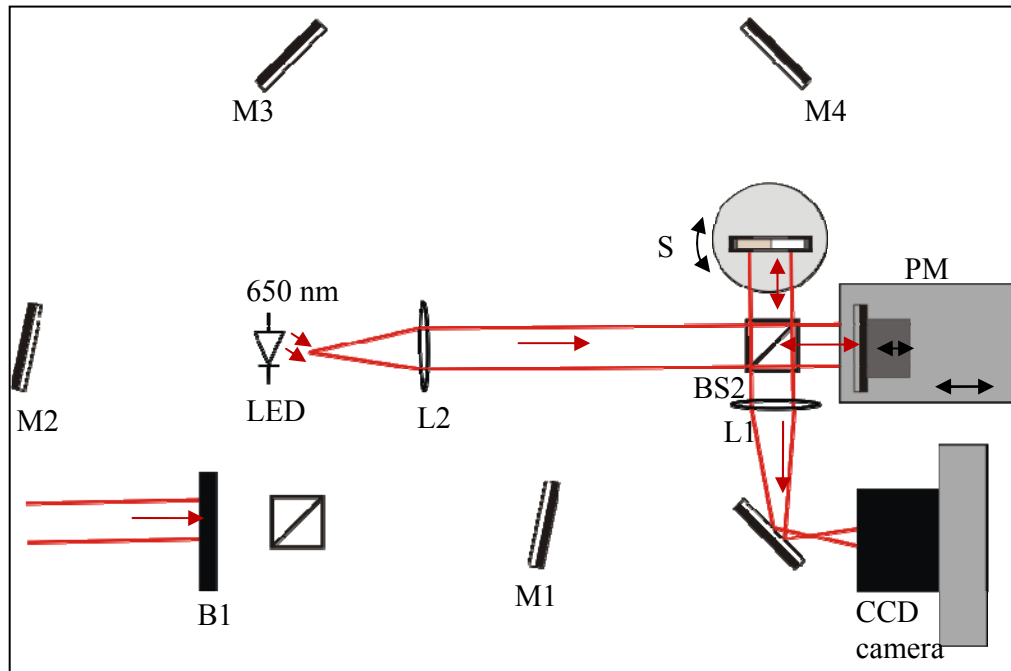Figure 3.6: Michelson Interferometer set up for measurement of surface deformation of the sample

3.5.1.3 Data Analysis

Both the "reflection mode" measurements involving Michelson interferometer setup and "transmission mode" measurement involving Mach-Zehnder interferometer setup require the calculation of the phase change from the interferograms obtained. For this purpose, the phase step method is used wherein

the interferogram phase can be shifted by a fixed amount with the mirror mounted on the combined translator stage. For each single measurement, three phase-shifted interferograms are considered. The intensity of the images are given by

$$I_1(x, y) = a(x, y) + b(x, y)\cos[\varphi(x, y) + 0],$$

$$I_2(x, y) = a(x, y) + b(x, y)\cos[\varphi(x, y) + \theta] \text{ and}$$

$$I_3(x, y) = a(x, y) + b(x, y)\cos[\varphi(x, y) + 2\theta]$$

where θ is the shift in phase. Here $a(x, y)$ is the background intensity, $b(x, y)$ is the amplitude of the interference fringes and $\varphi(x, y)$ is the phase.

A phase image $\Delta\varphi(x, y)$ can be obtained from three phase-shifted interferograms by:

$$\Delta\varphi = arctan\left(\frac{(I_3 - I_1)[\cos(\theta - 1) - (I_2 - I_1)[\cos(2\theta - 1)]}{sin\theta(I_3 - I_1) - sin2\theta(I_2 - I_1)}\right) \qquad (3.12)$$

The arc tangent in the equation above takes values only in between -π/2 and +π/2. As a result, discontinuities in the phase image show up. For correcting these discontinuities, several algorithms are available. A simple procedure usually leads to noise in the corrected images, because of jumps in phase and dirt or scratches on the sample surface. Hence removing the discontinuities from the phase images, the so-called "Unwrapping", turns out to be a demanding task [14-16] . For the computation of these tasks, the program FRAN was utilized. It was developed by T. R. Judge [17, 18]. Figure 3.19 shows a wrapped phase image and the corresponding unwrapped phase image of an ion implanted PMMA sample. To correct errors pertaining to the general alignment of the interferometer, a measurement in the transmission mode is carried out without a sample. The phase image of this "zero measurement" is subtracted from the phase image of the sample measurement.
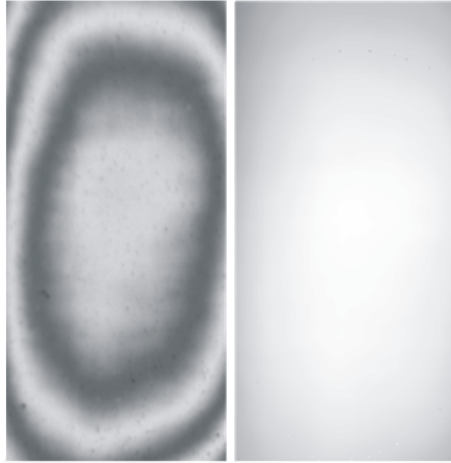
Figure 3.7: Left: Wrapped phase image of an ion implanted PMMA sample Right: Corresponding unwrapped phase image obtained from the program FRAN

The value of $\Delta n(x, y)$ is obtained with equation 3.9. The irradiation induced refractive index change $\Delta n_X(y)$ is finally given by

$$\Delta n_X(y) = \Delta n(x_2, y) - \Delta n(x_1, y)$$

(3.13)

where x_2 is in the irradiated region and x_1 is not. The index X highlights that here the radiation-induced quantity is given.

Error determination

From several measurements, a maximum error of 1×10^{-4} has been determined.

3.5.2 Optical Absorption Spectroscopy

Spectroscopy can be described as the study of the consequences of the interaction of electromagnetic radiation (light) with molecules, the most important interaction being "absorption".

3.5.2.1 Absorption spectroscopy

When atoms or molecules absorb light, the incoming energy excites a quantized structure to a higher energy level thereby increasing its energy. This increase is equal to the energy of the photon as expressed by the relation

$$E = h\nu = hc/\lambda$$

(3.14)

where h is the Planck's constant, ν and λ are the frequency and wavelength of the light respectively and c is the velocity of light. The change in energy may be in the electronic, vibrational or rotational energy of the molecule. Changes in

electronic energy involve relatively large quanta. Changes in vibrational energy involve smaller quantities of energy and changes in rotational energy involve quanta even smaller than those of vibrational energy. The electronic energy level of a molecule under normal conditions is called its ground state and the higher electronic levels represent the first and second excited states respectively. For each electronic level there are the ground and several possible excited vibrational states and similarly, for every vibrational level there are the ground and excited rotational levels (fig). The type of excitation due to energy absorption depends on the wavelength of the light. If a molecule absorbs a small amount of energy from a source of light in the far infra-red or the microwave region, only its rotational energy will change, no matter which vibrational or electronic state it is in. If the light source is of greater energy, say in the near infra-red region, then both the vibrational and rotational energies of the molecule will change. If the energy from the light source is much greater, as in the case of ultra-violet light or visible light, changes in the electronic, vibrational and rotational energies will take place[19]. This implies that electrons are promoted to higher orbitals by ultraviolet or visible light, vibrations are excited by infrared light, and rotations are excited by microwaves, predominantly.
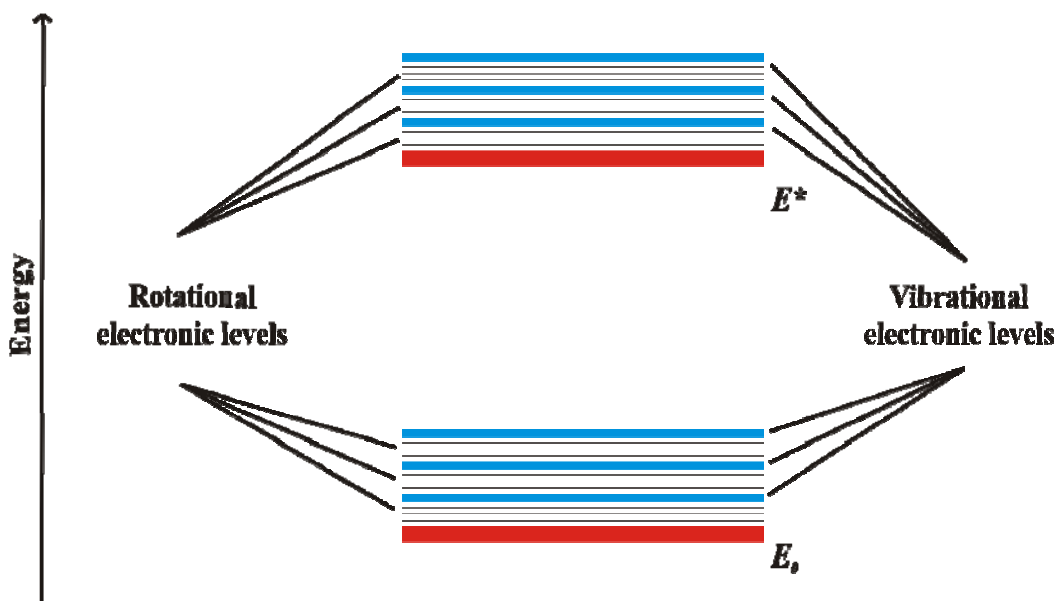

Figure 3.8: Energy levels of a polyatomic molecule [20]

Absorption spectroscopy uses the range of the electromagnetic spectra in which a substance absorbs. This includes Visible absorption spectroscopy and

Ultraviolet absorption spectroscopy which are often combined and known as UV/VIS spectroscopy.

3.5.2.2 UV-VIS absorption spectroscopy

Spectrophotometry, particularly in the VIS and UV portions of the electromagnetic spectrum (200 - 800 nm), is one of the most versatile and widely used techniques for qualitative and quantitative analysis of materials in chemistry and the life sciences.

Changes of optical properties of polymers caused by ion irradiation reflect the changes in the polymer structure. UV-Vis spectroscopy is employed for the characterization of degradation processes in irradiated polymers. In this study the changes in optical spectra can – at least qualitatively – be interpreted in terms of the disappearance of existing chemical groups and structures, and the appearance of new ones, resulting from the recombination of transient degradation products.

3.5.2.2.1 Theory

Molecular absorption spectroscopy is concerned with the measured absorption of radiation in its passage through a sample.

The visible region of the electromagnetic spectrum comprises photon energies of 36 to 72 kcal/mole, and the near ultraviolet region, up to 200 nm, extends this energy range to 143 kcal/mole. These energies are sufficient to cause electronic transitions within a molecule, promoting bonding and non-bonding electrons to higher, less stable antibonding orbitals. The molecule then loses this excess energy by rotational and vibrational relaxation. Consequently, absorption spectroscopy carried out in this region is sometimes called "electronic spectroscopy".

The energies associated with electronic transitions are sufficient for the dissociation of many molecules and hence these transitions are accompanied by changes in the electronic distributions of molecules. The degree of absorption of light by molecules is a function of the wavelength of the light. This wavelength-dependent capacity for absorbing photons depends on the energy spacing of the electronic levels of the molecule. Thus the **absorption characteristics in the UV-VIS region** of the electromagnetic spectrum can yield a considerable amount of information regarding the **electronic structure**.

Three types of electronic transition are considered:

1. Transitions involving π, σ and n electrons

2. Transitions involving charge-transfer electrons

3. Transitions involving *d* and *f* electrons

When sample molecules are exposed to light having an energy that matches a possible electronic transition within the molecule, some of the photons will be absorbed as the electron is promoted to a higher energy orbital.
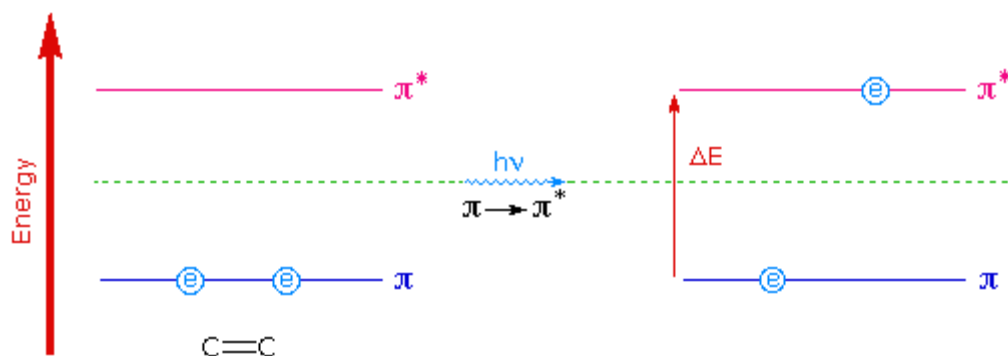
Figure 3.9: The diagram illustrates an electronic transition between the highest energy bonding π-orbital to the lowest energy antibonding π-orbital. The energy (ΔE) is required to effect the electron promotion [21].

The energy and wavelength of absorption is defined by the difference between energy levels of an electronic transition. This can be expressed as $\lambda = hc/\Delta E$, where $\Delta E = E_2 - E_1$, E_1 is the energy level of the molecule before absorption and E_2 is an energy level reached by absorption.
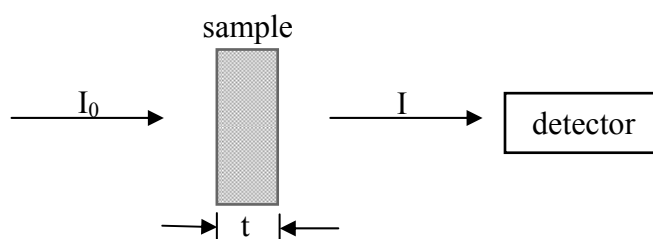
Figure 3.10: Light of intensity I_0 incident upon a sample of thickness t undergoes a loss of intensity upon passing through the sample. The intensity measured after passing through the sample of thickness t is I.

Optical absorption can be represented in units of absorbance or optical density, which is a dimensionless quantity defined as the negative of the base-10 logarithm of the transmission:

$$A = -log_{10}T \qquad\qquad 3.15$$

where the transmission, $T = (I_0/I)$, I_0 is the intensity of the incident light beam, and I is the intensity of the transmitted light beam.

3.5.2.2.2 Absorption in polymers

Absorption of ultraviolet and visible radiation in organic molecules is restricted to certain functional groups that contain valence electrons of low excitation energy. Such light absorbing groups are referred to as **chromophores**, i.e. "carriers of color" and appear coloured to the human eye. Organic chromophores which absorb strongly in the UV or visible portions of the electromagnetic spectrum nearly always involve multiple bonds such as C=C, C=O or C=N. The spectrum of a molecule containing these chromophores is complex. This is because the superposition of rotational and vibrational transitions on the electronic transitions gives a combination of overlapping lines. This appears as a continuous absorption band.

The various kinds of electronic excitations that may occur in organic molecules is shown in Figure 3.22. Of the six transitions outlined, only the two involving lowest energies (left-most, blue colored) can be achieved by the energies available in the 200 to 800 nm spectrum. These transitions need an unsaturated group in the molecule to provide the π electrons. As a rule, energetically favoured electron promotion will be from the highest occupied molecular orbital (HOMO) to the lowest unoccupied molecular orbital (LUMO), and the resulting species is called an excited state.
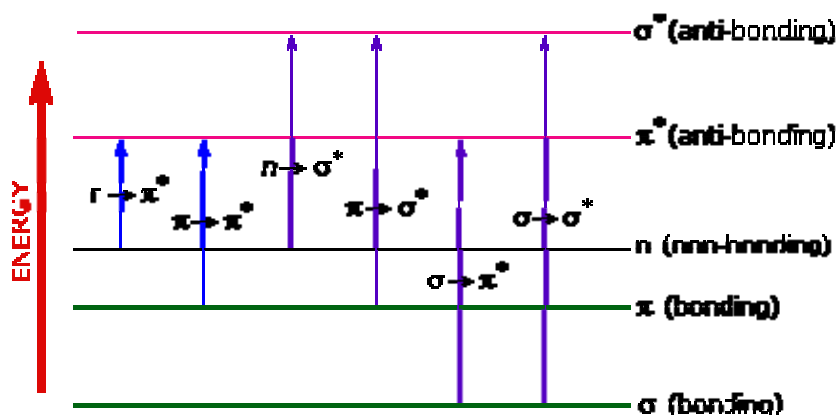

Figure 3.11 The six possible electronic transitions occurring in organic molecules [21]

48

Molecular excitation energy is dissipated as heat (kinetic energy) by the collision of the excited molecule with another molecule, as the molecule returns to the ground state. In turn, the intensity of the light transmitted by a collection of chromophores is less than the intensity of the incident light.

Ion irradiation leads to coloration of polymers. Most polymers show no specific absorption in the visible region of the spectrum and are therefore colourless in principle. Coloration of polymers upon ion irradiation leads to optical absorption in the ultraviolet and visible region of the spectrum.

3.5.2.2.3 Spectrophotometer

In principle, the role of a spectrophotometer is to determine the extent to which light of different wavelengths is absorbed by a sample. A spectrophotometer records the wavelengths at which absorption occurs, together with the degree of absorption at each wavelength and the resulting spectrum is presented as a graph of absorbance (A) versus wavelength. Instruments of this type require very stable light sources and detectors, and need to be relatively insensitive to background fluctuations. This is generally only feasible in the UV, VIS, and perhaps near-IR regions.

Cary 500 (Figure 3.24) is a high performance laboratory spectrophotometer functioning in the range from UV to NIR. This UV-VIS-NIR spectrophotometer was used to obtain absorption spectra of the samples in the wavelength range 175nm – 3300nm. It has a dual-beam design where the beam coming from the monochromator is split into two; one acts as a reference beam giving a continuous measure of the intensity of the incident light (I_0) whereas the other passes through the sample for the measurement of transmitted light (I_t). A mechanical chopper wheel carrying a mirror is employed to send the beam alternately along the two paths enabling sequential measurement of the incident light and the light transmitted by the sample. This compensates for any time dependent variations in the intensity of the light emitted by the source, thus improving sensitivity and reducing uncertainty.

The instrument uses a common light source, monochromators, and detector for both beams. The light source is usually a hydrogen or deuterium lamp for UV measurements and a tungsten lamp for visible measurements. The wavelengths of these continuous light sources are selected with a wavelength separator such as a prism or grating monochromator. Spectra are obtained by scanning the wavelength separator and quantitative measurements can be made from a spectrum or at a single wavelength. It incorporates a PbS detector which is thermoelectrically cooled to 0 °C to reduce photometric noise. A large sample

compartment and a removable floor plate provide maximum flexibility and easy access to the compartment when mounting samples. Most spectrometers, after measuring the transmittance T, use internal circuitry or operating software to obtain the absorbance.

The lamp turret has provision for a third lamp of your choice. The turret can be completely removed if you wish to install another light source

The slits can be fixed in the NIR as well as the UV-Vis

The out-of-plane design of the double Littrow monochromator reduces photometric noise and stray light, and produces excellent resolution

A 'floating' solid aluminium casting isolates the optics from external disturbances

The Cary 400/500 wavelength drive can change wavelengths at 16 000 nm/min in the UV-Vis and at 64 000 nm/min in the NIR

The monochromator and sample compartments have separate nitrogen purging plumbing

Schwarzchild coupling optics ensure a high level of light throughput. This produces more accurate measurements at low transmission levels

The sample compartment windows are tilted to prevent back-reflection and thus incorrect results

The PbS detector is thermoelectrically cooled to 0 °C to reduce photometric noise

A big sample compartment, with a removable floor plate, gives you maximum flexibility when mounting samples

The optics are silica overcoated, so that they can be cleaned without damage to the reflective surface

Electronics are also a very important design consideration. The extended dynamic range of the Cary instruments is a result of this. The Cary 400 and 500 instruments for example, are specified to measure up to 7 Abs with reference beam attenuation
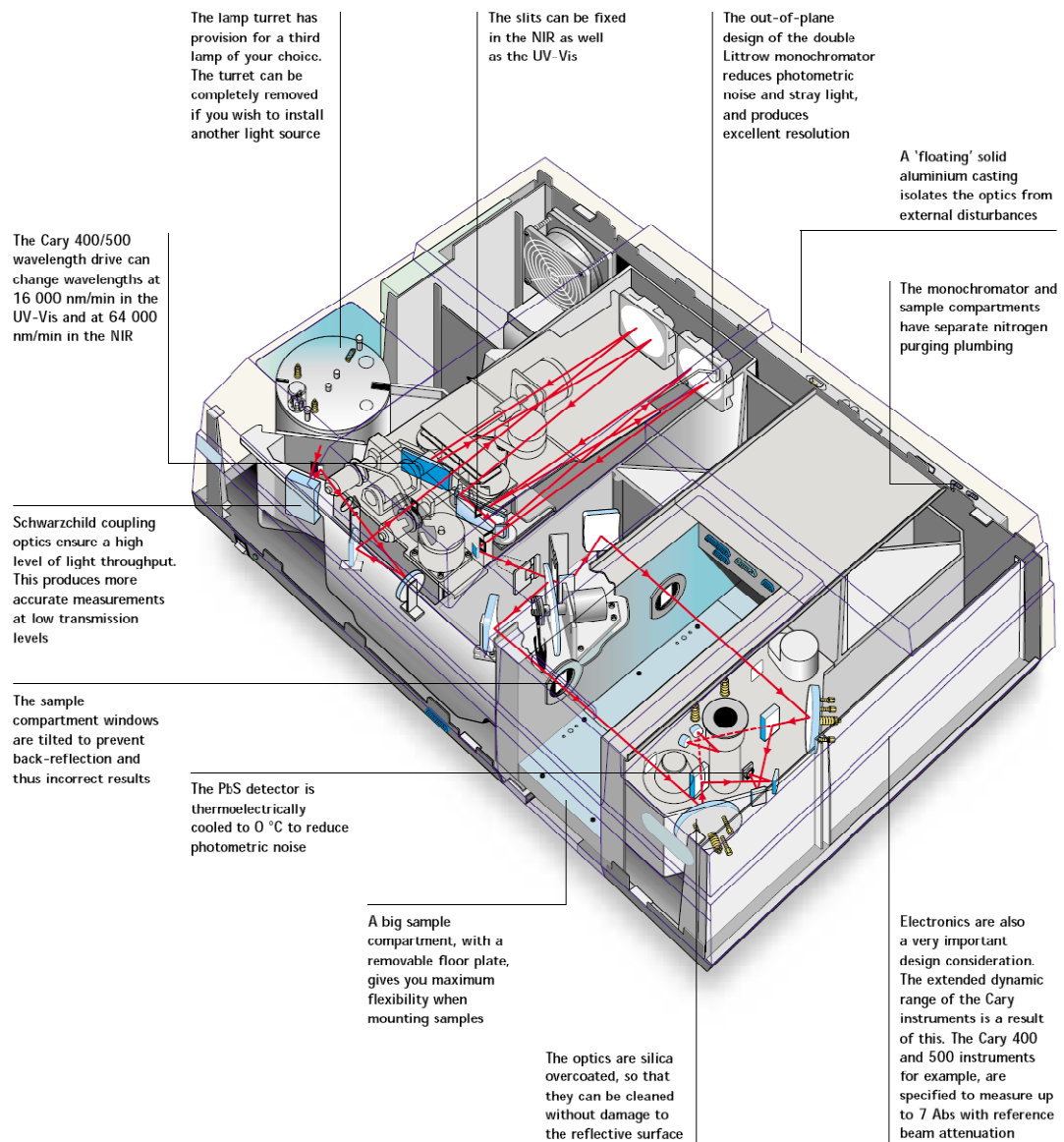
Figure 3.12: CARY 500 UV-VIS-NIR spectrophotometer [22]

3.5.2.2.4 Detector signal and absorption spectrum:

The detector registers the intensity of the transmitted light as a function of wavelength and compares it to the intensity of the reference beam at the same wavelength. Data sets are available in the computer as light intensity variation (proportional to detector signal) with wavelength.

At every wavelength, the following relationship holds:

$$[\log(V_0) - \log(V)] = (\log[I_0] - \log[I]) = log(I_0/I) = A(\lambda) \quad (3.16)$$

where $V = kI$; the proportionality constant k is set in the instrument construction,

V_0 is the detector signal measured from the reference beam,

V is the detector signal measured from the sample beam,

I_0 and I are the corresponding light intensities, and

A is the absorbance or the optical density which is provided as a function of wavelength in the outputted data set.

3.5.2.2.5 Presentation and analysis of absorption spectra:

An absorption spectrum is obtained by the spectroscopic analysis of the light transmitted by an absorbing medium which is placed between the light source and the spectroscope. An absorption spectrum gives the absorption of light as a function of wavelength.

The absorption intensity of an electronic transition at any wavelength is governed by the probability of the transition and the size of the absorbing molecule. The absorption maximum of a band therefore corresponds to the most probable transition in that region of absorption. The spectrum of an atom or molecule depends on its energy level structure, and absorption spectra are useful for identifying of compounds.

3.5.2.2.6 Measurement method

A 150µm wide slit was used to scan the sample for absorption measurements (Figure 3.25). An identical slit is placed in the reference beam path. A 100% transmission measurement is carried out with no sample in the sample compartment. Now, the sample slit is completely blocked and a 0% transmission measurement is carried out. These no-sample transmission measurements may need to be run only once a day acting as a reference for the

51

rest of the day. The light beam passing through the slit is incident on the sample surface perpendicular to the direction of ion irradiation. Hence, the light beam passes through the entire diameter of the implanted region. The absorption spectrum is collected at various depths of the implanted region along the direction of incidence of the ion beam in steps of 125 µm. Thus the entire width of the sample is scanned by the slit. Spectrum for an unirradiated sample is also obtained following the ion-implanted sample. The error involved in the measurements is upto 5%.
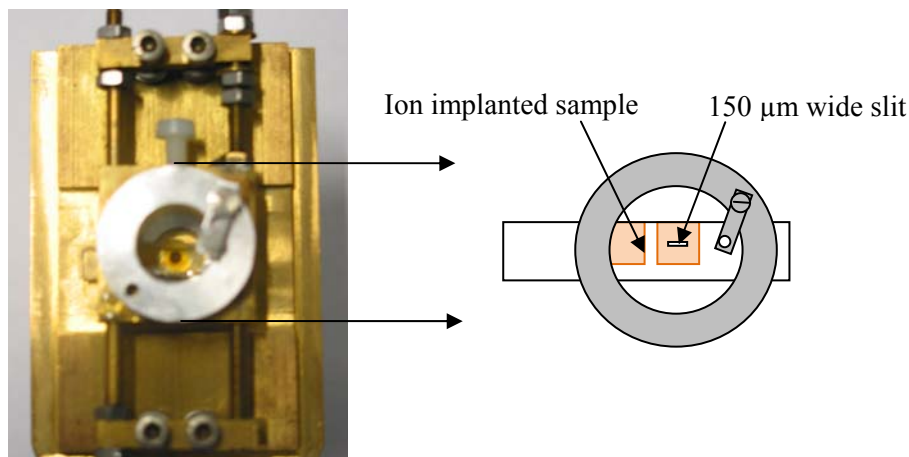

Figure 3.13: Sample holder with a sample mounted for optical absorption measurements. The 150 µm slit scans through the sample along the direction of irradiation in steps of 125 µm.

3.5.2.2.7 Background subtraction

Background subtraction is a term typically used in spectroscopy when one explains the process of acquiring a background radiation level (or ambient radiation level) and then makes an algorithmic adjustment to the data to obtain qualitative information about any deviations from the background, even when they are an order of magnitude less decipherable than the background itself. Background subtraction can affect a number of statistical calculations (Continuum, Compton) leading to improved overall system performance.

The measurement involved in obtaining the absorption spectra does not take into consideration the amount of light that might be scattered in the sample, the emission properties of the sample, nor the reflection losses at the surfaces of the sample. However, this problem can be compensated to an extent by using an absorption spectrum obtained from an non-irradiated sample as a

"background" correction to the spectra obtained from the actual sample of interest i.e. the ion implanted sample.

3.5.3 Optical Microscopy

Optical or **light microscopy** involves passing visible light transmitted through or reflected from the sample through a single or multiple lenses to allow a magnified view of the sample. The resulting image can be detected directly by the eye, imaged on a photographic plate or captured digitally. The single lens with its attachments, or the system of lenses and imaging equipment, along with the appropriate lighting equipment, sample stage and support, makes up the basic light microscope. The light microscope, so called because it employs visible light to detect small objects, is probably the most well-known and well-used research tool in many fields of science as a range of features are available in light microscopes.

Ion irradiation of polymers leads to colouration of polymers. Optical microscopic examinations are the traditional tool to examine changes in optical properties such as colour and absorption.

3.5.3.1 Bright field microscopy

Bright field illumination has been one of the most widely used observation modes in optical microscopy for the past 300 years. Bright field microscopy is the simplest of all optical or light microscopy illumination techniques. The technique is best suited for utilization with fixed, stained specimens or other kinds of samples that naturally absorb significant amounts of visible light. Sample illumination is via transmitted white light, i.e. illuminated from below and observed from above. Images produced with bright field illumination appear dark and/or highly coloured against a bright, often light gray or white, background. Bright field microscopy is used when there is enough contrast in the subject matter. The most common use of this technique involves the use of a sample mounted to a glass microscope slide.

Microscopes, from stereomicroscope to light microscope, allow polymer specimens to be examined in many ways and for many purposes. Examination of the polymer samples under bright field illumination proves to be the best technique to obtain maximum information of interest.

3.5.3.2 Light Microscope

Light from an incandescent source is aimed toward a lens beneath the stage called the condenser, through the specimen, through an objective lens, and to the eye through a second magnifying lens, the ocular or eyepiece. The condenser is

used to focus light on the specimen through an opening in the stage. After passing through the specimen, the light is displayed to the eye with an apparent field that is much larger than the area illuminated. The magnification of the image is simply the objective lens magnification times the ocular magnification. The magnification in our case is 50.

The light source has a wide dynamic range, to provide high intensity illumination at high magnifications, and lower intensities so as to view comfortably at low magnifications. Also the light intensity can be controlled. The illumination of the sample is adjusted so as to remain in the dynamic range of the sample and not in the saturated region. This is taken care of by making sure that the difference in colour in the sample region under view is not dramatic. When the difference in intensity between different regions is very large, it is not possible to know if the intensity of a pixel at a bright spot has reached saturation or not.

The digital image is captured with a Canon camera coupled to the microscope. The intensity of the light transmitted and in turn the absorbance of the ion implanted polymer samples is obtained from the captured images. Using the software Originlab7.5, the images are imported and are converted to Grayscale images (Figure 3.26). Vertical and horizontal scans through these intensity distribution images gives us a measure of the transmitted light intensity and hence absorbance of the samples.
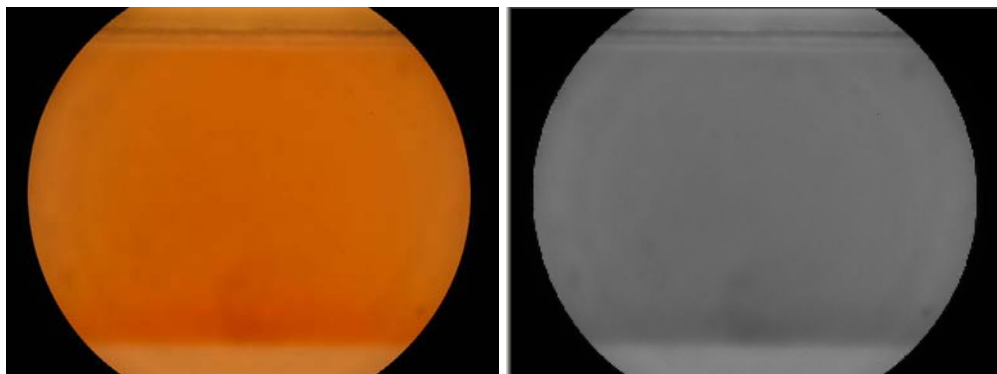

Figure 3.14: Left: The image of the sample obtained from the microscope. Right: The image after being converted to grayscale.

For lower magnification requirements, we take images of the samples using a stereo microscope.

3.5.4 Positron Annihilation Spectroscopy

Positron annihilation microscopy is a sensitive detection method for defects in materials like open volume defects in polymers.

3.5.4.1 Theory

Energetic positrons injected into solids thermalise and finally annihilate with an electron, yielding characteristic 511 keV γ-rays. The time between injection and annihilation characterizes the material and its structure. In polymeric materials, the positron either annihilates right away with an electron or links to an electron in a cavity and forms positronium (Ps), i.e. the quasi-stable neutral bound state of an electron and a positron. The typical free positron annihilation lifetime is about 100 - 500 ns. The Ps annihilation lifetime is correlated with the cavity size (i.e. with the free volume in a polymer). Positronium can exist in the two spin states, S = 0, 1. The singlet state (S = 0), in which the electron and positron spins are antiparallel, is termed para-positronium (p-Ps), whereas the triplet state (S = 1), in which the electron and positron spins are parallel, is termed ortho-positronium (o-Ps). Because of the two possible spin orientations of the two particles, the Ps exists in an ortho- and a para- form corresponding to the parallel or antiparallel orientation of electron and positron spins, with an abundance ratio of 3:1 due to spin statistics. These two positronium forms annihilate in quite different ways. The p-Ps annihilates with emission of two 511 keV photons with the mean lifetime of about 125 ps (in vacuum). The o-Ps lives in vacuum for 142 ns and decays via emission of three photons. In matter, however, the o-Ps positron lifetime is reduced to 10^3 - 10^4 ps due to interaction with surrounding electrons by the so-called pick-off process. In a 3γ-decay, the total energy $2m_0c^2$ is distributed between three photons resulting in photons with energies less than 511 keV. The formation and annihilation of positronium varies from one substance to another, being sensitive to the presence of chemically active agents such as free radicals, and to the size of the free volume. An increase in free volume can lead to an increase in o-Ps formation and hence an increase in 3γ-decay of o-Ps. This results in an increase in photons having energy less than 511 keV. A shallow increase in the signal between the Compton edge (due to Compton scattering of 511 keV photons) and the 511 keV photopeak occurs and the counts in the 511 keV photopeak (2γ-decay of p-Ps) decreases. The region between the Compton edge and the 511 keV photopeak (valley) is used in the analysis of the 3γ-decay of o-Ps and the region consisting of the whole 511 keV photopeak is used in the analysis of 2γ-decay of p-Ps. Although the pick-off

process is more probable than the 3γ-decay of o-Ps, the ratio between 3γ and 2γ-decay gives a measure of the open volume in the material.

In the positron annihilation process, the momentum of the electron-positron pair is conserved in the annihilation radiation. The momentum component in the gamma-ray propagation direction leads to a small Doppler shift of the annihilation energy. Statistically, the Doppler shift will give a different peak shape to the annihilation spectrum that reveals the distribution of the electron-momenta at the annihilation site. The shape of the annihilation peak is quantified by the S-parameter, which is given by the ratio of the counts in the central part of the annihilation peak at 511 keV to the total counts in the peak (Figure 3.25). The S-parameter is in fact a parameterization of the annihilation peak shape that is influenced by the environment in which the positron annihilates (positron delocalized, trapped at defects or surfaces, etc)[23].
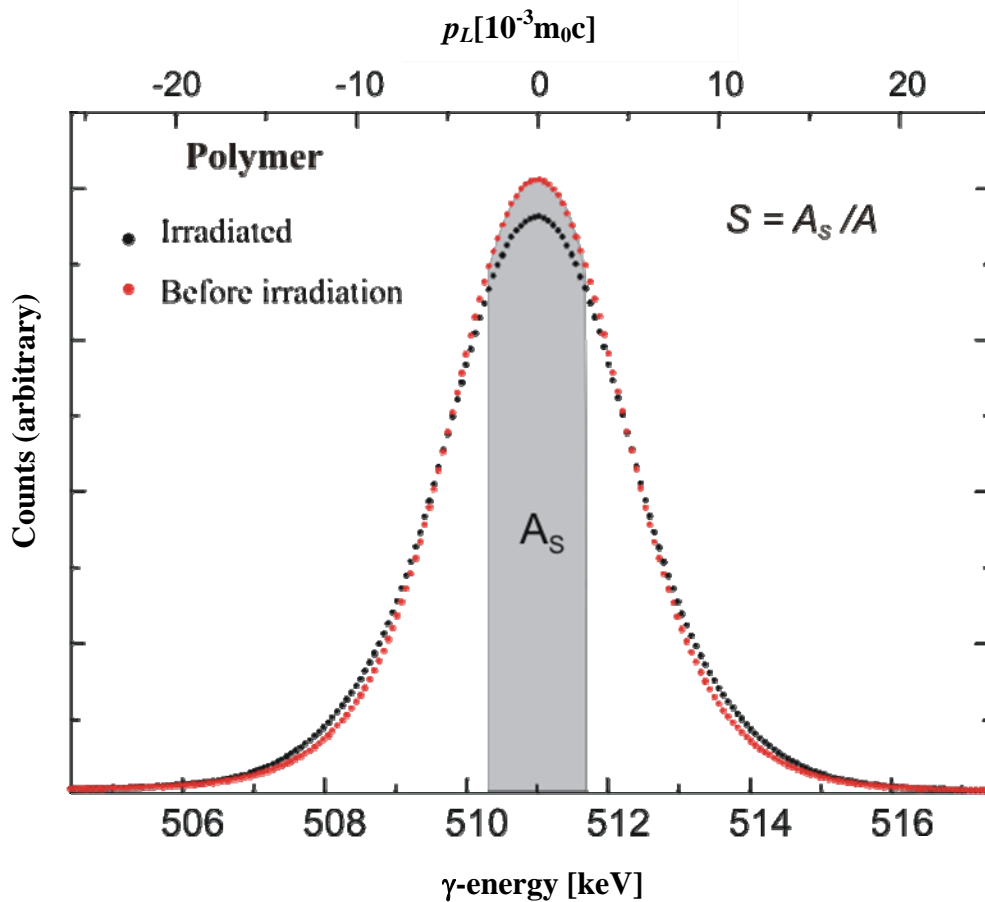

Figure 3.15: The definition of S-parameter [2]

56

3.5.4.2 The Bonn Positron Microprobe

A monoenergetic positron beam has been integrated in the electron optical system of a scanning electron microscope with the help of a magnetic prism. This permits positron-annihilation measurements with a spatial resolution in the micron range.

The monoenergetic positrons are generated by a combined source-moderator setup consisting of a 12 mCi ^{22}Na source 0.5mm in diameter. The spatial resolution limit is about 5 μm. A motorized x-y table is used to position the sample[2][2, 24].
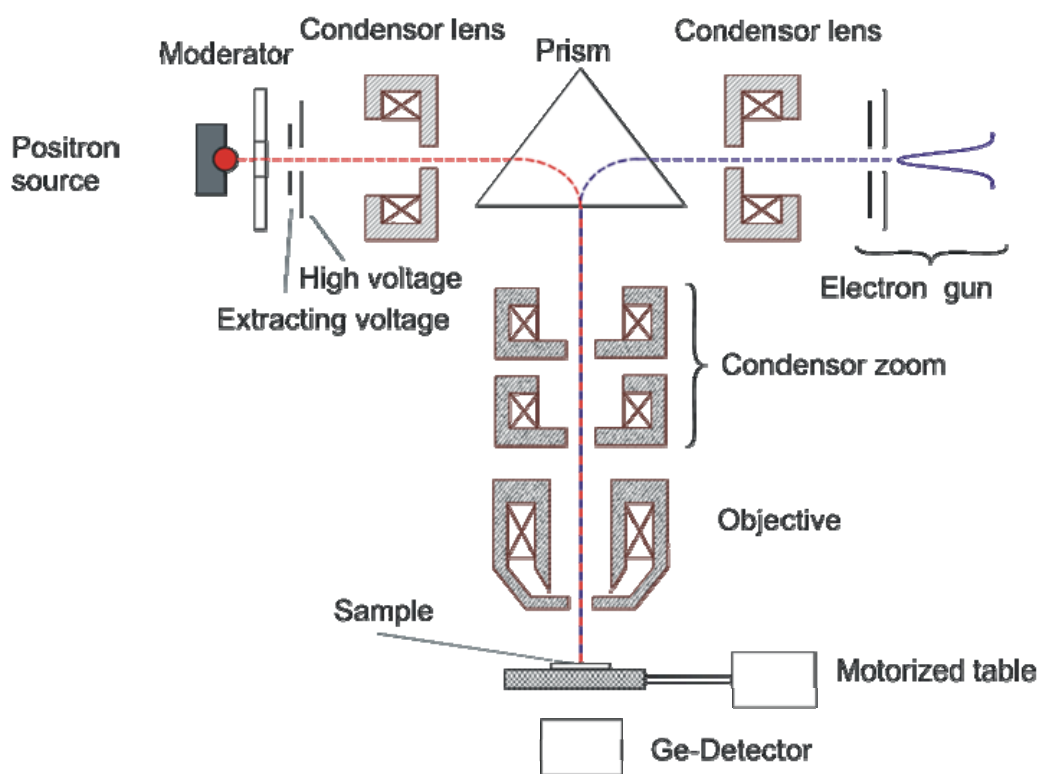
Figure 3.16: The Bonn positron microprobe consists of a finely focussed positron beam combined with a Scanning Electron Microscope (SEM).

3.5.4.3 Measurement and analysis

The ion implanted specimen is polished using SiC paper. Enough material is removed so that the surface of the specimen consists of the implanted region. At the Bonn positron microprobe, the specimen is first imaged using the instrument

---

[2] For more information on The Bonn Positron Microprobe, refer [19].

in the electron mode (as a conventional SEM) and the region of interest is selected for local positron annihilation studies. Care is taken to focus the electron beam only on the aluminium holder and not on the polymer samples. The electron beam, if focussed on the sample, will lead to charging of the material and hence the position given by the deflection coils will turn out to be wrong. The electron beam will also cause damage to the polymer samples. The adjustment of all lens currents will be preserved after going over into the positron-annihilation mode. The scanning coils and the electron gun are switched off. The 511 keV annihilation quanta are registered by a Ge detector attached to the specimen chamber below the specimen site. The motorized x-y positioning table permits an automatic operation of the system in the positron mode.

The data obtained are analysed using M-Spec to obtain the S parameter. The M-Spec program allows us to define borders of the peak width in the annihilation spectra to be used for calculation of the S parameter. Also the program reduces the background to a great extent. The ratio between 3γ and 2γ-decay was also obtained using M-Spec program[25, 26].

4 Polycarbonate

4.1 Results

4.1.1 Interferometric measurements

The distribution of the change in refractive index in a polycarbonate sample irradiated with 4000 nC is presented in Figure 4.1. The deuteron energy was 26 MeV and the peak to peak amplitude of ultrasonic waves was maintained at 30V.
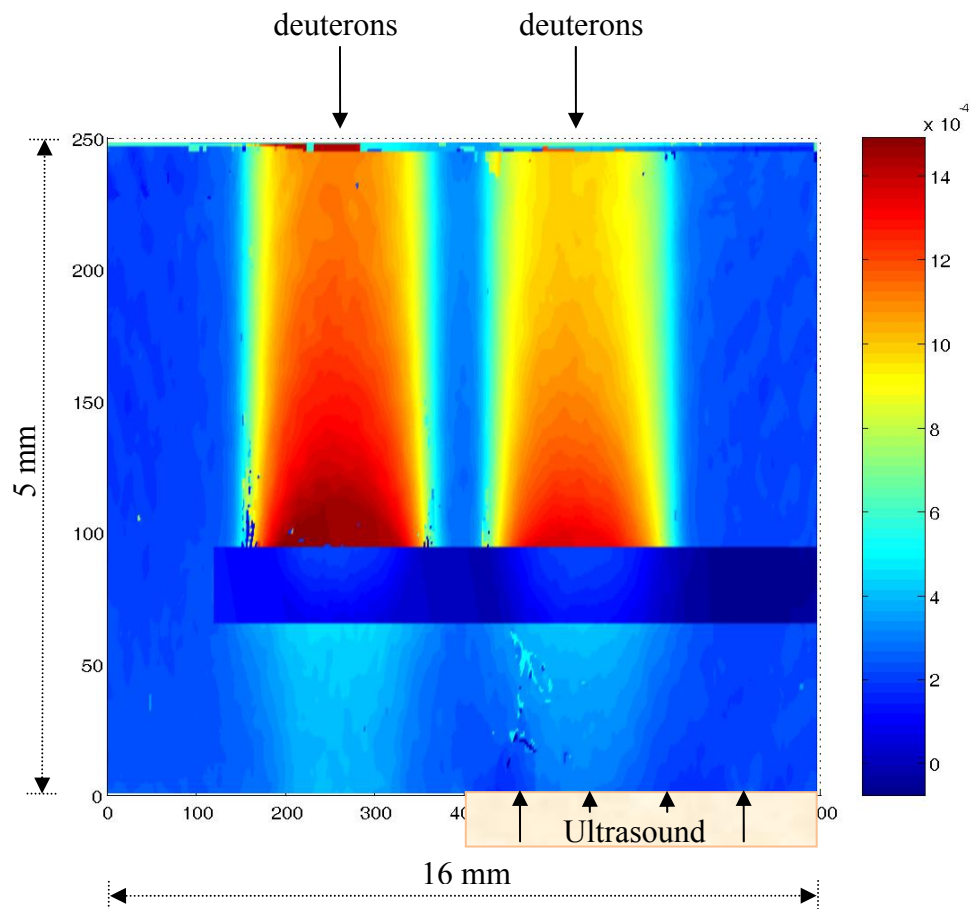
Figure 4.1 The distribution of refractive index modulation in an irradiated PC sample. The projection of the modulation (radiation damage in the sample volume) on the surface perpendicular to the direction of irradiation is seen. The two regions of radiation damage are distinctly seen. The colour scale gives a measure of the change in refractive index with reference to a pristine sample. The $V_{peak-peak}$ of ultrasonic waves was maintained at 30 V throughout the irradiation time. The ion charge deposited is 4000 nC.

59

The difference in refractive index modulation in the irradiated region and the region subjected to ultrasound during irradiation is distinctly seen (in Figure 4.1). A decrease in the refractive index modulation with the introduction of ultrasonic waves is observed and is clearly indicated (in Figure 4.2) by a horizontal scan (very close to the stopping range of the deuterons) through the refractive index modulation distribution in Figure 4.1. The refractive index modulation between the non-irradiated region, irradiated region and the region subjected to irradiation and ultrasound simultaneously is observed. An increase in refractive index modulation is observed due to ion irradiation. A decrease in refractive index modulation is observed with the introduction of ultrasound during irradiation.
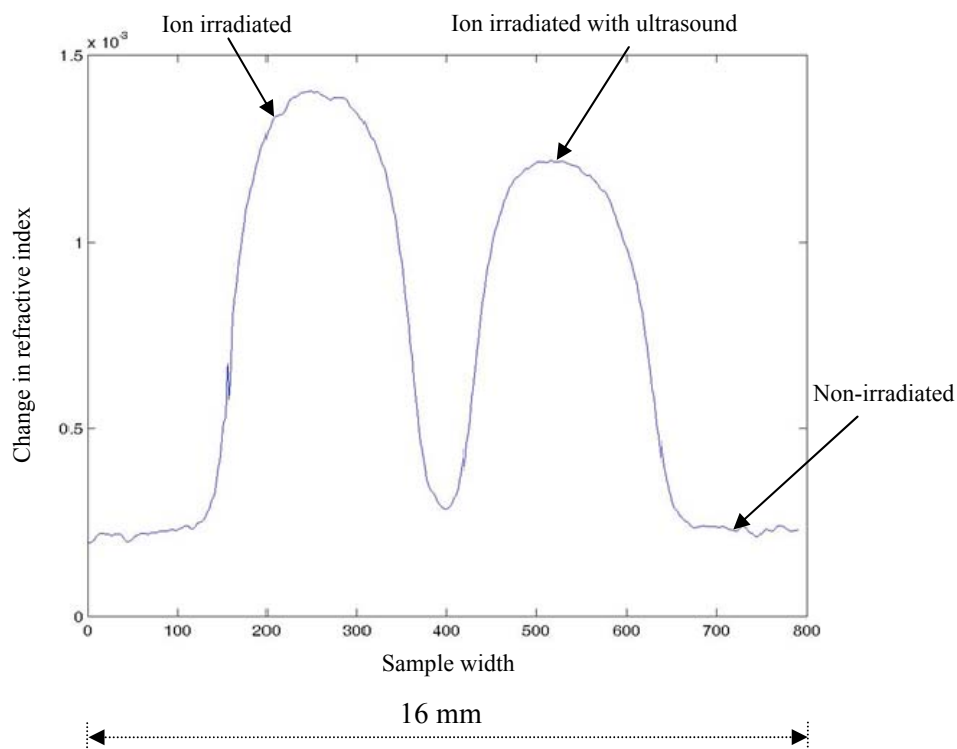
Figure 4.2: A horizontal scan through the distribution of refractive index modulation in Figure 4.1 is plotted. A measure of the change in refractive index due to irradiation and due to the introduction of ultrasound during irradiation can be obtained.

A comparison of the profile of the refractive index modulation along the direction of irradiation and the electronic energy loss (simulated using SRIM 2006) is presented in Figure 4.3 which shows that the profile of the refractive index modulation deviates from the electronic energy loss of the impinging ions in the sample indicating that the refractive index modulation in the sample is not entirely

due to electronic energy losses. Also the introduction of ultrasonic waves during irradiation brings about an almost constant reduction in the refractive index modulation. The maximum change in refractive index is observed at the end of the stopping range of the implanted ions (so-called Bragg peak) which coincides with the position of maximum electronic energy loss in the sample. The maximum change in refractive index due to ion irradiation was $\approx 1.65 \times 10^{-3}$. The reduction in refractive index modulation due to introduction of ultrasound during irradiation was $\approx 1.5 \times 10^{-4}$.

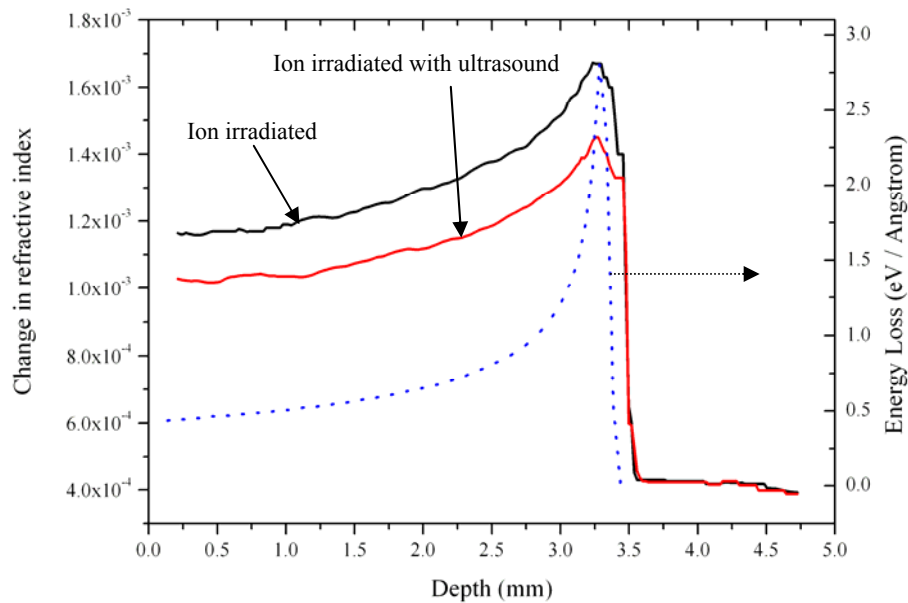Figure 4.3: Vertical scans through the ion irradiated region and the region introduced with ultrasound during ion irradiation in the distribution of refractive index modulation in Figure 4.1 is plotted. The profile of the variation of the refractive index modulation and the electronic energy loss of the incident ions along the sample depth in the direction of irradiation are compared.

In an irradiated Polycarbonate sample with a deposited dose of 200nC, a small change in refractive index modulation is observed and a smaller change in the same is observed due to introduction of ultrasound during irradiation. A horizontal scan through the projection of the distribution of refractive index modulation (similar to Figure 4.1) in this sample is plotted in Figure 4.4. The change in refractive index due to irradiation was $\approx 3 \times 10^{-5}$ and the reduction in refractive index modulation brought about by the introduction of ultrasound during irradiation was $\approx 5 \times 10^{-6}$.
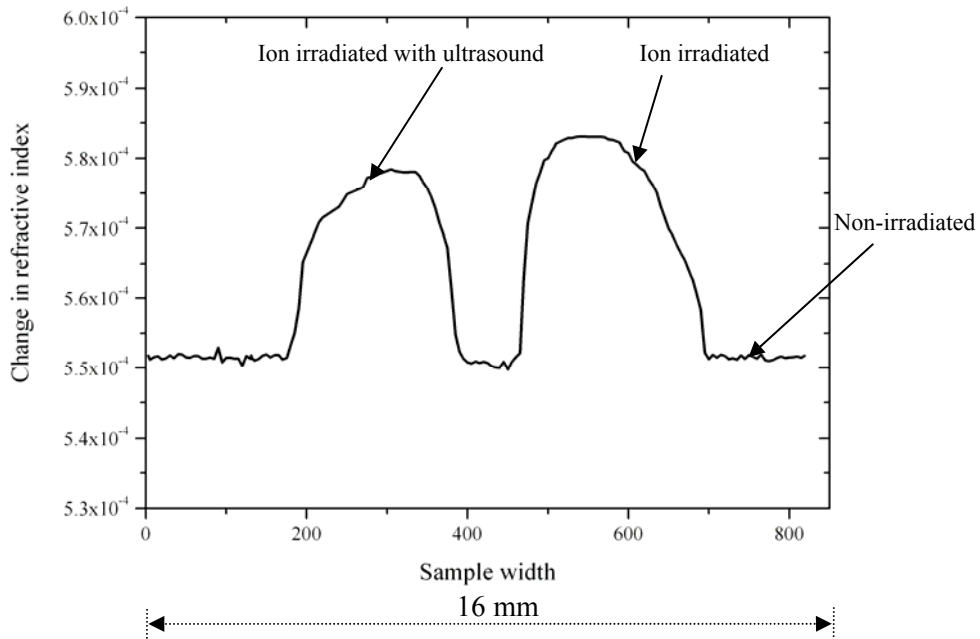
Figure 4.4: A horizontal scan through the distribution of refractive index modulation in an irradiated PC sample with a deposited dose of 200 nC is plotted. The $V_{peak-peak}$ of the ultrasonic waves was maintained at 30 V. A measure of the change in refractive index due to irradiation and due to the introduction of ultrasound during irradiation can be obtained.
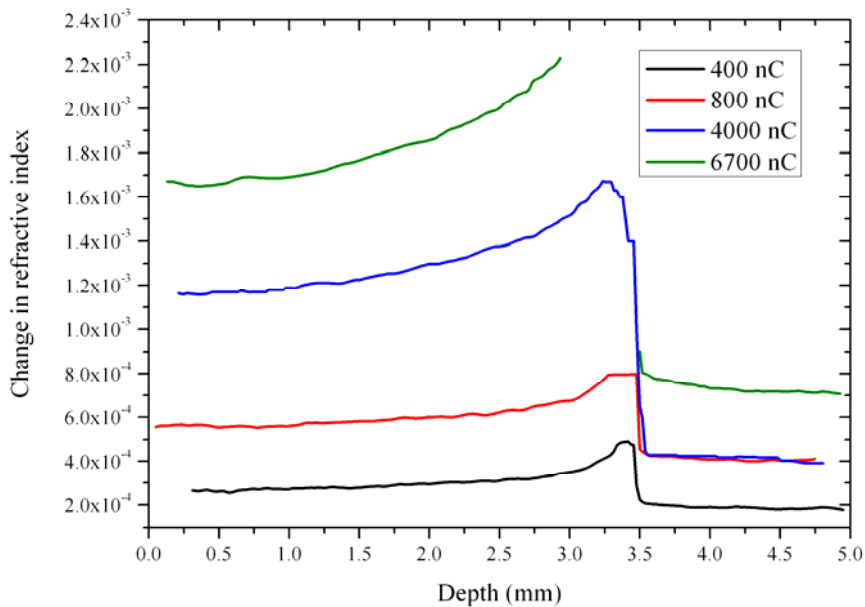
Figure 4.5: The refractive index modulation along the sample depth in the direction of irradiation is plotted for Polycarbonate samples with deposited charges as indicated in the plot.

62

Figure 4.5 shows the refractive index modulation along the sample depth in the direction of irradiation for Polycarbonate samples with deposited doses of 400nC, 800 nC, 4000 nC and 6700 nC. We see an increase in refractive index modulation with the deposited dose. The refractive index near the stopping range goes out of scale for a high deposited dose of 6700 nC. The maximum change in refractive index modulation is observed at the calculated stopping range of the incident deuterons in the Polycarbonate sample.

4.1.2 Optical absorption measurements

Figure 4.6 shows the absorption spectra of a polycarbonate sample in an ion irradiated region, an ion irradiated region simultaneously introduced to ultrasound and a region unaffected by radiation. The implanted dose was 4000 nC and the peak to peak amplitude of ultrasound was 30 V.
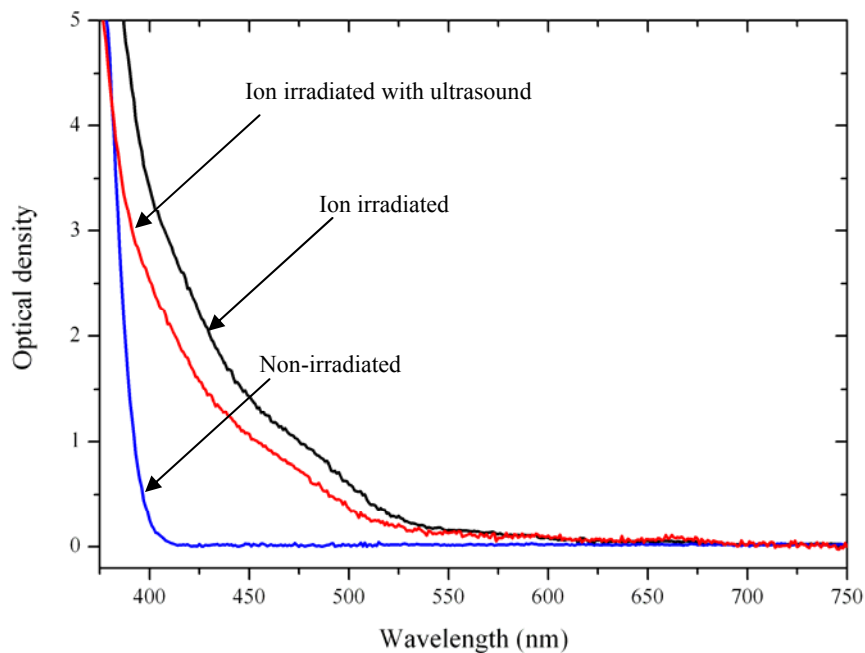
Figure 4.6: The absorption spectra obtained from different regions of an irradiated Polycarbonate sample with a deposited dose of 4000 nC at a depth of 625 μm in the sample along the direction of irradiation.

The absorption spectrum obtained for a region unaffected by radiation was taken to be a reference spectrum and subtracted from the absorption spectra obtained at various depths along the direction of irradiation. The resultant spectra were normalized which give a measure of the change in optical density (Figure 4.7).

63

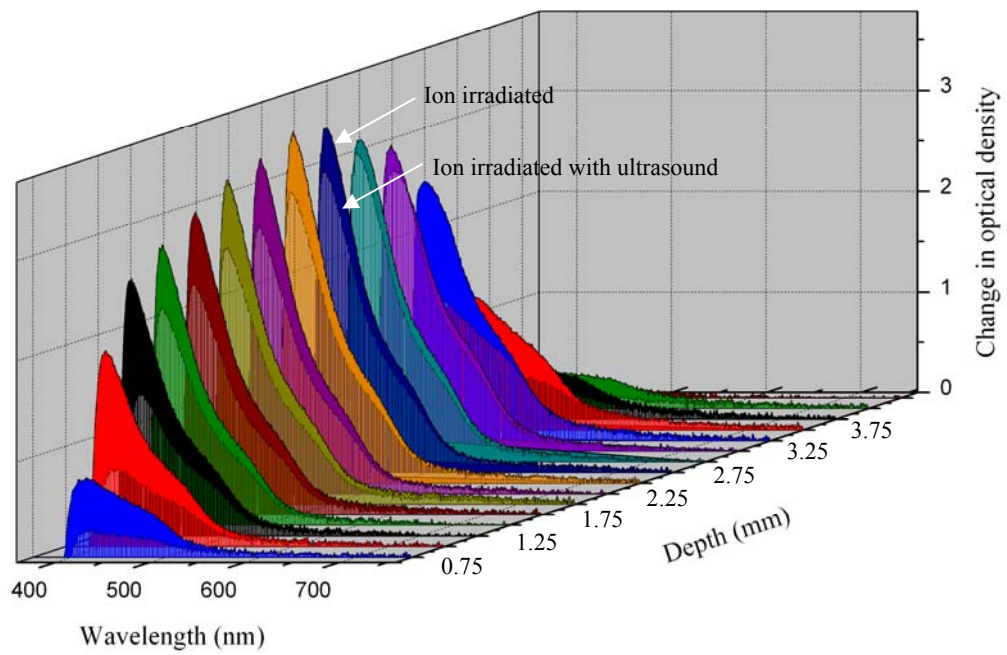Figure 4.7: The change in optical density is plotted as a function of sample depth in the direction of irradiation for an irradiated Polycarbonate sample with a deposited dose of 4000 nC.
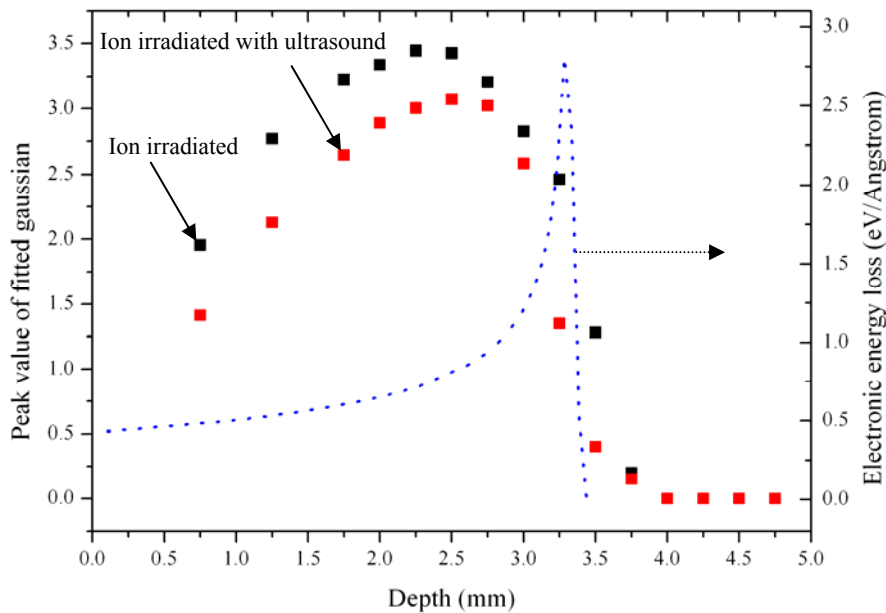

Figure 4.8: Peak values of the Gaussian fitted to the absorption spectra in Figure 4.6 at a wavelength of 410 nm as a function of sample depth in the direction of irradiation.

A multi-gaussian fit of the normalized spectra gives a measure of the maximum change in optical density at a particular wavelength of absorption. The peak values of optical density at a particular wavelength obtained by fitting multi-gaussian to the normalized spectra are plotted as a function of the depth in the sample along the direction of irradiation in Figure 4.8. Change in optical density at a particular wavelength in the visible region clearly does not follow the electronic energy loss of the imcident deuterons in the Polycarbonate sample.

For a sample with an implanted dose of 200 nC, the absorbance in the visible region is negligible. No significant changes were seen in the near-infrared range.

4.1.3 Microscope measurements

Ion irradiation causes coloration of Polycarbonate samples. The transparent material becomes gradually opaque to visible light. The coloration of a sample with a deposited dose of 200 nC is feeble and fades away rapidly whereas that of a sample implanted with a dose of 4000 nC is orange in colour (Figure 4.9) and takes a few months to fade away completely in room temperature. Visual inspection of the samples (with deposited dose of 4000 nC and above) allowed to stand at room temperature in air reveals a dark interior region within the coloured implanted region as seen inFigure 4.9. This dark interior region seems to originate from a darker spot at the centre of this dark region (not seen in Figure 4.9). The dark interior region observed in the samples soon (in hours to days) begins to fade and eventually cannot be seen anymore. Also very light yellow coloration is seen beyond the stopping range of the deuterons in the sample, which fades away quickly.
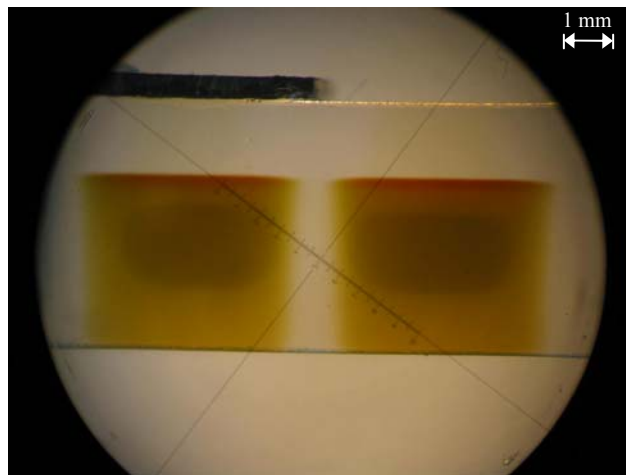
Figure 4.9: Image of ion implanted Polycarbonate sample under microscope implanted with 4000 nC.

Digital images of the sample viewed under microscope were obtained for intensity and therefore absorption measurements of the samples. The images were obtained with optimum illumination in the dynamic range in order to view and understand the radiation damage in the sample in greater detail. The images were then converted to Grayscale using OriginLab7.5 and the intensity of the light transmitted through the sample was extracted. The absorption of white light by the sample was calculated in turn and plotted as a function of the depth along the direction of irradiation (Figure 4.10). The profile of white light absorption in the irradiated regions along the sample depth in the direction of irradiation projects the position and nature of the dark interior region within the implanted region. Ultrasound induction has brought about an almost uniform decrease in white light absorption in the entire irradiated region in the sample.
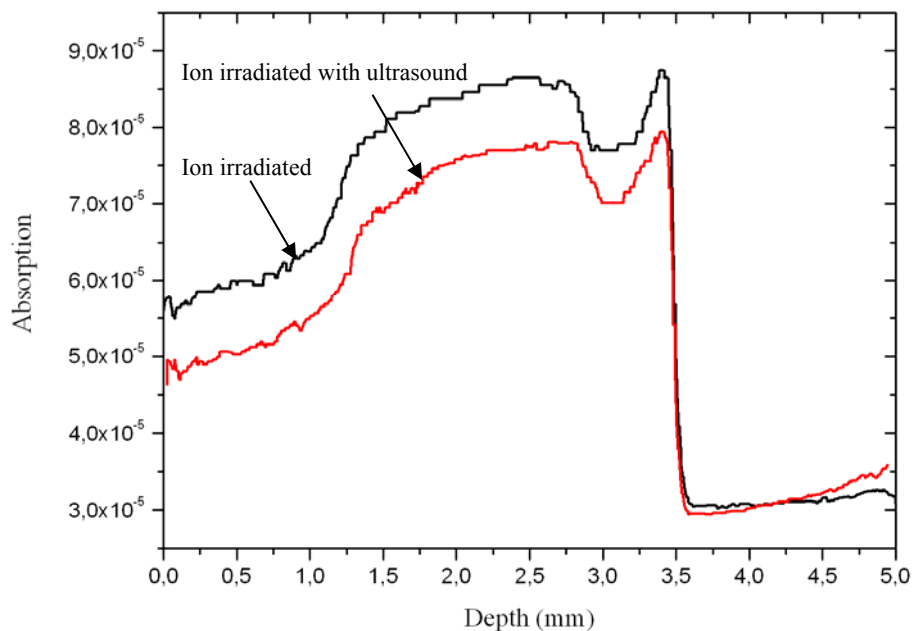
Figure 4.10: Absorption of white light is plotted along the sample depth in the direction of irradiation in a Polycarbonate sample with a deposited dose of with 4000 nC

4.1.4 Positron annihilation measurements

Measurements were made at the Bonn Positron Microprobe. Figure 4.11 shows the distribution of S-parameter along the sample depth in the direction of irradiation in a Polycarbonate sample with a deposited dose of 4000 nC. No

remarkable variation in S-parameter is observed in the irradiated regions of the sample.
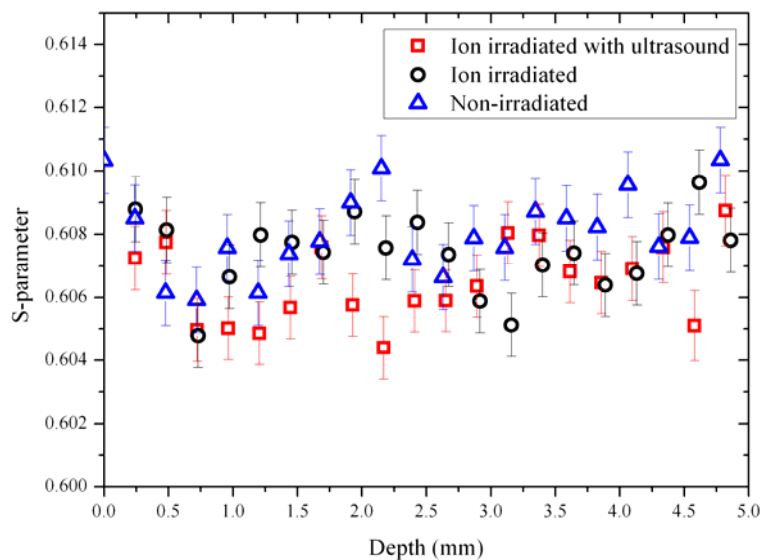
Figure 4.11: Distribution of S-parameter along the implantation depth of Polycarbonate sample implanted with 4000 nC.

4.2 Discussion (PC)

Degradation is the main effect induced in Polycarbonate due to ion irradiation. The functional groups in Polycarbonate include methyl, phenyl ring, carbonyl, ether and hydroxyl. Ether forms the skeleton of the macromolecule. Bond breaking occurs at the carbonyl group, ether group, methyl group and the phenyl group in Polycarbonate under ion irradiation. Double bonds are very sensitive to irradiation, whereas on the contrary phenyl rings are most stable under irradiation and attack at these points in the chain is unlikely to result in chain scission. The aromatic character of Polycarbonate and radical recombination reactions are considered to reduce the degree of chain scission due to ion irradiation.

Under the influence of ionizing radiation, degradation via chain scission occurs predominantly at the carbonate linkage in Polycarbonate. The possible breakdown mechanisms of diphenyl carbonate are schematically represented in Figure 4.11 [27, 28]. The breakdown of diphenyl carbonate to **PhOCO•** is a favoured reaction. **PhOCO•** being unstable, breaks down to the phenoxy radical and the phenyl radical. The formation of benzene and phenol may arise from hydrogen abstraction

67

reactions of the phenyl and phenoxy radicals. Recombination reactions of the various products formed may also occur.
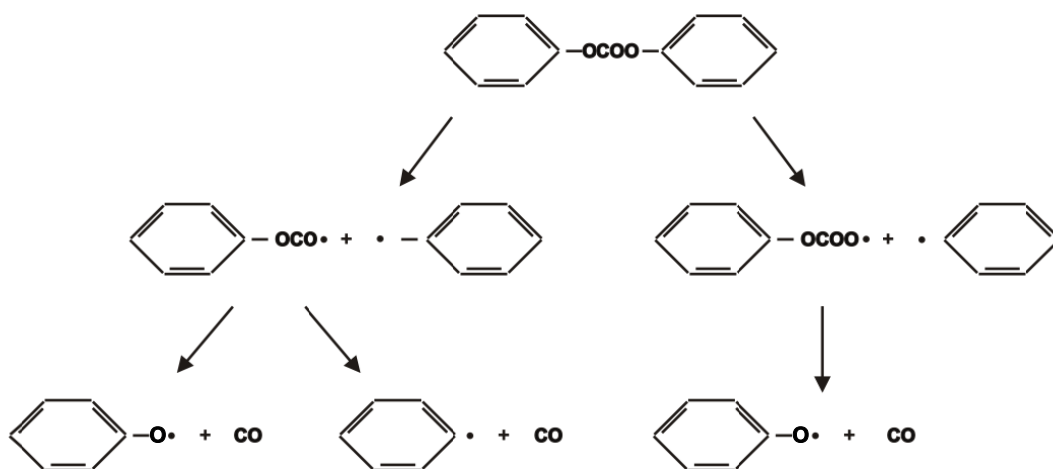
Figure 4.12: Breakdown mechanisms of the carbonate linkage in Polycarbonate chain resulting in the formation of phenoxy radical and phenyl radical. Recombination of the products formed may also occur.

Refractive index variation depends on the degree of degradation, molecular modifications which involve electronic modifications and structural modifications in the polymer. The comparison of measured refractive index changes with the electronic energy loss in the sample shows that the observed effects are predominantly due to electronic processes, although various other chemical and structural modifications seem to contribute to the changes in refractive index.

Modifications in optical absorption of ion irradiated Polycarbonate samples depends on the ion fluence. A strong absorbance in the visible region is seen in the ion implanted samples seen similar to what has been observed in different polymers bombarded with keV and MeV ions. Chromophores confer colour on substances. Auxochromes (such as C—OH, C—NH_2, C—Br etc) are groups which by themselves do not confer colour on a substance but tend to increase the colouring power of a chromophore [19, 29]. The presence of a chromophore, i.e. a multiple bond, generally causes absorption in the 200-800 nm region. Carbon – carbon bond conjugation is known to induce absorption of visible light by the material. The increase in absorption and the colouration of the Polycarbonate samples may be attributed to the formation of a conjugated system of bonds (chromophore groups) that absorb at a certain wavelength, as a consequence of the beam induced bond breaking and recombination reactions [30, 31].

Deuterons have a very low nuclear binding energy. Assuming that the deuteron is split into a neutron and a proton on impinging the sample surface, each possessing half the energy of the deuteron, the range of the protons largely differs from that of the neutrons. Protons cause maximum damage at the end of their range in the material. The calculated stopping range of 13MeV protons (protons split from the deuteron) in the Polycarbonate sample lies at the centre of the dark interior within the coloured implanted region indicating that this dark colouration within is caused by the interaction of these protons with the already modified polymer volume.

Ion irradiation in polymers is known to broaden 511 keV positron annihilation radiation which is caused by a reduction of para-positronium, the spin-antiparallel bound state between a positron and an electron. Annihilation peak broadening decreases the S parameter. The reason for observing no changes in the S parameter of the ion implanted Polycarbonate samples could be the large addition to the already existing free volume, due to ion irradiation which leaves no integral difference between the ion implanted region and non-implanted region of the sample [32].

A decrease in refractive index modulation, change in optical density and white light absorption is observed due to the introduction of ultrasound in the Polycarbonate sample during ion irradiation. The standing wave of ultrasound induces a stationary pressure wave pattern in the Polycarbonate sample thereby creating a stationary vibration pattern in the sample during ion irradiation. The ultrasound power was maintained at sub-threshold values so as to avoid temperature effects. Exposure to ultrasonic waves adds energy to the molecules of the sample system in addition to the energy imparted by energetic deuterons impinging on the sample. However, this additional energy results in a reduction in the modulation of properties caused by ion irradiation in the Polycarbonate sample. In other words, the simultaneous introduction of ultrasound and high energy deuterons in a Polycarbonate sample brings about a suppression of radiation damage.

5 Polymethylmethacrylate

5.1 Results

5.1.1 Interferometric measurements

Figure 5.1 shows the distribution of the change in refractive index in deuteron irradiated PMMA sample. The graph covers the region irradiated with deuterons and the region which is irradiated with deuterons and simultaneously treated with ultrasound. The two regions can be distinctly seen. The energy of the deuterons was 26 MeV and the implanted dose was 4000 nC. A standing wave of ultrasound with a peak to peak amplitude of 20 V was set up in the sample during ion irradiation. An increase in refractive index modulation with the introduction of ultrasound is observed.

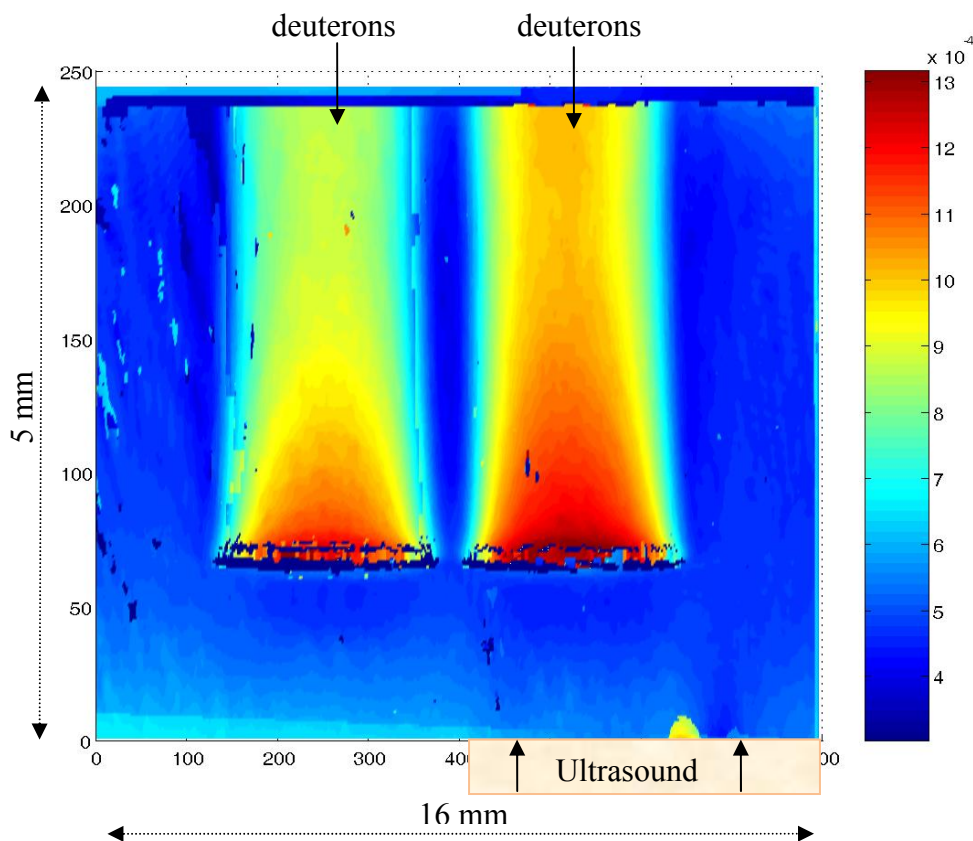Figure 5.1: The plot shows the projection of the distribution of refractive index modulation in an irradiated PMMA sample with a deposited dose of 4000 nC. The two regions of radiation damage are distinctly seen. The colour scale gives a measure of the change in refractive index with reference to a pristine sample. The $V_{peak-peak}$ of ultrasonic waves was maintained at 20 V throughout the irradiation time.

A comparison of the profile of refractive index modulation along the direction of ion irradiation and the electronic energy loss is presented in Figure 5.2 which shows a deviation between the two. Hence the refractive index modulation in the sample cannot be entirely due to electronic energy losses. Also the introduction of ultrasound during ion irradiation brings about an increase in the change in refractive index along the sample depth in the direction of irradiation. The maximum change in refractive index is observed near the end of the stopping range of the implanted ions (so-called Bragg peak) which coincides with the position of maximum electronic energy loss in the sample.
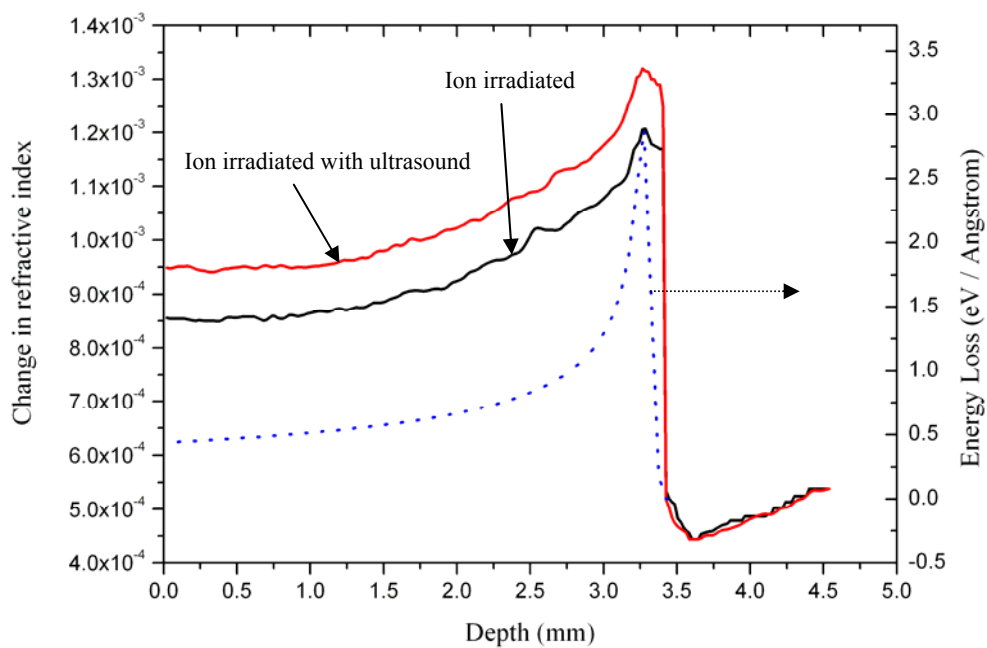
Figure 5.2: Vertical scans through the ion irradiated region and the region introduced with ultrasound during ion irradiation in the distribution of refractive index modulation in Figure 5.1 is plotted. The profile of the variation of the refractive index modulation and the electronic energy loss of the incident ions along the sample depth in the direction of irradiation are compared. The deposited dose is 4000 nC.

Figure 5.3 shows the refractive index modulation along the width of an irradiated PMMA sample with a deposited dose of 200 nC. A decrease in refractive index due to ion irradiation is observed and an enhancement of the change in refractive index is observed due to the introduction of ultrasound. The peak to peak voltage of ultrasound was 16V.

71
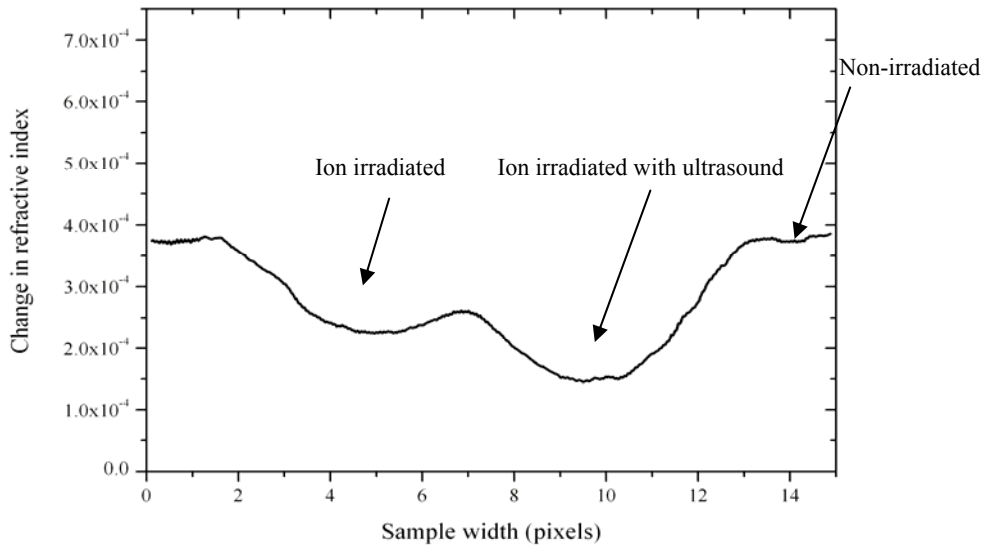
Figure 5.3: A horizontal scan through the distribution of refractive index modulation in an irradiated PMMA sample with a deposited dose of 200 nC is plotted. The $V_{peak-peak}$ of the ultrasonic waves was maintained at 16 V. A measure of the change in refractive index due to irradiation and due to the introduction of ultrasound during irradiation can be obtained.

Figure 5.4 shows the refractive index modulation profile in PMMA samples which were irradiated with 26 MeV deuterons. These samples were not introduced with ultrasonic waves. The total deposited charge was 200nC, 400 nC, 800 nC and 4000 nC. Vertical scans through the irradiated regions in the graphs of distribution of refractive index modulation of the samples are plotted as a function of th sample depth in the direction of irradiation. We observe an increase in refractive index modulation for deposited doses of 800 nC and 4000 nC, and a decrease in refractive index modulation for deposited doses of 200 nC and 400 nC.
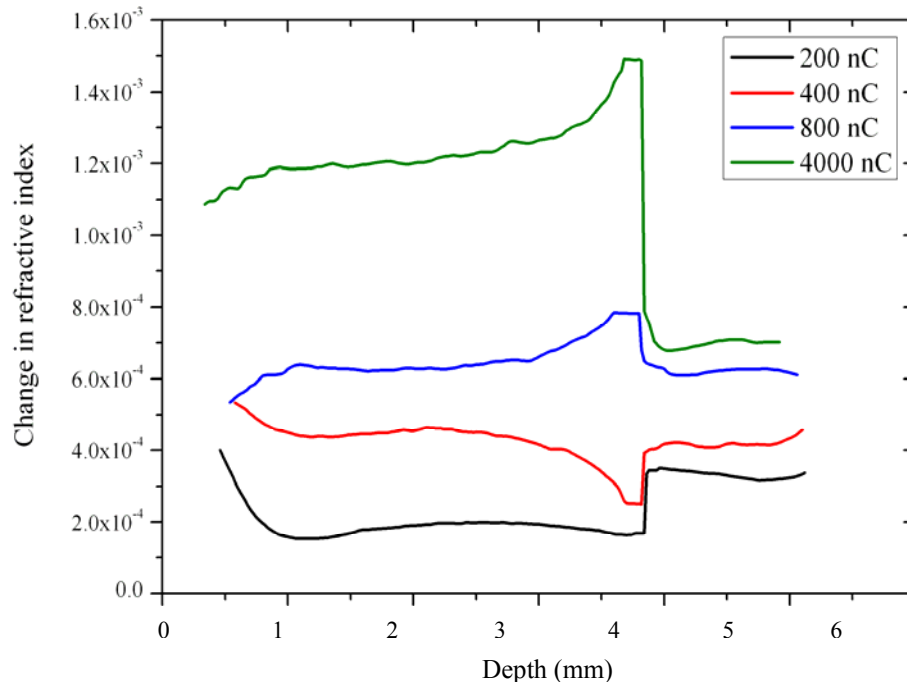
Figure 5.4: The refractive index modulation along the sample depth in the direction of irradiation is plotted for PMMA samples with deposited charges as indicated in the plot.

5.1.2 Optical absorption measurements

The optical absorption spectra obtained for the deuteron irradiated PMMA sample is shown in Figure 5.5. The absorption spectra of a PMMA sample in an ion irradiated region, an ion irradiated region simultaneously introduced to ultrasound and a region unaffected by radiation at a sample depth of 625 μm in the direction of irradiation are plotted. The deposited dose was 4000 nC and the peak to peak amplitude of ultrasound was 20 V.
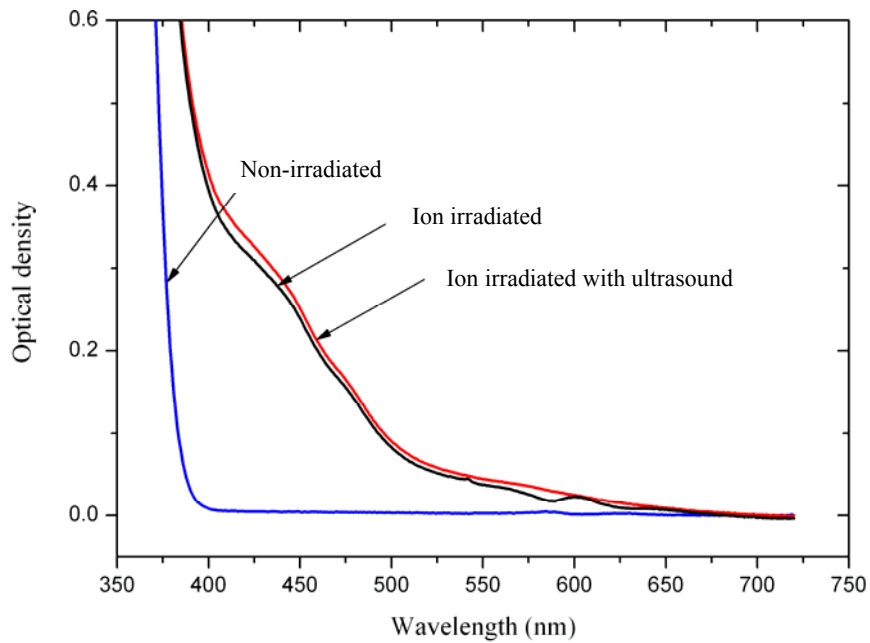
Figure 5.5: The absorption spectra (in the visible region) obtained from different regions of an irradiated PMMA sample with a deposited dose of 4000 nC at a depth of 625 µm in the sample along the direction of irradiation.

A strong absorbance in the visible region is observed in the ion irradiated region. A small reduction in absorption with the induction of ultrasound is seen in Figure 5.5. Figure 5.6 shows the change in optical density along the implantation depth in the sample in the ion irradiated region and the region subjected to simultaneous ion irradiation and ultrasound induction. The change in optical density at various depths in the sample along the direction of irradiation is obtained (as described in Section 4.1.2) and plotted in Figure 5.7. The change in optical density over the wavelength range is small and along the sample depth is very small. No significant changes can be seen in the near-infrared range.
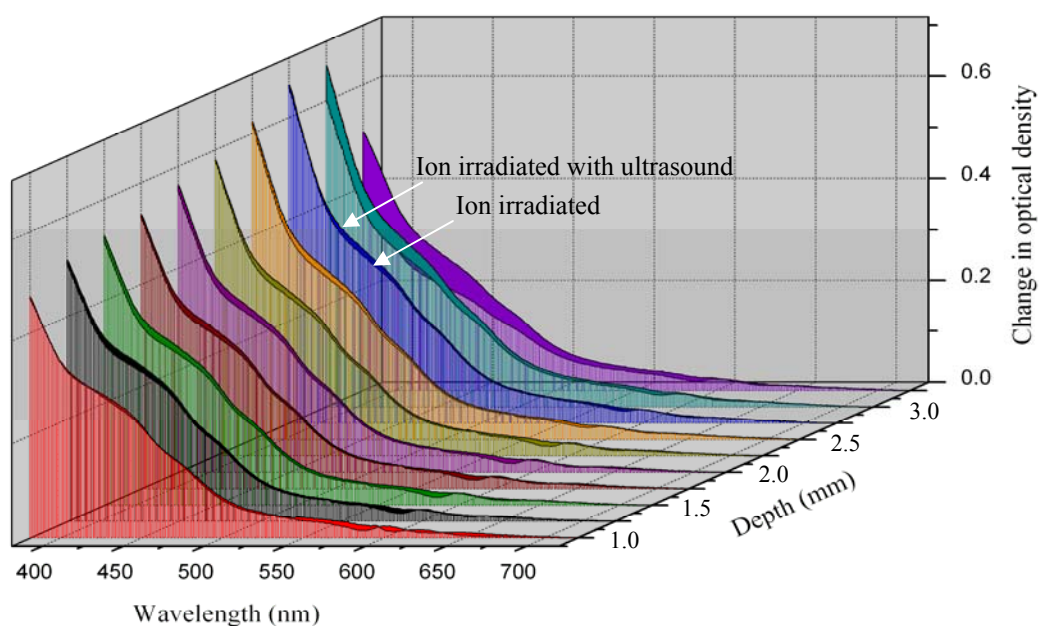
Figure 5.7: The change in optical density is plotted as a function of sample depth in the direction of irradiation for an irradiated PMMA sample with a deposited dose of 4000 nC.

5.1.3 Microscope measurements

On ion irradiation, PMMA turns yellow. This coloration depends on the deposited dose and vanishes soon. Figure 5.8 shows an ion irradiated PMMA sample. A light yellow coloration is seen at the irradiated regions.

Figure 5.8: An image of a PMMA sample irradiated with 4000 nC. A light yellow colouration of the sample at the irradiated regions can be seen. This colouration fades away in a few weeks.

Images of the irradiated samples were taken using light microscope. The profile of white light absorption of the samples is obtained by analysing the images (using

the software OriginLab7.5) and presented in Figure 5.9. An increase in absorption is observed due to introduction of ultrasound.
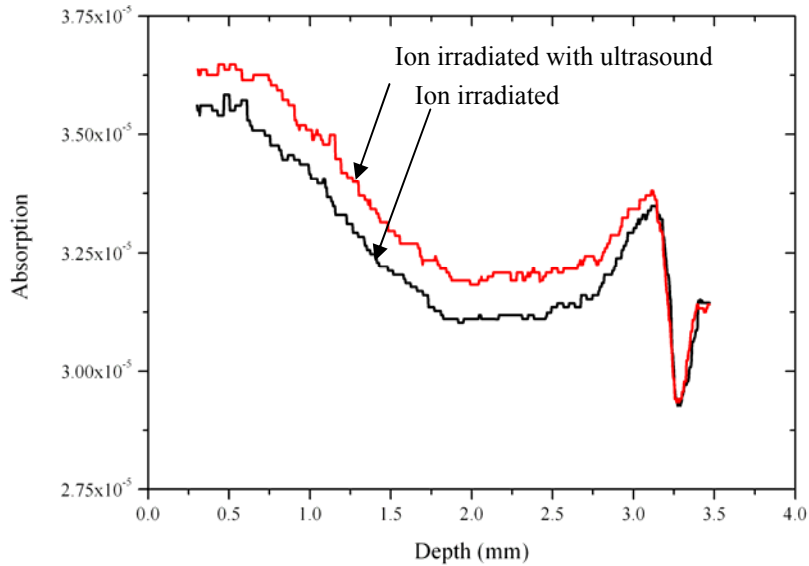
Figure 5.9: Absorption of white light is plotted along the sample depth in the direction of irradiation in a PMMA sample with a deposited dose of with 4000 nC.

5.1.4 Positron annihilation measurements

Positron annihilation measurements were made at the Bonn Positron Microprobe. Figure 5.10 shows the distribution of S-parameter along the sample depth in the direction of irradiation for a PMMA sample with a deposited dose of 4000 nC. No measurable difference in the S-parameter was observed between the non-irradiated region and ion irradiated regions of the sample. No effects due to ultrasound were observed.
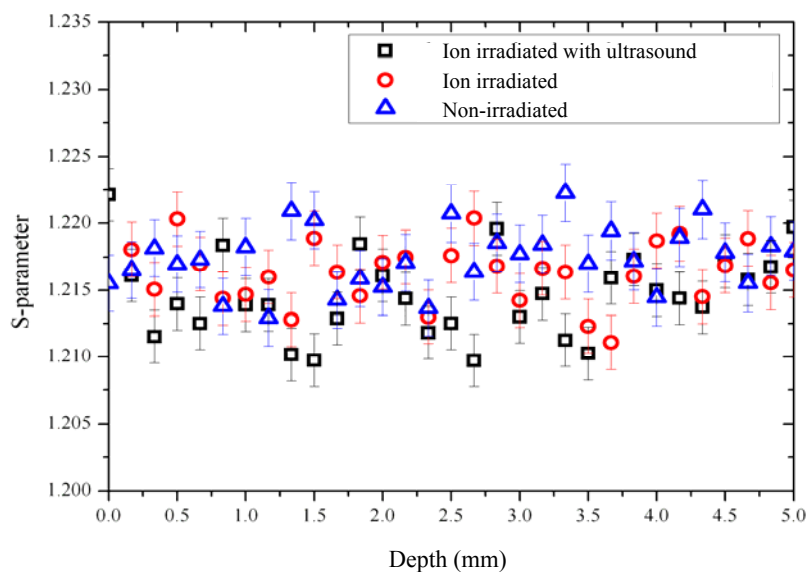
Figure 5.10: The distribution of S-parameter along the sample depth in the direction of irradiation for a PMMA sample with a deposited dose of 4000 nC.

5.2 Discussion (PMMA)

PMMA has one of the highest known radiation sensitivities with respect to chain scission and splitting off side groups containing C=O. When PMMA in the solid form is irradiated with deuterons, two reactions predominate: degradation of the main chain, and the evolution of gases arising from the breakdown of the side chains. The degradation is thought to proceed by random rupture of main-chain C-C bonds by rearrangement of the excited polymer. Cleavage of pendent methyl ester groups also occurs. For each main-chain rupture, approximately one ester side chain is decomposed. These reactions lead to the release of various gaseous molecular species such as hydrogen, molecular scission products from the end groups as well as pendant atoms and groups of the polymer such as $H^{°}$, $CH_3^{°}$, and $CH_3OOC^{°}$, and their reaction products resulting in the creation of radicals or dangling bonds. Cross-linking occurs when two free dangling bonds on neighbouring chains unite, whereas double or triple bonds are formed if two neighbouring radicals in the same chain unite.

PMMA responds sensitively to electronic energy transfers and offers a wide range of variation in the refractive index. Drastic increase of the refractive index is observed after ion irradiation at doses of the order of 10^{14} ions/cm^2. Both the refractive index change and the ionization energy density vary strongly over the range of ion penetration [33]. The incident deuterons are stopped in the polymer

losing their energy following the electronic energy loss curve. The profile of the index of refraction does not entirely follow the electronic energy loss curve of the deuterons in PMMA, calculated using SRIM 2006. The comparison of measured refractive index modulation, with the ionization energy density shows that although the electronic processes play the main role in the observed effects, other processes also contribute to the damage created. Refractive index changes in PMMA result predominantly from the change of the material density, and only at higher doses additionally from a chemical modification [34, 35]. Chemical modification of the polymer due to energy deposition during ion irradiation comes into play as high energy ions are implanted in large doses. Chemical modifications influence the refractive index owing to changes of the molecular polarizability. The modifications in the chemical and physical structure of the polymer together lead to compaction and densification of the material, thus increasing the refractive index. The largest change of refractive index occurs near the end of range as the maximum amount of energy is deposited at the end of the range. The increase of the refractive index may be due to the complete or partial separation of the side chain from the PMMA molecule [36]. This implies a volume contraction by van der Waals interactions leading to a local increase of the mechanical density and consequently of the refractive index [37]. The modification of refractive index is also attributed to the formation of a relatively high concentration of unsaturated bonds in the ion implanted volume of the polymer. Chemical modifications of PMMA are directly related to the absorbed dose. A suggested chemical mechanism for degradation of PMMA due to light ion irradiation is schematically shown in Figure 5.21. Irradiation of PMMA with energetic light ions leads to a deterioration of almost all characteristic functional groups, with similar destruction efficiency, and formation of carbon-carbon double bonds [5].

$$
\begin{array}{ccccc}
CH_3 & & CH_3 & & CH_2 \\
| & & | & & \| \\
-CH_2-C- & \longrightarrow & -CH_2-C^{\bullet}+ & \longrightarrow & -CH_2-C \\
| & & | & & | \\
C=O & & C=O & & C=O \\
| & & | & & | \\
O & & O & & O \\
| & & | & & | \\
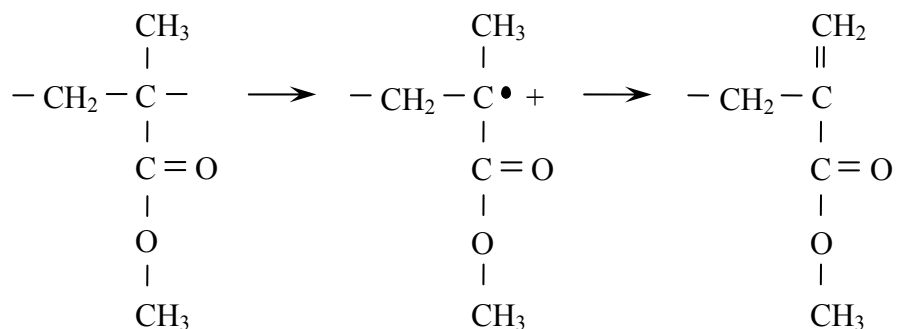CH_3 & & CH_3 & & CH_3 \\
\end{array}
$$

Figure 5.21: Characteristic suggested mechanism for PMMA damaging after light-ion irradiation

78

The introduced changes in the chemical and physical structure together result in a change of the optical absorption. The absorption in the visible region may be attributed to an anionic species for the following reasons: the anionic species of PMMA has an absorption maximum in this wavelength region. It should be noted that the anionic species of molecules having an ester or ketone structure have absorption maxima in the 400-500 nm region [38].

Coloured free radicals, trapped within the irradiated solid matrix may be correlated with the coloration of the samples. These trapped coloured radicals may form colourless products upon reaction with oxygen or reaction with other (nearby) radicals (since the samples are thick), thereby leading to the gradual decay of coloration in the sample. Colored radical-radical reactions can proceed either by coupling to form a carbon-carbon sigma bond, or disproportionation thus creating a double bond.

Ion irradiation is capable of inducing free volume in polymers additionally to the pre-existing intrinsic one. More free volume is created by the volatile products formed during irradiation. Positrons annihilate in the already existing free volume in the polymer. The increase in free volume leads to more positron annihilation which however does not make an integral difference.

An increase in refractive index modulation, optical density and light absorption is observed due to the introduction of ultrasound in the Polymethylmethacrylate sample during ion irradiation. The standing wave of ultrasound sets up a stationary mechanical vibration pattern in the PMMA sample. The mechanical vibration increases the energy of the molecules inducing molecular vibrations. This increase in energy does not cause any measurable modifications in the analysed properties of the PMMA sample (sub-threshold ultrasound power). During ion irradiation, energy is imparted into the sample system by impinging ions. The increase in energy of the sample system due to exposure to ultrasound together with the enhancement of energy due to ion irradiation enables the molecules and the molecular fragments formed to overcome the activation energy for displacement. Thus the added energy due to introduction of ultrasound enhances the radiation damage in the PMMA sample.

6 Polyvinylchloride

6.1 Results

6.1.1 Interferometric measurements

The Polyvinyl chloride samples used are transparent but blue in colour. This is because of a blue dye added to it during the process of production. The blue colouration of the sample makes it not suitable for measurements with the interferometer where a red He-Ne laser is used as the measurement light. The absorption of the sample is close to the maximum of absorption in the visible region. As a result, the images obtained from interferometer measurements show no measurable effects in the sample.

6.1.2 Optical absorption measurements

Optical absorption measurements of Polyvinyl chloride samples implanted with deuterons of energy of 26 MeV were made with CARY 500, spectrophotometer. The absorption spectra were obtained along the depth of the sample in the direction of irradiation in steps of 125 μm in the deuteron irradiated region simultaneously exposed to ultrasound, region irradiated with deuterons alone and non- irradiated region of the sample. Figure 6.1 shows the absorption spectra of a polyvinyl chloride sample in the above mentioned three regions at a depth of 2mm in the sample in the direction of irradiation. The deposited dose was 200 nC and the peak to peak amplitude of ultrasound was 20 V. Figure 6. shows similar absorption spectra for a Polyvinyl chloride sample with a deposited dose of 400 nC and a peak to peak amplitude of ultrasound of 20 V. The absorption spectra presented are obtained at a depth of 2mm in the sample in the direction of irradiation. Absorption bands in the visible region of the electromagnetic spectrum are observed in the ion irradiated regions. No significant changes in absorption were observed in the near-infrared region. We observe an increase in optical density as the effect of introduction of ultrasound in the sample during deuteron irradiation. The absorption spectrum obtained at a non irradiated region (same as pristine sample) was taken to be a reference spectrum and subtracted from the absorption spectra obtained at various sample depths and the resulting spectra were normalised. These normalised spectra display the change in optical density as a function of implantation depth for deposited doses of 200 nC and 400 nC in Figure 6.7 and Figure 6.4.
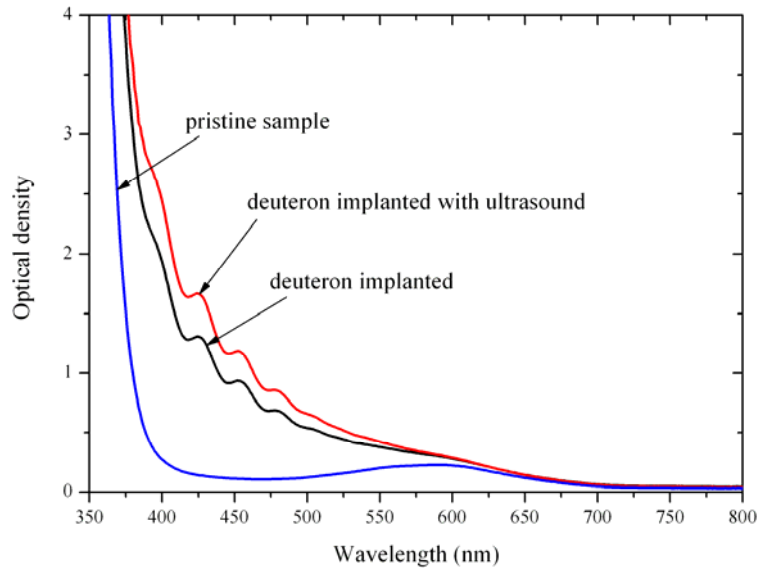
Figure 6.1: Absorption spectra of a PVC sample implanted with 200 nC.
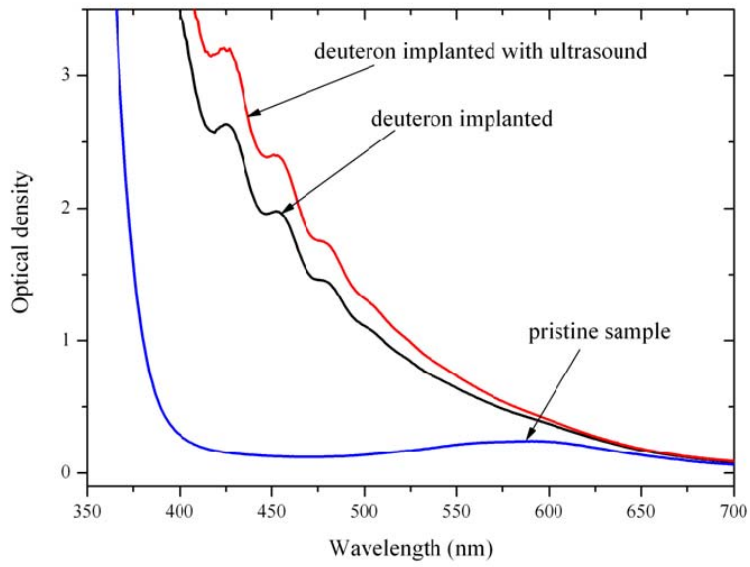
Figure 6.2: Absorption spectra of a PVC sample implanted with 400 nC.

81
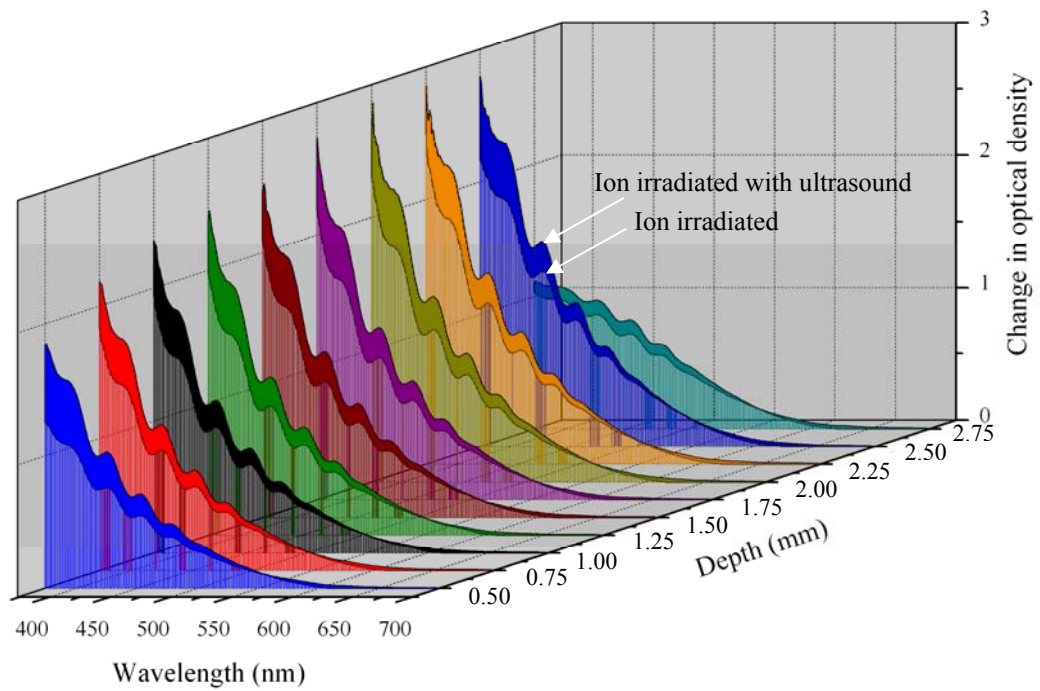
Figure 6.3: The normalised absorption spectra in the visible region are plotted as a function of the ion implantation depth for a PVC sample implanted with 400 nC.
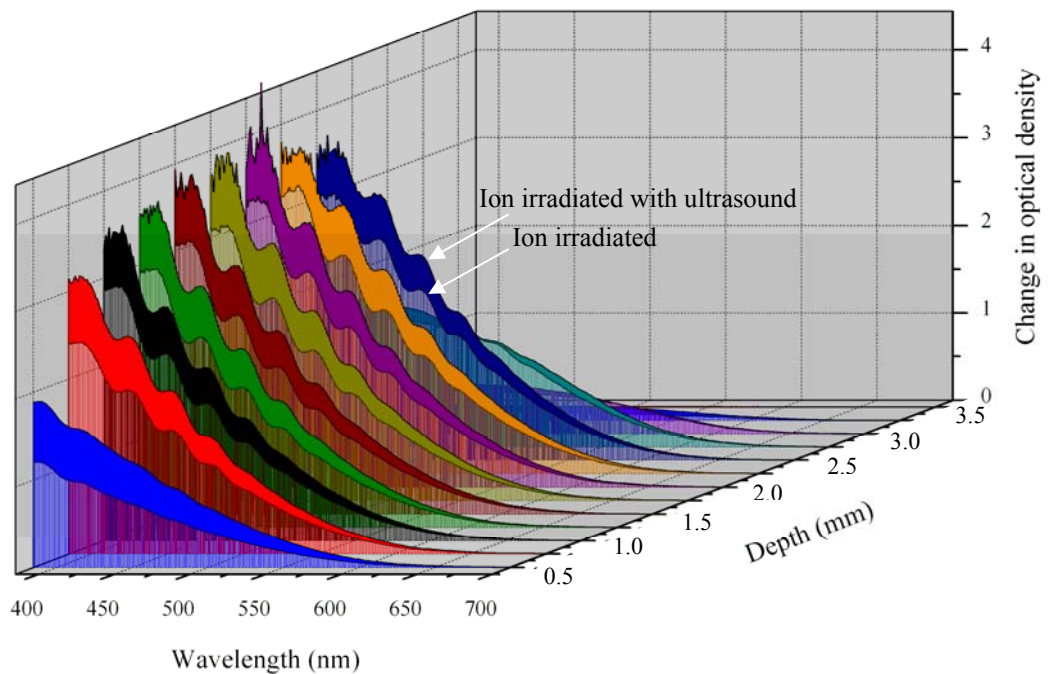
Figure 6.4: The normalised absorption spectra in the visible region are plotted as a function of the ion implantation depth for a PVC sample implanted with 400 nC.

An increase in the change in optical density is observed along the implantation depth until the calculated stopping range of the deuterons in the sample. Here the change in optical density decreases steeply and vanishes at further depths. The ultrasound seems to bring about a constant effect on the change in optical density in the implanted region.

To compare the profile of variation in optical density in a deuteron implanted PVC sample with the simulated electronic energy loss in the same sample, spectra were fitted with a Gaussian function at an absorption wavelength and the peak values of the gauss fit were plotted as a function of implantation depth in the sample (Figure 6.5). The simulated electronic energy loss is plotted in the same graph. The profile of the variation in optical density deviates from that of the electronic energy loss suggesting other processes of radiation damage in PVC samples.
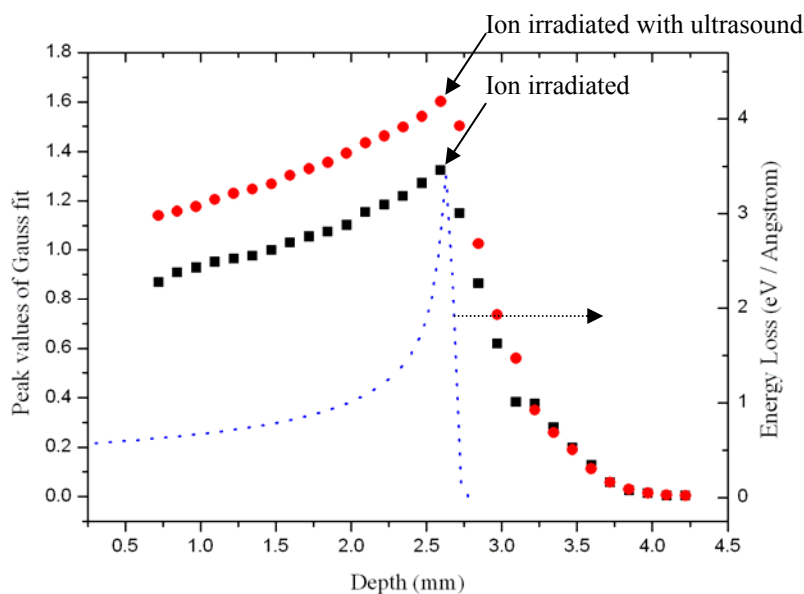
Figure 6.5: The peak values of Gaussian fitted to absorption spectra in Figure 6.3 at a wavelength of 425 nm is plotted as a function of implantation depth. The plot shows the profile of the change in optical density in comparison with the electronic energy loss in the PVC sample implanted with 200 nC.

6.1.3 Microscope measurements

PVC samples develop a dark yellow coloration on deuteron irradiation. The coloration ranges between dark yellow to dark brown depending on the ion dose. Figure 6.6 shows a PVC sample implanted with a dose of 200 nC.
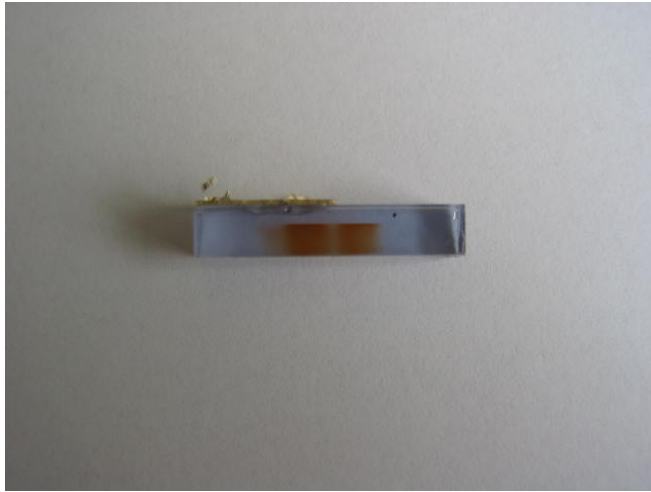
Figure 6.6: A PVC sample implanted with deuterons of energy 26 MeV. The ultrasound transducer is fixed on top-left. The implanted regions are seen as brown colourations. The implanted volume on the left was exposed to ultrasound during implantation.

Images of the implanted samples were taken using light microscope. The profile of light absorption of the samples is obtained by analysing the images (using the software OriginLab7.5) and presented in Figure 6.7 and Figure 6.8 for irradiated PVC samples with deposited doses of 200 nC and 400 nC. An increase in absorption is observed on the introduction of ultrasound.
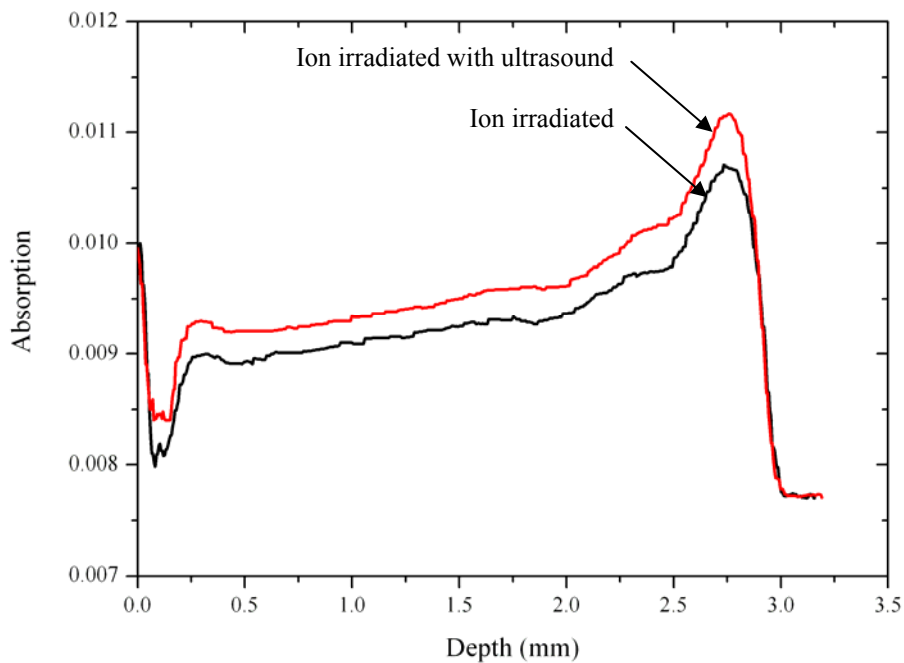
Figure 6.7: The absorption of light by a PVC sample implanted with 200 nC is plotted as a function of the implantation depth.
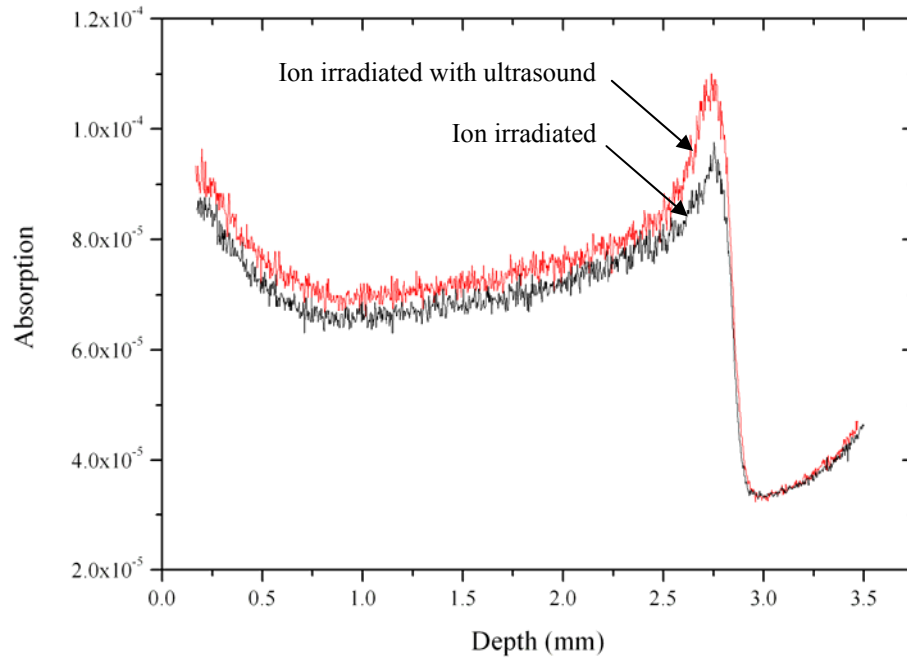
Figure 6.8: The absorption of light by a PVC sample implanted with 400 nC is plotted as a function of the implantation depth. The sample colouration is dark and there is very little light transmitted. This accounts for the distortions in the absorption curves.

6.1.4 Positron annihilation measurement

Positron annihilation measurements were made at the Bonn Positron Microprobe. The data analysis was carried out using M-Spec. Figure 6.9 shows the distribution of S-parameter along the implantation depth an ion-implanted PVC sample. Figure 6.10 shows the distribution of S-parameter in the irradiated regions along the width of the sample. No distinct difference in the S-parameter measured at a non-implanted region and ion-implanted regions of the sample was observed. No variation due to ultrasound was seen.

Figure 6.9: The distribution of S-parameter along the sample depth in the direction of irradiation for a PMMA sample with a deposited dose of 400 nC.

Figure 6.10: The distribution of S-parameter along the sample width for an irradiated PVC sample with a deposited dose of 400 nC. Horizontal scans along the width of the sample are made.

6.2 Discussion (PVC)

Polyvinyl chloride belongs to the group of polymers that preferentially undergo cross-linking under irradiation. When exposed to high energy radiation, the main effect is the formation of new bonds, free radicals, double bonds, etc. Thus a new chemical system, with functional groups and electronic structure different with respect to the pristine material, is formed [39].

The main effects of ion irradiation in PVC are crosslinking, chemical dissociation of the molecular structure leading to formation of unsaturation with accompanying discoloration, and hydrogen chloride evolution [40].

Miller [41] has suggested a free-radical chain reaction initiated by the radical $-CHCl-\overset{\bullet}{C}H-CHCl-$ in accordance with the mechanism of thermal degradation proposed by Winkler [42]. The first step is the formation of $\overset{\bullet}{}-CH_2-CH-CH_2-$ radical. The abstracted Cl atom can detatch a hydrogen atom from a methylene group, forming HCl and the relatively instable $-\overset{\bullet}{C}HCl-CH-CHCl-$ radical. This alkyl radical can be stabilized by transformation into an allyl or polyenyl radical with the formation of HCl by the so-called "zipping" mechanism:

$$\text{WWW } CHCl-\overset{\bullet}{C}H-\underset{\underset{Cl}{|}}{C}H-\underset{\underset{H}{|}}{C}H \text{ WWW} \xrightarrow{-HCl} \text{WWW } CHCl-CH=CH-\overset{\bullet}{C}H \text{ WWW}$$

This process may proceed without a "free" Cl atom by simultaneous dissociation and abstraction, and can result in up to nine conjugated double bonds.

When polymers are exposed to ionizing radiation, colour centers are produced resulting in the formation of visible absorptions and coloured ion implanted volume. Degree of colouration (yellowing) usually increases with an increase in radiation dose. Visible absorptions are usually associated with annealable color centers. It is likely that the visible absorptions are associated with polymeric radicals and possibly other structurally-related, conjugated radicals which may be present in low concentrations.

No distinction between the S-parameter in an irradiated region and a non-irradiated region is observed in PVC samples as ion irradiation induces free volume in addition to the pre-existing intrinsic one. Evolution of volatile products formed during irradiation leads to an increase in free volume in the polymer. Positrons annihilate in the already existing free volume in the polymer in a very short time.

87

Hence an increase in free volume does lead to more positron annihilation but it does not make an integral difference.

Introduction of ultrasound brings about an increase in the degree of coloration and optical density of the Polyvinyl chloride samples in the visible region of the electromagnetic spectrum. The standing wave of ultrasound creates a stationary pattern of sound pressure in the PVC sample. This pressure causes mechanical vibration to occur. The mechanical vibrational energy introduced into the sample alone does not induce measurable changes in the properties of the PVC sample as sub-threshold ultra. But the same mechanical vibrational energy of ultrasound introduced into the sample during ion irradiation causes the displacement of the constituents of the sample system. This can be understood by considering that the energy imparted into the sample by the impinging ions, together with the mechanical vibrational energy enable the molecules and molecular fragments of the sample system undergoing damage to overcome the activation energy required for their displacement thereby increasing the damage caused by irradiation. Thus the introduction of ultrasound enhances the radiation damage in PVC as in the case of PMMA.

7 Discussion

The observed effect of ultrasound on the polymers PC, PMMA and PVC are summed up in Table 1.

Property / Polymer	Refractive index modulation (Interferometry)	Change in optical density (Optical absorption spectroscopy)	White light absorption (Optical microscopy)	S-parameter (Positron annihilation spectroscopy)
PC	Decrease	Decrease	Decrease	No measurable change
PMMA	Increase	Increase	Increase	No measurable change
PVC	Not measurable	Increase	Increase	No measurable change

Table 1. The observed effect of ultrasound on the modulation of properties in the polymers used is listed.

We observe a decrease in modulation of the measured properties in PC and an increase in the modulation of the measured properties in PMMA and PVC, due to the simultaneous introduction of ultrasound with energetic deuterons in the samples. As seen in Figure 7.1 and Figure 7.2, the effect of ultrasound is observed over the entire deuteron implantation depth in the samples. Also the effect of ultrasound was observed over the entire wavelength scale in the absorption spectra of the samples

and not just at particular wavelengths. The profile of refractive index modulation along the implantation depth is comparable for PC and PMMA although it deviates from the electronic energy loss (simulated using SRIM 2006) in the two samples at higher implantation depths (Figure 7.1). This deviation could be because of the chemical modification of the polymer samples which comes into play at high doses. Also the software SRIM 2006 assumes a virgin polymer material as target for every impinging ion (out of a total of 10000 ions) while simulating the electronic energy loss of incident particles in the target, which is not the case in practice.

The observed modulation of properties due to introduction of ultrasound is not an effect of temperature. The temperature of the sample was constantly monitored during the implantation of deuterons in the polymer samples. No measurable change in temperature was observed. The ultrasound power was kept low enough to have no measurable changes in the sample due to heating. Also the duty cycle of the deuteron beam and ultrasound were kept very low to avoid heating up of the sample. Hence we rule out the possibility of effect of temperature on the observed modulations due to introduction of ultrasound.

The introduction of ultrasound inputs energy to the polymer constituents in addition to the energy imparted by the impinging deuterons. This increase in energy enables the constituents of the polymer samples to overcome the activation energy required for displacement. Thus the introduction of ultrasound produces mechanical displacement of polymer constituents thereby affecting the radiation damage caused by deuterons impinging on the polymer samples.
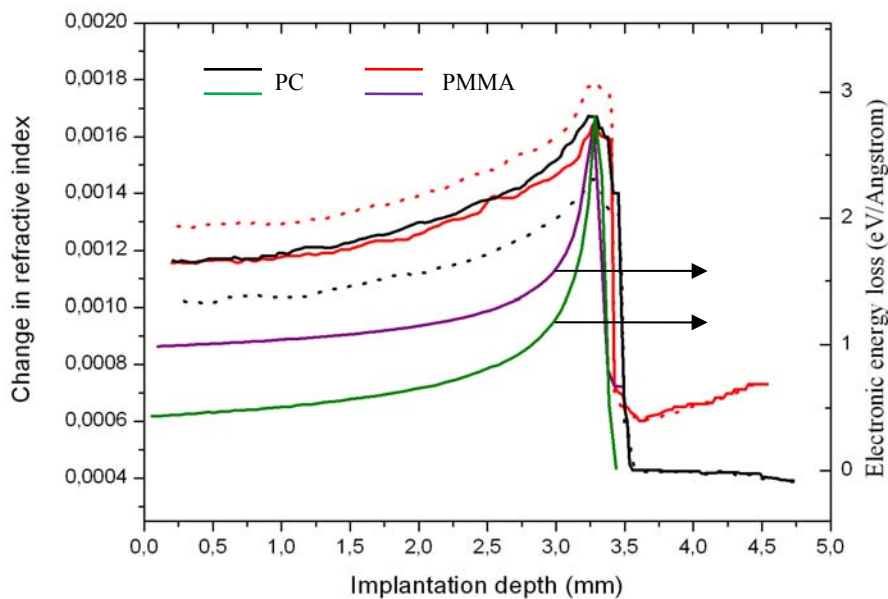

Figure 7.1: The refractive index modulation along the penetration depth in PMMA is calibrated and plotted along with that in PC. The dotted lines represent the profile due to radiation damage along with ultrasound introduction. The electronic energy loss along the implantation depth is also plotted.
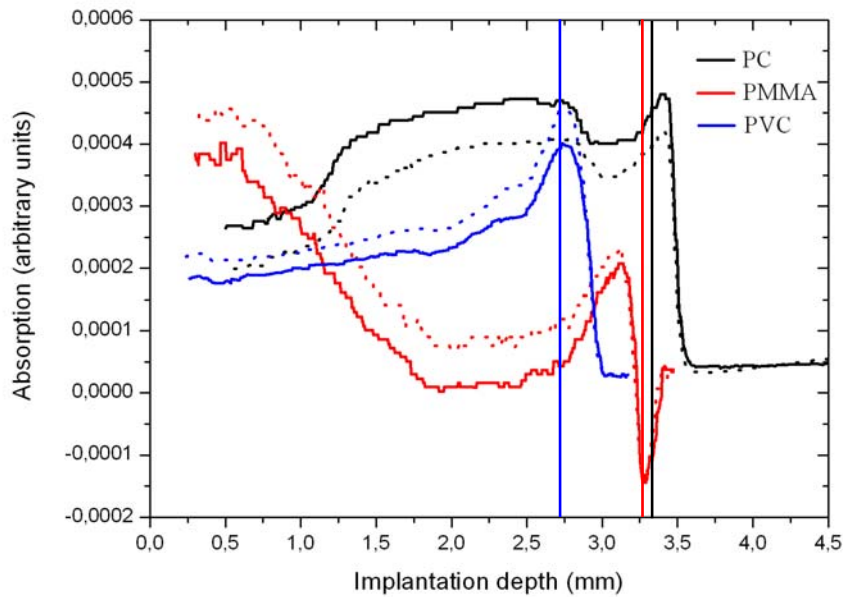
Figure 7.2: The variation of white light absorption along the penetration depth is calibrated and plotted for PC, PMMA and PVC. The dotted lines represent the variation of white light absorption in the region subjected to radiation damage and simultaneous ultrasound introduction. The solid vertical lines represent the stopping range of the incident deuterons in the samples. The absorption values are arbitrary. The plot is intended to compare the profile of the variation of absorption in PC, PMMA and PVC.

PMMA has one of the highest known radiation sensitivities with respect to chain scission and is extremely sensitive to radiation in comparison with inorganic materials. It responds sensitively to electronic energy transfers and offers a wide range of variation in the refractive index. Drastic change in the refractive index is observed after ion irradiation at doses of the order of 10^{14} ions/cm^2 and a lensing effect is observed at the stopping range of the deuterons in the PMMA sample (seen in Figure 7.1 and Figure 7.2).

PVC is also very sensitive to radiation. Deep colouration of PVC is observed for a deposited dose of 400 nC and blackening of PVC occurs for higher deposited doses.

Both PMMA and PVC, being aliphatic compounds, are highly sensitive to radiation enabling radiation damage to a large extent. PC, being an aromatic compound, is stable and reasonably resistant to radiation damage in comparison with PMMA and PVC. The addition of energy by introduction of ultrasound is observed to increase

91

the radiation damage in PMMA and PVC whereas in the case of PC, we observe an ultrasound driven repair mechanism which brings about a decrease in the radiation damage. This contradictory effect of ultrasound in different polymers can be attributed to the different structural stability of the polymers and the polymer constituents.

8 Summary and Outlook

8.1 Summary

The effect of ultrasound on radiation damage in polymers was studied. 26 MeV energetic deuterons were implanted in polymers namely, Polycarbonate, Polymethylmethacrylate and Polyvinyl chloride. Ultrasound was introduced into the samples simultaneously during deuteron irradiation. The chosen polymers were all transparent enabling their analysis using various optical techniques. The stopping range of the deuterons was within the polymer samples enabling the study of the entire implanted region. The frequency, amplitude and pulse length of ultrasound were chosen such that the ultrasound alone does not cause any measurable damage in the polymer samples. Thus sub-threshold ultrasonic waves were used in the experiments. The simultaneous introduction of ultrasound and energetic deuterons into the sample is carried out so as to study the final damage resulting from the effect of ultrasound on the polymer which is being rapidly modified during ion irradiation. The methods used for analysing the irradiated samples were Optical interferometry, Optical absorption spectroscopy, Optical microscopy and Positron annihilation spectroscopy.

Radiation damage in polymers is a complex process involving structural and chemical degradation of the material. In this work, the radiation damage caused in the polymers is reflected as refractive index modulation, variation in optical density and changes in white light absorption in comparison with the pristine polymers. The profiles of these modulations in properties do not follow the electronic energy loss (simulated) curve entirely. An effect of ultrasound is observed in the radiation induced damage in the polymers used. A decrease in refractive index modulation, change in optical density and white light absorption is observed in Polycarbonate, as an influence of ultrasound. In Polymethylmethacrylate, an increase in refractive index modulation, change in optical density and white light absorption is observed as an influence of ultrasound. In Polyvinyl chloride, an increase in change in optical density and light absorption is observed. In all three polymers, the effect caused by ultrasound is observed over the entire implantation depth. The effect of ultrasound is observed over the entire wavelength scale and not at particular wavelengths in optical absorption measurements. The observed modulation of properties due to introduction of ultrasound is not an effect of temperature as ultrasound power used in the experiments was sub-threshold. The introduction of ultrasound inputs kinetic energy to the polymer constituents in addition to the energy imparted by the impinging deuterons. This added can be sufficient to overcome the activation energy required for displacement of constituents of the polymer samples. Thus the introduction of sub-threshold ultrasonic waves produces mechanical displacement

of polymer constituents thereby affecting the radiation damage caused by deuterons impinging on the polymer samples.

A decrease in modulation of the measured properties in PC and an increase in the modulation of the measured properties in PMMA and PVC, due to the simultaneous introduction of ultrasound with energetic deuterons in the samples, is observed. PMMA and PVC are highly sensitive to radiation whereas PC is relatively stable under irradiation. The energy increase due to introduction of ultrasound is observed to increase the radiation damage in PMMA and PVC whereas an ultrasound driven repair mechanism resulting in a decrease in the radiation damage is observed in PC. This contradictory effect of ultrasound in different polymers seems to be due to the varied stability of the polymers under irradiation.

8.2 Outlook

The polymer samples have been used as a model system to study the effect of ultrasound upon radiation damage created by ion irradiation. Ion irradiation is largely implemented in many fields of science, especially in the medical field for radiation therapy. The experiment is more like a simulation of ion irradiation used in radiation therapy wherein the effect of ultrasound on the damage created by ions is studied. An effect of ultrasound has been observed which implies that this is a sensible approach to control the effects of radiation damage. Further research in other sample systems needs to be done to obtain a sophisticated method for implementing this idea in the medical field.

9 Bibliography

[1]   *Plastic Scintillators and Fast Pulse Techniques*.   [cited; Available from: http://www.pma.caltech.edu/~ph77/labs/exp13.html.

[2]   Haaks, M., *Positronenspektroskopie an Ermüdungsrisse und Spanwurzeln*. 2003, Rheinischen Friedrich - Wilhelms - Universität: Bonn.

[3]   Krevelen, D.W.v., *Properties of Polymers*. Second ed. 1976, Amsterdam - Oxford - New York: Elsevier Scientific Publishing Company.

[4]   American Piezo Ceramics Inc, A.I., Ltd, *Piezoelectric Ceramics: Principles and Applications*. 2002: APC International.

[5]   Fink, D., *Fundamentals of Ion-Irradiated Polymers*. Materials Science. Vol. 63. 2004, Germany: Springer.

[6]   Perez, J., *Physics and Mechanics of Amorphous Polymers*. 1998, Rotterdam: Taylor & Francis.

[7]   Daniels, C.A., *Polymers: Structure and Properties*. 1989, Lancaster - Basel: Technomic Publishing Co., Inc.

[8]   1994. **88**.

[9]   Leo, W.R., *Techniques for Nuclear and Particle Physics Experiments*. Second ed. 1987: Springer-Verlag.

[10]   Nordlund, K., *Molecular dynamics simulations of atomic collisions for ion irradiation experiments*. 1995, University of Helsinki.

[11]   El'piner, I.E., *ULTRASOUND Physical, Chemical and Biological effects*. 1964, New York: Consultants Bureau.

[12]   Gooberman, G.L., *ULTRASONICS Theory and Application*. 1968, London: The English Universities Press Ltd.

[13]   Hariharan, P., *Basics of Interferometry*.

[14]   Birk Andreas, I.B.K.B., *Modeling of X-ray-Induced Refractive Index Changes in Poly(methyl methacrylate)*. ChemPhysChem, 2005. **6**(8): p. 1544-1553.

[15]   D. C. Ghiglia, M.D.P., *Two Dimensional Phase Unwrapping*. 1998, New York: John Wiley & Sons.

[16]   Andreas, B., *Modifikation des Brechungsindexes von Dielektrika mit Hilfe ionisierender Strahlung*. 2005, Bonn University: Bonn.

[17]   D. P. Towers, T.R.J., and P. J. Bryanston-Cross, *Automatic Interferogram Analysis applied to Quasi-heterodyne Holography and ESPI*. Opt. Laser. Eng., 1991. **14**.

[18] T. R. Judge, a.P.J.B.-C., *A Review of Phase Unwrapping Techniques in Fringe Analysis.* Opt. Laser. Eng., 1994. **21**.

[19] Rao, C.N.R., *Ultra-violet and Visible Spectroscopy*.

[20] *UV-Vis Absorption Spectroscopy: Theoretical principles*. [cited; Available from: http://teaching.shu.ac.uk/hwb/chemistry/tutorials/molspec/uvvisab1.htm.

[21]   [cited;   Available   from: http://www.cem.msu.edu/~reusch/VirtualText/Spectrpy/UV-Vis/spectrum.htm.

[22] *Cary 100/300/400/500 Spectrophotometer specifications brochure*. [cited; Available from: www.varianinc.com.cn/products/spectr/uv/brochure/1604.pdf.

[23] I.K. MacKenzie, J.A.E., R.R. Gingerich, *The Interaction between Positrons and Dislocations in Copper and in Aluminium Alloy.* 1970. **33**.

[24] H. Greif, M.H., U. Holzwarth, U. Männig, M. Tongbhoyai, T. Wider, K. Maier, J. Bihr, B. Huber, *High-Resolution Positron Annihilation Spectroscopy with a New Positron Microprobe.* 1997. **71**.

[25] Mills, A.P., *Positronium Formation at surfaces.* 1978. **41**.

[26] P.J. Schultz, K.G.L., *Interaction of positron beams with surfaces, thin films and interfaces.* 1988. **60**.

[27] Hazell, J.H.G.a.E.A., *Degradation of a Polycarbonate by Ionizing Radiation.* Journal of Polymer Science: Part A, 1963. **1**: p. 1671-1686.

[28] Golden, J.H., *II. Effect of Radiation on Model Compounds*, in *Degradation of Polycarbonates*

1963, Materials Reasearch Laboratories, Explosives Research and Development Establishment, Ministry of Aviation, Waltham Abbey, Essex, England.

[29] Rao, C.N.R., *Ultra-Violet and Visible Spectroscopy*. Third ed. 1975, London - Boston: Butterworths.

[30] Balanzat, E., N. Betz, and S. Bouffard, *Swift heavy ion modification of polymers.* Nuclear Instruments and Methods in Physics Research Section B: Beam Interactions with Materials and Atoms, 1995. **105**(1-4): p. 46-54.

[31] Farenzena, L.S., et al., *Modifications in the chemical bonding and optical absorption of PPS by ion bombardment.* Nuclear Instruments and Methods in Physics Research Section B: Beam Interactions with Materials and Atoms, 1995. **105**(1-4): p. 134-138.

[32] Wang, Y., et al., *Chemical modification of polycarbonate induced by 1.4 GeV Ar ions.* Nuclear Instruments and Methods in Physics Research Section B: Beam Interactions with Materials and Atoms, 2000. **164-165**: p. 420-424.

[33]   Hoover, B.G., et al. *Laser-array generators produced by patterned ion irradiation of acrylic films*. in *Photonics for Space Environments X*. 2005. San Diego, CA, USA: SPIE.

[34]   Biersack, J.P. and R. Kallweit, *Ion beam induced changes of the refractive index of PMMA*. Nuclear Instruments and Methods in Physics Research Section B: Beam Interactions with Materials and Atoms, 1990. **46**(1-4): p. 309-312.

[35]   T. Venkatesan, L.C., B. S. Elman and G. Foti, *Ion beam effects in organic molecular solids and polymers*, in *Ion Beam Modification of Insulators*, P.M.a.G.W. Arnold, Editor. 1987, Elsevier.

[36]   Sum, T.C., et al., *Proton beam writing of passive waveguides in PMMA*. Nuclear Instruments and Methods in Physics Research Section B: Beam Interactions with Materials and Atoms, 2003. **210**: p. 266-271.

[37]   Schmoldt, A. 1994, TU Berlin.

[38]   A. Torikai, T.M., K. Fueki, *Radiation-Induced Degradation of Polycarbonate: Electron Spin Resonance and Molecular Weight Measurements*. Polymer Degradation and Stability, 1984. **7**.

[39]   Calcagno, L. and G. Foti, *Ion irradiation of polymers*. Nuclear Instruments and Methods in Physics Research Section B: Beam Interactions with Materials and Atoms, 1991. **59-60**(Part 2): p. 1153-1158.

[40]   Wündrich, K., *Influence of molecular motions on radiation-induced reactions in polymers*. Journal of Polymer Science, 1973. **11**.

[41]   Miller, A.A., J. Phys. Chem., 1959. **63**: p. 1755.

[42]   Winkler, D.E., Journal of Polymer Science, 1959. **35**.

Acknowledgement

In the first place, I would like to convey my gratitude to Prof. Dr. Karl Maier for providing me the opportunity to work under his supervision and for his able guidance and valuable support throughout the course of my research work. It would not be an exaggeration to say that discussions with him have been more informative than hours of book reading. I would also like to thank PD Dr. Reiner Vianden for kindly accepting to be my second referee.

I gratefully acknowledge Dr. Matz Haaks for his valuable advice and for spending time to read this thesis and giving critical comments. I am also grateful to PD Dr. Torsten Staab and Dr. Konrad Peithmann for their generous help and useful comments. I am thankful to Dipl.Ing. Mr. Bernd Habenstein for his valuable advice and fruitful discussions.

I am deeply indebted to Dr. Doris Thrun for accepting me in the Bonn International Graduate School. I am also thankful to Mrs. Petra Weiss for helping me in the initial phase of my stay in Bonn.

I would like to take this opportunity to thank Mrs. Maier for her kind hospitality. I would also like to thank all my colleagues and ex-colleagues. I am thankful to Dr. Andre Engelbertz for helping me in the initial stage of my research work. I also thank Ms. Christine Negrini for being an amiable work partner in the initial stages of my research work. I am thankful to all my colleagues in the NMR group, the Positron group and the Material Science group for their friendship and support throughout my study. They have made me feel at home in the working group and made my life more adventurous than it has ever been with the group trips.

I would like to express my sincere gratitude to the entire Bonn cyclotron operating group for their support especially during the beam times. I am also thankful to the Electronic workshop group and the Fine Mechanics workshop group for their support. I am thankful to the Secretaries in the Institute for their administrative help and all the members of the Institute who have supported me in the last few years.

Special thanks to Girisan Venugopal for his unconditional support throughout my stay in Germany. Innumerable thanks to Ingo Müller for being a helpful colleague and a wonderful friend till date. I would like to thank all my friends in Germany for their support and nice company during my stay in Bonn. I am also thankful to all my friends who have been there for me no matter in which part of the world they are.

Finally I wish to thank my parents for their unconditional love and encouragement. I am also thankful to my sisters, Suganyashree and Pallavee, and my brother Thirumal for their continuous support, encouragement, and love.

Curriculam Vitae

Personal Data

Name	:	Poornnima Anbalagan
Date & Place of Birth	:	05 September, 1979, Chennai, India
Nationality	:	Indian Citizen
Marital Status	:	Unmarried
Present Address	:	Helmholtz Institut für Strahlen- und Kernpysik
		University of Bonn, Nußalle 14-16,
		Bonn D-53115, Germany
		Tel: +49-228-733540, Fax: +49-228-732505
		e-mail: anbalaga@iskp.uni-bonn.de

Education and Degrees

School	:	Kendriya Vidyalaya II, Chennai, India
		July 1987 – July 1996
University	:	

- Madras Christian College, Madras University, India.
  August 1996 – August 1999
  Bsc Degree (Physics) : First Class
- Indian Institute of Technology, Madras. India.
  July 1999 – June 2001
  Msc Degree (Physics) : GPA 7.5/10
- Helmholz Institut für Strahlen- und Kernphysik, University of Bonn.
  April 2004 – April 2008.
  Advisor: Prof. Dr. Karl Maier

Dissertation

Ph.D thesis	:	Radiation Damage of Polymers in Ultrasonic Fields
		Advisor: Prof. Dr. Karl Maier